Spring 5-7-2016

Recurrent Mutations of T-Cell Receptor and CO-Stimulatory Signaling Proteins in Peripheral T-Cell Lymphomas

Joseph Rohr
University of Nebraska Medical Center

RECURRENT MUTATIONS OF T-CELL RECEPTOR AND CO-STIMULATORY SIGNALING PROTEINS IN PERIPHERAL T-CELL LYMPHOMAS

by

Joseph Rohr

A DISSERTATION

Presented to the Faculty of

the University of Nebraska Graduate College

in Partial Fulfillment of the Requirements

for the Degree of Doctor of Philosophy

Pathology & Microbiology
Graduate Program

Under the Supervision of Professor Wing C. Chan

and Professor Javeed Iqbal

University of Nebraska Medical Center
Omaha, Nebraska

April, 2016

Supervisory Committee

Kai Fu, MD, PhD	Julie Vose, MD, MBA
Shelley Smith, PhD	Dennis Weisenburger, MD

ACKNOWLEDGMENTS

This work could never have come to be without the efforts of many others across the United States and around the world. I am grateful to Dr. John Chan for setting me up for success and allowing me to choose a project which, despite being my primary preoccupation for years, still continues to interest me, and for continuously having new ideas to push me further in my work. I am equally grateful to Dr. Javeed Iqbal for taking over the primary committee responsibilities when we moved to California, and for teaching me so much about the bioinformatics that makes our field possible.

To Dr. Timothy McKeithan, thank you for the years of lunches, elaborate puns, and even more importantly, the conversations about life, liberty, and lymphocyte biology. Without your direct input this would not exist, and I cannot thank you sufficiently.

To Drs. Kai Fu, Shelley Smith, Julie Vose, and Dennis Weisenburger, I thank you for taking part in the many meetings with the multi-city logistical nightmares, and for your contributions to the directions this project went.

I want to thank heartily Dr. Shuangping Guo, who took over the project (including lots of cloning) in my intervening medical school year, who taught me how to keep the cells happy, and with whom I am extremely fortunate to be able to continue working, despite the date line between us.

Thanks to Qiang Gong and Weiwei Zhang, for the magic on the screen that leads to discovery at the bench.

Thanks to Cindy Lachel, Alyssa Bouska, Tayla Heavican, and Jennifer Yu, for working with me and together to further this project and others, and for all the emails (even if their content wasn't what I wanted to hear). Thanks to Andrew Cannon for being an important part of the data in my first year, and for the spots on the couch afterwards.

Thanks to Chao Wang for the sequences, and to Bei Jiang for working together in the cross-country move. Thanks especially to Yuping Li for being so knowledgeable to help me develop many of my experiments. Thanks also to Jianbo Yu, Gehong Dong, Xinhua Wang, Valerie Valenzuela, and Micheline Sepilian for making the lab at City of Hope a good place to be.

I have been extremely fortunate to directly work with many excellent members of labs throughout the world to further particular parts of the discovery in this thesis, and without them the conclusions could not have been drawn. These include Drs. Simon Davis and Jiangdong Huo of the University of Oxford, UK, who performed and analyzed the affinity analyses; Drs. Gloria Borgstahl and Peter Simone of UNMC and Florida International University, respectively, who performed the molecular modeling; and Drs. Christian Steidl, Anja Mottok, Stacy Hung, and Elizabeth Chavez of the British Columbia Cancer Agency for parsing the complexities of specific components of the sequencing and validation.

I have been equally fortunate to work with talented members of core labs both in Omaha and Duarte. At the University of Nebraska, particular thanks to Victoria Smith and Dr. Philip Hexley in the UNMC flow cytometry core, and to Ron Redder, Dr. Alok Dhar, and Dr. James Eudy of the UNMC sequencing core. At City of Hope, thanks to Lucy Brown, Alex Spalla, Ni Feng, and Shaun Hsueh of the COH analytic cytometry core, and Loren Quintanar and Dr. Brian Armstrong of the COH light microscopy core. Without your expertise, I could not have been able to gather the cells and data to draw any conclusions, and I am particularly grateful that you went above and beyond to answer questions and work with me to find ways to ask new ones.

I am lucky to work, albeit indirectly, with so many established medical professionals in obtaining patient samples and data the world over; Drs. Andreas Rosenwald, Randy Gascoyne, Françoise Berger, Tim Greiner, Lou Staudt, and Wenming Xiao. Thank you.

Gratitude cannot be expressed enough to my family. Thanks to my parents, Wendy and Stephen Rohr, for all the phone calls between point A and point B, especially during the Los Angeles commute, and for being supportive whatever happens.

And most importantly, thank you to my wife, Ariella, for more than I can possibly express (but I'll try anyway): for moving across the country with me three times in five years, for the day-to-day and the week-to-week, all those dinners, all those dishes, for giving me the tools and space to compile and write this thesis but the insisting I take breaks too, and for the love.

RECURRENT MUTATIONS OF T-CELL RECEPTOR AND CO-STIMULATORY SIGNALING PROTEINS IN PERIPHERAL T-CELL LYMPHOMAS

Joseph Rohr, Ph.D.

University of Nebraska, 2016

Supervisors: Wing C. Chan, MD and Javeed Iqbal, PhD

Peripheral T-cell lymphomas (PTCLs) comprise a heterogeneous group of mature T-cell neoplasms with a poor prognosis. Recently, mutations in TET2 and other epigenetic modifiers as well as RHOA have been identified in these diseases, particularly in angioimmunoblastic T-cell lymphoma (AITL). CD28 is the major co-stimulatory receptor in T-cells which, upon binding ligand, induces sustained T-cell proliferation and cytokine production when combined with T-cell receptor stimulation, through many signaling molecules including VAV1. This thesis identifies recurrent mutations in CD28 in PTCLs, as well as mutations in VAV1. Two residues of CD28 – D124 and T195 – were recurrently mutated in 11.3% of cases of AITL and in one case of PTCL, not otherwise specified (PTCL-NOS). Surface plasmon resonance analysis of mutations at these residues with predicted differential partner interactions showed increased affinity for ligand CD86 (residue D124) and increased affinity for intracellular adaptor proteins GRB2 and GADS/GRAP2 (residue T195). Molecular modeling studies on each of these mutations suggested how these mutants result in increased affinities. We found increased transcription of the CD28-responsive genes CD226 and TNFA in cells

expressing the T195P mutant in response to CD3 and CD86 co-stimulation and increased downstream activation of NF-κB by both D124V and T195P mutants. VAV1 mutations affect many important domains and may also enhance co-stimulatory signal. Together, these mutations suggest a novel potential pathway for therapeutic targeting in PTCLs.

TABLE OF CONTENTS

LIST OF FIGURES

LIST OF TABLES

LIST OF ABBREVIATIONS

5hmC	5-hydroxymethylcytosine
5mC	5-methylcytosine
Ac	Acidic region
AITL	Angioimmunoblastic T-cell lymphoma
ALCL	Anaplastic large cell lymphoma
ALK	Anaplastic lymphoma kinase
AM	Acetomethoxyl
APC	Antigen presenting cell
ATLL	Adult T-cell leukemia/lymphoma
BCL6	B-cell lymphoma 6
BLIMP1	B-lymphocyte-induced maturation protein 1
bp	base pairs
BSA	Bovine serum albumin
BTLA	B- and T-lymphocyte attenuator
CD	Cluster of differentiation
cDNA	Complementary DNA
CFSE	Carboxyfluorescein succinimidyl ester
CH	Calponin homology
CHOEP	Cyclophosphamide, doxorubicin, vincristine, etoposide, and prednisone
CHOP	Cyclophosphamide, doxorubicin, vincristine, and prednisone
CLP	Common lymphoid progenitor
CMP	Common myeloid progenitor
COO	Cell of origin
CR	Clinical remission
CTCL	Cutaneous T-cell lymphoma
CTLA4	Cytotoxic T-lymphocyte antigen 4
CXCL13	CXC chemokine ligand 13
CXCR5	CXC chemokine receptor 5
DAG	Diacyl glycerol
DC	Dendritic cell
DN	Double negative
DNA	Deoxyribonucleic acid
DP	Double positive
EBER	Epstein Barr virus-encoded RNA
EBV	Epstein Barr virus
EPOCH	Etoposide, prednisone, vincristine, cyclophosphamide, and doxorubicin
EVS	Event-free survival
FDA	Food and Drug Administration
FDC	Follicular dendritic cell
FFPE	Formalin-fixed, paraffin-embedded

GAP	GTPase-accelerating protein
GDI	guanine dissociation inhibitor
GDP	guanine diphosphate
GEF	guanine exchange factor
GEP	Gene expression profiling
GOF	gain-of-function
GTP	guanine triphosphate
H&E	Hematoxylin and eosin
HCT	Hematopoietic cell transplant
HDAC	Histone deacetylase
HEV	High endothelial venule
HSC	Hematopoietic stem cell
HSCT	Hematopoietic stem cell transplant
HVEM	Herpes virus entry mediator
ICOS	Inducible co-stimulator
IFNγ	Interferon gamma
Ig	Immunoglobulin
IgV	V-set immunoglobulin domain
IL	Interleukin
IPI	International Prognostic Index
I-PTCL	International Peripheral T-cell Lymphoma Study Group
kbp	kilobase pairs
LCK	Leukocyte C-terminal Src kinase
LFA-1	Lymphocyte function-associated antigen 1
LLMPP	Leukemia/Lymphoma Molecular Profiling Project
LOF	loss-of-function
LT-HSC	Long-term hematopoietic stem cell
MHC	Major histocompatibility complex
MPP	Multipotent progenitor
MPS	Massively parallel sequencing
NFAT	Nuclear factor of activated T-cells
NGS	Next-generation sequencing
NK	Natural killer cell
NKCL	Natural killer cell lymphoma
NSG	NOD/SCID/Il2rg-null
OS	Overall survival
PBMC	Peripheral blood mononuclear cell
PBS	Phosphate buffered saline, pH 7.4
PCR	Polymerase chain reaction
PD-1	Programmed death 1
PDX	Patient-derived xenograft
PH	Pleckstrin homology
PI3K	Phosphatidylinositol 3-kinase
PIP2	Phosphatidylinositol diphosphate
PIP3	Phosphatidylinositol triphosphate

PIT	Prognostic Index for T-cell Lymphoma
PLCG1	Phospholipase C γ-1
PTCL	Peripheral T-cell lymphoma
PTCL, NOS	Peripheral T-cell lymphoma, not otherwise specified
RAG	Recombination-activation gene 1/2
RNA	Ribonucleic acid
RRM	RNA recognition motif
SCA1	Stem cell antigen 1
SH2	Src homology 2
SH3	Src homology 3
SNP	Single nucleotide polymorphism
SP	Single positive
STAT	Signal transducer and activator of transcription
ST-HSC	Short-term hematopoietic stem cell
TCR	T-cell receptor
T_H1	T-helper 1
T_H2	T-helper 2
T_{FH}	Follicular helper T-cell
TM	Transmembrane domain
Treg	Regulatory T-cell
WES	Whole-exome sequencing
WGS	Whole-genome sequencing
WT	Wild-type
WTS	Whole-transcriptome sequencing
ZAP-70	ζ-associated protein of 70 kilodaltons

Introduction

Epidemiology and clinical characteristics of peripheral T-cell lymphomas

Peripheral T-cell lymphomas (PTCLs) are a large group of uncommon, heterogeneous diseases which comprise up to 20% of all non-Hodgkin lymphomas depending on geographic region.[1,2] Most are derived from mature helper T-cells which express cluster of differentiation 4 (CD4), and besides anaplastic lymphoma kinase positive (ALK+) anaplastic large cell lymphoma (ALCL), most subtypes carry a dismal prognosis.[1,2] In the Western world, the incidence of PTCLs has increased dramatically in recent years, amounting to 3.8% per annum in the United States,[3] sharply augmenting both clinical and research interest. A clinical diagnosis requires pathologic examination by expert hematopathologists, but because of their rarity and variable clinical presentations, these entities remain difficult to diagnose. Since the publication of the WHO guidelines for the classification of lymphoid tumors and their later update,[4,5] inter-observer classification is fairly consistent depending on subtype. How-ever, even with these guidelines, approximately 10% of cases initially diagnosed as a PTCL or related NK-cell lymphoma (NKCL) were misdiagnosed in the 2008 International Peripheral T-cell Lymphoma (I-PTCL) Group study[1] which examined 1,314 cases of PTCL and NKCLs, the largest cohort ever examined for these diseases. Such a margin of error highlights the necessity of expert review. In general, the PTCLs have a poor overall survival, but depending on subtype (by pathologic review) and staging (by any or all of the Ann Arbor method,[6] International Prognostic Index [IPI],[7] or Prognostic Index for T-cell lymphoma [PIT]),[8] prognosis can vary widely. Diagnosis and proper clinical evaluation of the

particular entity, therefore, is extremely important for prognostication and choice of therapy.

The two most common PTCLs worldwide are PTCL, not otherwise specified (NOS; approximately 30%) and angioimmunoblastic T-cell lymphoma (AITL; approximately 20%).[1] In North America, PTCL, NOS accounts for 34.4% of all cases and AITL for 16.0%. Both of these diseases often present with focal or generalized lymph-adenopathy, and constitutional B-symptoms (fatigue, fever, night sweats, and/or unintentional weight loss) are variably present (see Table 1). Both of these entities primarily affect older individuals with a median age of 60 years for PTCL, NOS and 65 years for AITL. Although AITL has several unique histologic and immunophenotypic features, including a strong association with infection with Epstein-Barr virus (EBV), PTCL, NOS is a diagnosis of exclusion.

In the I-PTCL study, 69% of PTCL, NOS patients presented at Ann Arbor stage III or IV, and 29% had greater than one extranodal site; for AITL, 89% presented at Stage III or IV, with 27% having more than one site of extranodal involvement. Physical and blood exams were non-specific for both diseases, though hypergammaglobulinemia was more common in AITL than PTCL, NOS. A summary of the findings can be found in Table 1.

Given the geographical differences found in PTCL subtypes, it follows that different races and ethnicities may have differential predispositions to various PTCLs. A recent survey of PTCL cases in America has found this to be the case;[9] compared to whites, American Indians and Alaskan natives were 40% less likely to be diagnosed with PTCL, NOS, and too few were diagnosed with AITL to draw conclusions. Conversely, blacks were 67% more likely to be diagnosed with PTCL, NOS, but 29% less likely to have AITL than whites. Still, to contribute ethnicity as a major predetermining factor in PTCL likely ignores many broad, mostly unclear, factors.

This introductory section will serve to outline the current state of diagnosis and treatment of PTCL, NOS and AITL, to describe the current understanding of these diseases' genetic and biological bases, and to discuss relevant background information on T-lymphocyte signaling pathways.

	PTCL, NOS (N=340)	AITL (N=243)
Age, years		
Median	60	65
Range	19-87	20-86
	Number (% of total) as available	
Male	223 (65)	137 (56)
Stage III-IV	232/334 (69)	214/241 (89)
Extranodal sites >1	99 (29)	66 (27)
Systemic (B) symptoms	118 (35)	168 (69)
IPI > 1	72%	192/222 (79)
PIT > 1	42%	154/233 (63)
Clinical exam findings		
Skin involvement	16%	21%
Hepatomegaly	17%	26%
Splenomegaly	24%	35%
Serum findings (not available for all cases)		
Elevated LDH	49%	146/223 (60)
Elevated CRP	50%	84/127 (35)
Hypercalcemia	5%	3/184 (1)
Elevated β2-microglobulin	36%	53/92 (22)
Hypergammaglobulinemia	29/201 (14)	74/166 (30)
Survival		
5-year OS	32%	32%
5-year PFS	20%	18%

Table 1. Clinical characteristics of AITL and PTCL, NOS. Legend on next page.

Table 1. Clinical characteristics of AITL and PTCL, NOS. Clinical findings are usually non-specific, and clinical suspicion is usually low, contributing to the difficulty in diagnosis. Both entities affect older individuals with a slight male preference, and the majority are diagnosed at late stage. AITL tends to have a higher proportion of clinical exam findings, but serum findings between the two are inconclusive. Both have a deplorable 5-year overall survival (OS) and progression-free survival (PFS). Adapted and reprinted with permission. Includes data from from Weisenburger et al.[3]

Pathologic characteristics of PTCL, NOS and AITL

As stated previously, review by expert hematopathologists is crucial for diagnosis, and agreement on diagnosis is fairly consistent across experts. Still, first-diagnosis inter-observer accord has been pegged at 75% for PTCL, NOS and 81% for AITL.[1,3,10] Clinical data in addition to pathologic data are important and informative for accurate diagnosis. Still, even the experts can disagree on the best characterization.

AITL

Histologically, hematoxylin and eosin (H&E) staining will reveal various degrees of effacement of normal lymphoid architecture by small-to-medium sized lymphocytes (see Figure 1a).[4,11] These lymphocytes may display nuclear atypia. Usually, there is marked proliferation of high endothelial venules (HEVs), with clusters of atypical cells, often intermixed with plasma cells, eosinophils, and/or histiocytes. Most cases display an increased follicular dendritic meshwork, and in some hyperplastic follicles are evident. Because the neoplastic cells partially mimic the normal function of their putative cell of origin, the follicular helper T-cell (T_{FH}; see "Genetics/Cell of Origin), the B-cell compartment may be perturbed as well. Frequently the B-cells are infected with EBV,

resulting in mild-to-moderate atypia and the appearance of a B-immunoblastic proliferation. Rarely, Reed-Sternberg-like cells may be present, which may confound diagnosis. There may also be an inflammatory infiltrate.

On immunohistochemical staining, AITL cells express pan-T markers CD2, CD3 (Figure 1b), and CD5, plus CD4. A CD8 stain, however, may reveal large numbers of infiltrating cytotoxic T-cells, which may obscure diagnosis. CD10, may be expressed in the neoplastic cells(Fig. 1d), as is the transcription factor responsible for T_{FH} identity, BCL6. Cells are usually negative for CD30, but any Reed-Sternberg-like cells may be positive for CD30 (Fig. 1e) or rarely CD15 (Fig. 1f). Staining for T_{FH} markers CXC chemokine ligand 13 (CXCL13) and programmed death-1 (PD1)[12] will almost always be positive, and these two are particularly informative for the distinction between AITL and PTCL, NOS. Stains for inducible co-stimulator (ICOS) will be generally high, though this is not thought to be particularly specific.[13] Also, as AITL is characterized by the expansion of the follicular dendritic meshwork, markers of follicular dendritic cells (FDCs) – CD21 (Fig. 1c), CD23, CD35, and CNA42 – are often observed. As AITL frequently occurs in the background of EBV infection, *in situ* hybridization (ISH) for Epstein-Barr virus-encoded small RNAs (EBER) highlights EBV-infected B-cells (Fig. 1f, inset); these $EBER^+$ B-cells may be of various sizes, and may separately progress to, or be founders of, a B-cell malignancy.

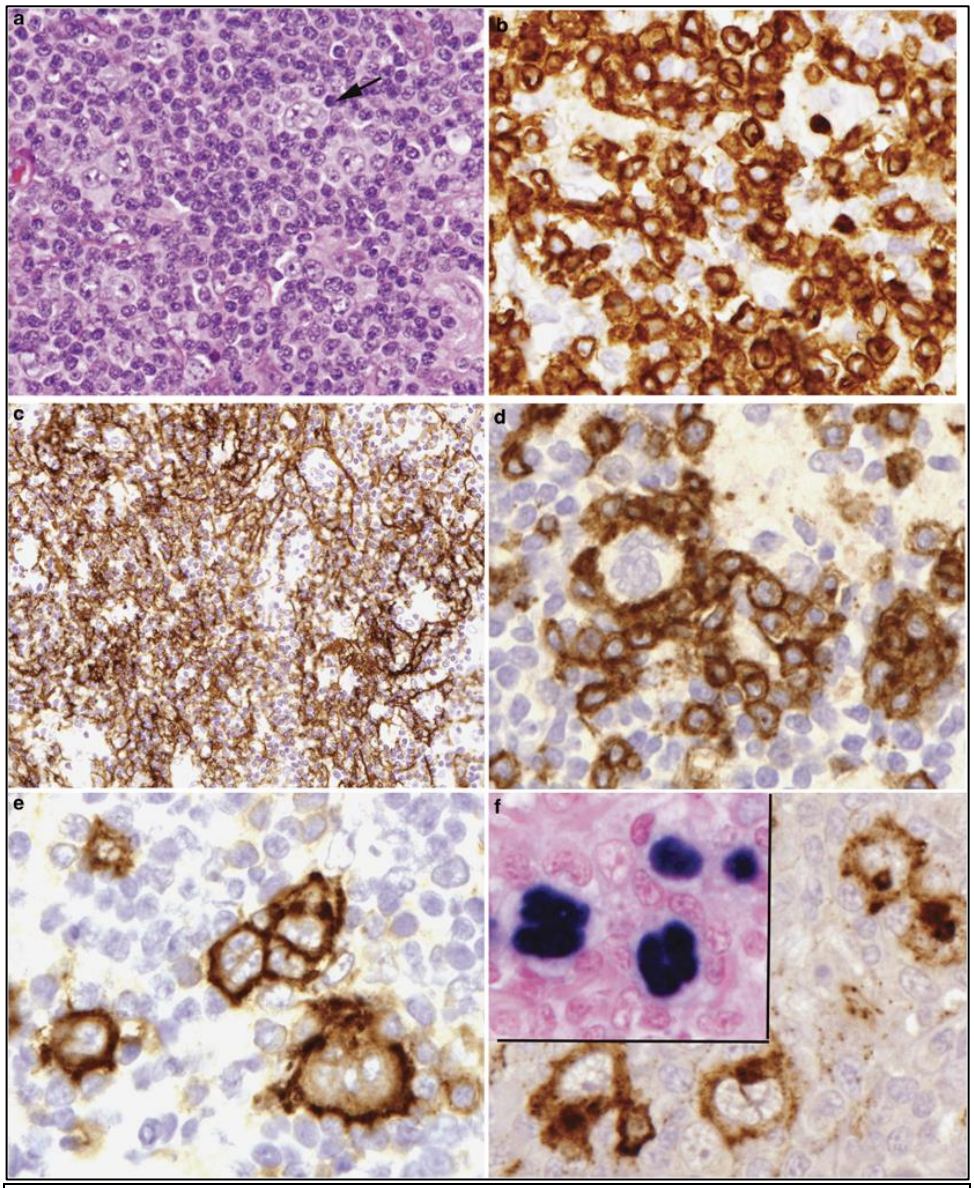

Figure 1. Pathologic characteristics of angioimmunoblastic T-cell lymphoma with Hodgkin-Reed Sternberg-like cells positive for EBV. (a) Atypical large cells, some binucleate (arrow) are seen in a background of atypical lymphocytes. (b) Cytological atypia is evident in the T cells, highlighted with a CD3 stain. (c) Follicular dendritic cell meshworks are expanded, as seen with a stain for CD21. (d) CD10-positive atypical lymphocytes rosette large atypical cells with Hodgkin-like features. The Hodgkin-like cells are positive for CD30 (e), CD15 (f), and EBER (inset). Reprinted by permission from Macmillan Publishers Ltd: *Modern Pathology* **26** S71-S87 doi:10.1038/modpathol.2012.181 (ref. [5])© 2013

PTCL, NOS

The morphology of NOS ranges broadly but usually effaces normal nodal architecture (see Figure 2A,B).[1,4,14] Cellular infiltrates may be monomorphous to highly polymorphous. Nuclei are often irregular and hyperchromatic. Large cells may have prominent nucleoli and mitoses. Reed-Sternberg-like cells may be present, and HEVs are not prominent. Because PTCL, NOS is a diagnosis of exclusion, there is no specific morphologic feature that points to its identification.

Immunophenotypically, the neoplastic cells may express some or all mature T-cell antigens, or aberrantly lose some: CD5, CD7, and CD4 or CD8. Some cases are CD30, CD56, CD20, CD79a, or CD52 positive; some are double positive for CD4 and CD8.

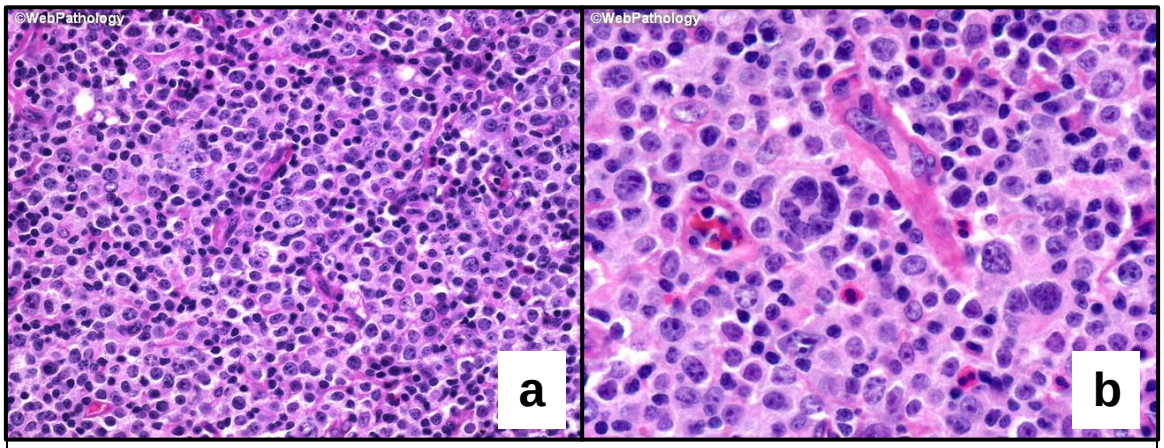

Figure 2. Pathologic characteristics of peripheral T-cell lymphoma, not otherwise specified. (a) The tumor cells are variably-sized and consists of small cells with only minimal cytologic atypia and larger cells with irregular nuclear contours, prominent nucleoli, and brisk mitotic activity. Large cells with clear cytoplasm and Reed-Sternberg-like cells may be seen in some cases. Evidence of neoangiogenesis in the form of high endothelial venules is often seen. There is often a prominent component of reactive cells in the background, including small lymphocytes, eosinophils, macrophages, and plasma cells. (b) Some cases of PTCL, NOS show Reed-Sternberg-like cells. One such cell can be seen near the center of this image. The presence of a reactive infiltrate in the background consisting of eosinophils, lymphocytes, plasma cells, and histiocytes creates further resemblance to Hodgkin's lymphoma. From Webpathology.com.[15] Used with permission.

Some cases may have a substantial number of $CD30^+$ tumor cells which raises the possibility of ALCL. The T-cell receptor (TCR) β-chain is usually positive, which allows differentiation from γδ-PTCL subtypes. Ki-67, a marker of proliferation, is usually fairly high. Notably, it can be challenging to differentiate this entity from AITL due to the large variation in PTCL, NOS, so the markers which are on the neoplastic component of AITL – CD10, CXCL13, PD-1, ICOS, BCL6 – should be low to negative in PTCL, NOS. However, the follicular meshwork is variable, though low staining decreases the likelihood of AITL.

Cytogenetic characteristics[4] of both PTCL, NOS and AITL have been studied in very few cases, and these rare findings can be found in Table 2. These changes are not diagnostic and their functions are not known.

	PTCL, NOS	AITL
TCR clonality	+	+
Chromosomal loss	4q, 5q, 6q, 9p, 10q, 12q, 13q	13q
Chromosomal gain	7q, 8q, 17q, 22q	3, 5, 19, X; 22q, 11q13

Table 2. Cytogenetic characteristics of PTCL, NOS and AITL. Although not frequent, these cytogenetic findings[4] are sometimes identified in each entity.

Treatment and outcomes of PTCL, NOS and AITL

There exists no standard of therapy for PTCL, NOS or AITL, but the anthracycline-based regimen of cyclophosphamide, doxorubicin, vincristine, and prednisone (CHOP), is usually used. However, no treatment has been found that works consistently well. Thus, the major recommendation is to include patients on clinical trials, if possible.[16] This approach has led to the use of several new drugs, trials for most of which are still ongoing.

Despite its prevalence, outcomes associated with the use of CHOP in PTCLs are poor. The addition of etoposide (CHOEP or EPOCH)[16] has been shown to improve event-free survival (EVS) but not overall survival (OS), particularly in younger patients (<60 years). These formulations and dosages are based primarily on trials in aggressive B-cell non-Hodgkins lymphomas, and work fairly well in those diseases but much less well in PTCL, NOS. Other, more intensive regimens have also been tried in the past, but uniformly these have shown no improvement in outcomes but increases in treatment toxicities.[16,17] For AITL, retrospective analysis has found CHOEP to be superior to any other regimen.[16]

Consolidation therapy remains somewhat controversial,[16,17] but radiation therapy is used to some success for controlling localized disease. However, because of the high relapse rate for PTCLs, current recommendations strongly suggest the chemotherapeutic regimen as a bridge to either autologous (preferred) or allogeneic hematopoietic stem cell transplant (HSCT or HCT).[18-20] This is not true for lowest-risk tumors, which have a notably high OS after therapy with monitoring, but PTCLs only rarely present at low stage.

Auto-HCT, in which hematopoietic stem cells are collected from patients and then returned after marrow-ablative chemotherapy, works best for younger patients in their first clinical remission post-chemotherapy, though only a few large studies have been performed on which these statements have been based. There have been more studies with smaller patient populations, using various induction and consolidation regimens and patients of various ages, stages and diagnoses; predictably, these studies have a wide range of outcomes, making it challenging to draw meaningful conclusions when taken together. Understandably, relapse is not uncommon in autotransplant, but the outcomes are generally better than without transplant. Allo-HCT is the only possible curative therapy in the case of relapsed or refractory disease. Unfortunately, given the age and health of the majority of patients with PTCL, NOS and AITL, many are poor candidates for an allotransplant, leading to difficult clinical decisions. Patients who are successfully engrafted may achieve clinical remission (CR), particularly in chemosensitive patients, and some may be cured.[18-20] Graft-versus-host disease (GVHD), in which the transplanted immune cells attack recipient tissue, remains a major complication.[17,18]

Patients who are poor candidates for transplant and/or who fail chemotherapy are generally given other chemotherapeutic regimens with variable but generally poor efficacy. Patients may opt for palliative care, or for trials if applicable.

Even in the past five years, many new drugs have become available which show promise in treating PTCLs.

- Pralatexate, an antifolate, has been approved by the United States Food and Drug Administration (FDA) for PTCL when administered with leucovorin rescue to minimize side effects.[21-23] This treatment has not been as effective in AITL as other PTCL subsets, including NOS. Interestingly, there was no correlation between number of prior therapies and response to the drug,[23]

suggesting that the pathways targeted may be independent of the cancers' clonal evolution in response to other chemotherapies.

- Brentuximab vedotin, is an anti-CD30 antibody conjugated to monomethyl auristatin E, an anti-tubulin agent. It is approved for use in CD30-positive PTCLs.[24-26] In one study, effect was not directly correlated with tumor CD30 expression, suggesting that drug activity is measurable even with low levels of CD30. Unfortunately, its side effect profile is fairly serious, with many patients experiencing peripheral neuropathy which may not regress depending on length of brentuximab therapy, and a small percentage of patients developing progressive multifocal leukoencephalopathy.[27]
- Histone deacetylase (HDAC) inhibitors, including romidepsin[28,29] and belinostat[30,31], are approved for use in patients who have failed at least one prior therapy. Serious cardiotoxic side effects have been found in cutaneous T-cell lymphomas[29] (CTCLs, a separate subset of PTCLs), so patients with moderate-to-severe cardiovascular disease (a large portion of the patient population) are ineligible.

Further, there are currently 195 listed drug trials for PTCLs, many of which are attempting to perfect dosages of known drugs. Some, however, aim to investigate the use of novel agents approved for other malignancies, including:

- Mogamulizumab,[32] an inhibitor of chemokine receptor CCR4
- Tipifarnib,[33] a farnesyltransferase inhibitor which prevents the activation of Ras-family GTPases
- Selinexor,[34] an inhibitor of nuclear exporter XPO1, which has been shown to maintain tumor suppressor activity in suppressor-mutated tumors
- Alemtuzumab,[35,36] an anti-CD52 antibody

- Lenalidomide,[37,38] a strong immunomodulatory agent which works through many, mostly incompletely understood, mechanisms
- Bendamustine,[39,40] a nitrogen mustard with DNA-alkylating and anti-metabolic properties[41]
- Bortezomib,[42-44] carfilzomib,[45] and ixazomib,[46] second-generation proteosome inhibitors, have shown promise in CTCLs.

With the use of CHOP or other anthracycline-based therapies for PTCL subtypes, overall survival for most subtypes is fairly low[1] (Figure 3). For both AITL and PTCL, NOS, 5-year overall survival is 32% with CHOP-like chemotherapy, and failure-free survival is 18% and 20%, respectively. At one point, this figure was similar for most hematologic malignancies. Since the use of rationally designed drugs like rituximab for B-cell lymphomas, including high-risk diffuse large B-cell lymphomas, these diseases have seen remarkable improvements in overall survival and progression-free survival,[47,48] a trend that has not extended to PTCLs.

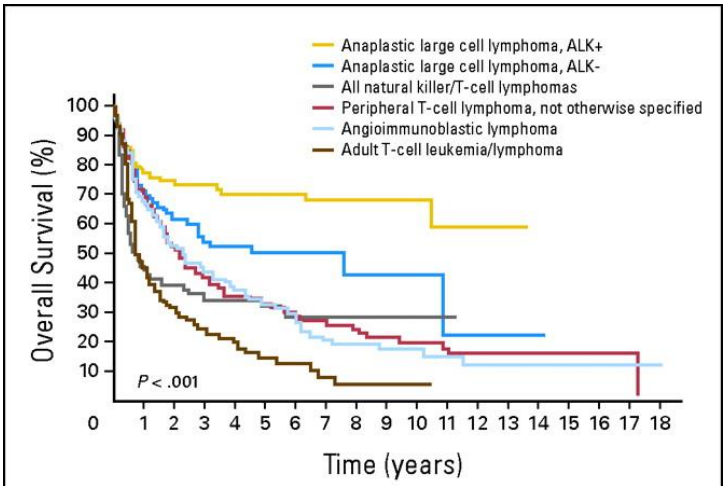

Figure 3. Overall survival of patients with the "common" peripheral T-cell lymphomas, by subtype. AITL and PTCL, NOS both have 5-year survival rates of 32%. Reprinted with permission[1].

T-cell development and activation: an overview

To explain specifically the development of peripheral T-cell lymphomas, it is first necessary to trace T-cell development. This section briefly discusses T-lymphocyte generation in the post-natal human, and how T-lymphocytes become activated.

From stem cell to mature αβ-T-cell

Hematopoietic stem cells (HSCs) reside in the bone marrow and generate all blood cells through asymmetric cell division; when a long-term (LT) HSC divides, one daughter cell retains hematologic pluripotency whereas the other moves toward a committed lineage. They are identified by surface expression of stem cell antigen 1 (Sca1) and c-Kit without expression of any lineage-specific markers.[49] In the case of cells that will become T-lymphocytes, a LT-HSC differentiates into a short-term HSC, which is further differentiated into a multipotent progenitor (MPP). MPPs then divide to terminal, e.g. irreversible lineage commitment. Classically, these progeny are either common lymphoid progenitors (CLPs) from which the entire lymphoid lineage is derived, or common myeloid progenitors (CMPs) from which the myeloid, megakaryocyte and erythroid lineages develop. Recent work has suggested some trans-differentiation between CLPs and CMPs depending on the cytokine milieu, thymic environment, and bone marrow cellularity,[50] but this complexity is beyond the scope of this chapter.

To generate T-cells, CLPs, identified by the expression of IL-7Rα and low levels of c-Kit and Sca1, emigrate from the bone marrow to the thymus.[51] What causes this emigration is not fully elucidated, but adhesion molecules CD44 and lymphocyte function-associated antigen 1 (LFA-1) are both absolutely required. Expression of B220

identifies a thymus-bound subset of CLPs known as CLP-2s which efficiently enter the thymus at its corticomedullary junction via CD44, LFA-1, and nearly a dozen other adhesion molecules.[52,53] CLP-2s are believed to enter the thymus the same way that more mature lymphocytes enter peripheral organs: adhesion and tethering to ligand; rolling along the endothelia that line the capillary wall adjacent to the organ; and extravasation through the endothelial wall into the organ.[54]

Mature T-cells can broadly be separated into two categories based on TCR chain expressed;[55] the α-chain always pairs with β, which is termed an αβ T-cell. T-cells expressing the αβ TCR are up to 98% of mature T-cells in humans. The remaining 2% or so of T-cells express the γ and δ chains of the TCR which will not be further described here. The maturation process allows for the generation of appropriately functional β and α TCR chains, in that order.

Pre-T-cells in the thymus go through three distinct phenotypic stages based on expression of CD4 and CD8, and the first stage is further divided into four substages.[55] The double-negative (DN) stages express neither CD4 nor CD8, and the cells migrate within the thymic outer cortex, but can be further subdivided based on surface expression of CD44 and CD25. DN1 is $CD44^{+}CD25^{-}$; DN2, $CD44^{+}CD25^{+}$; DN3, $CD44^{-}CD25^{+}$; and DN4, $CD44^{-}CD25^{-}$. As the thymocyte progresses through the stages, it is sequentially attempting to make a functional T-cell receptor β-chain through recombination by action of recombination-activation gene 1 (RAG1) and RAG2, which is a hallmark of adaptive immunity in vertebrates. At the DN3 stage, a pre-α chain (non-recombined) is synthesized, to form a pre-TCR with the β-chain and components of CD3: γ, δ, and multiple ε and ζ chains. In the event that the β-chain is non-functional, the pre-T-cell will not be stimulated through its pre-TCR and therefore die.

Once the DN4 stage is complete and there is a functional β-chain, the cells divide several times and then individually recombine the α-chain gene to encode a functional,

mature αβ-TCR; the pre-α chain is quickly lost.[55] The cells also begin to upregulate CD8, followed by CD4, to begin the double-positive (DP) stage. The cells migrate into the deep cortex of the thymus and interact with thymic cortical epithelial cells, which express major histocompatibility complex (MHC) classes I (which interacts with TCR and CD8) and II (which interacts with TCR and CD4) and present some self-peptides. Thus, the DP cells are able to receive stimulation by MHC through their TCR, which sets up the next round of selection. If the TCR is unable to interact with MHC, the T-cell undergoes apoptosis, termed "by neglect." But if the TCR interacts with MHC, usually weakly to moderately, it receives enough positive signal to stay alive, termed "positive selection." The nature of this positive signal transduction is discussed later in this section. These selection steps theoretically ensure that T-cells which proceed to the next step in development are able to function.

T-cells that pass positive selection then migrate to the thymic medulla to interact with medullary epithelial cells and dendritic cells, which are also coated with MHC presenting self-peptides. At the end of this developmental stage, the T-cells will be single-positive (SP) and express only one of CD4 or CD8, which will limit their ability to interact to only MHC II or MHC I, respectively. How these final maturation steps occur has only fairly recently been elucidated, and only after protracted experiments with conflicting data; the accepted model is called "instructional," as opposed to a stochastic method of a random assortment of MHC interactions.[55]

DP cells interacting with epithelial cells receive moderate signaling through MHC I / CD8 or MHC II / CD4. When one signal is stronger, however, the T-cell first downregulates the receptor gene that received the primary signal,[55] e.g. if signaling came through CD4, *CD4* is mildly downregulated, so shortly after receiving signal, future $CD4^{+}$ cells may appear $CD4^{med}CD8^{hi}$. Eventually, *CD8* will be methylated and downregulated, and *CD4* transcription will be restored.

During the DP-SP transition as discussed above, the T-cells are still interacting heavily with epithelial cells in the medulla. If the TCR reacts strongly with MHC, the T-cell also undergoes apoptosis, termed “negative selection.” This ensures that the nascent T-cells will not react strongly with peptides derived from the body’s own tissues, preventing autoimmunity. The cells are still selected positively as well, such that cells that cannot maintain TCR signal throughout thymic migration will still undergo apoptosis.

The particularities of the DN-DP transition, and to a slightly lesser degree DP-SP transition, are quite complex and are important for the understanding of T-cell leukemogenesis.[56] T-cell leukemias are derived primarily from the various immature T-cell subsets, so failures of negative selection, or oncogenic mutations which render cells unlikely to undergo apoptosis, are very important for leukemia biology. T-cell lymphomas, however, are almost exclusively derived from mature T-cell subsets, which means this entire process of thymocyte maturation likely proceeded correctly and any directly lymphomagenic mutation occurred after maturation. For one gene, this actually may not be the case (see “TET2” under “mutations” below).

Once SP cells have completed their migration through thymic stroma, they are released into blood to circulate and migrate through secondary lymphoid tissue until an activation signal is found.

$CD4^+$ T-cell activation cascade

Mature, naïve $CD4^+$ T-cells circulate throughout the body and enter peripheral tissues by random or following chemokine attraction. At any one time, the majority of T-cells are likely within peripheral lymphoid organs – spleen, lymph nodes, and oral and gastrointestinal mucosa – in a quiescent state, expressing a mature TCR (αβ-complex and CD3γ, -δ, two -ε and two-ζ chains) interacting at random with antigen-presenting

cells (APCs) via MHC II. When a T-cell finds an MHC presenting an antigen with which it can successfully interact above a certain threshold of affinity, it experiences signal transduction activation with pleiotropic effects, but as will be shown, sustained activation requires a second, co-stimulatory signal (see Figure 4). To explain the pathways, first the canonical TCR activation cascade is described.

Most of the early activation proteins are residents of the plasma membrane. Several are modified by fatty acid chains (palmitoyl and miristoyl groups) which anchor them in the membrane and prevent them from diffusing away, ensuring rapid transduction of signal on ligation. Upon ligation of TCR/CD3 with a cognate antigen, the MHC II interaction with CD4 causes CD4 to recruit leukocyte C-terminal Src kinase (LCK). In turn, LCK phosphorylates the immunoreceptor tyrosine-based activation motifs (ITAMs) on the CD3ζ chains, which allows binding by Src kinase ζ-associated protein of 70 kilodaltons (ZAP-70). LCK then phosphorylates ZAP-70, which phosphorylates linker of activated T-cells (LAT). LCK also separately interacts with and phosphorylates FYN, another Src tyrosine kinase. LAT serves as the scaffold for binding a variety of signaling intermediates, including growth factor receptor-bound protein 2 (GRB2), and the VAV family, especially VAV1, both of which have many functional domains to interact with many different proteins.

FYN, once activated, activates MEK and ERK through a variety of mechanisms, intermediate steps in the RAS-RAF-MEK-ERK classical cascade which phosphorylates dozens of other proteins as well as allows the nuclear translocation of transcription factors, including nuclear factor κ-B (NF-κB), Fos, Jun, MYC, and nuclear factor of activated T-cells (NFAT) among others. FYN, along with LCK and ZAP-70, activates phosphatidylinositol 3-kinases (PI3K), which generate phosphatidylinositol triphosphate PIP_3 and others, as well as activate protein kinase B (PKB/AKT), and phospholipase C γ-1 (PLCG1), described below.[57,58]

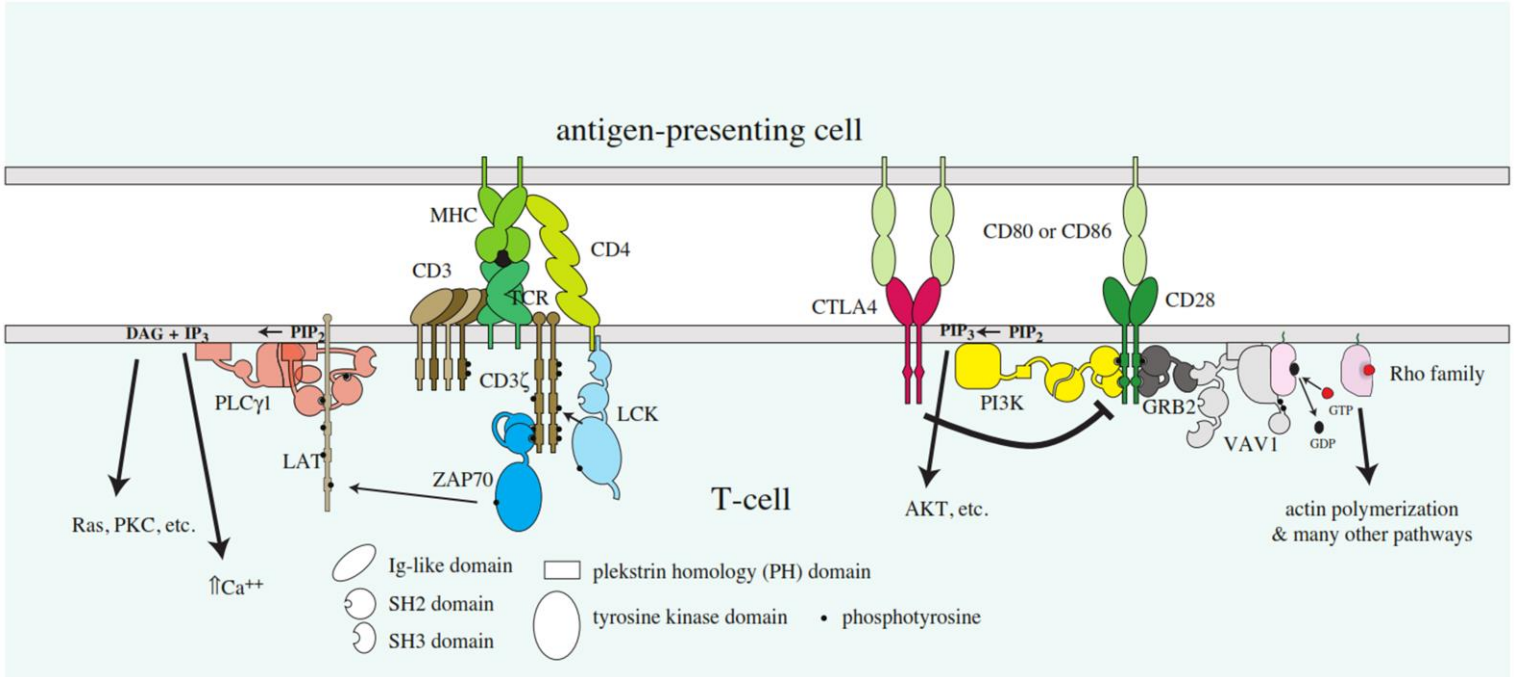

Figure 4. Simplified diagram of the TCR/CD3 stimulation and CD28 co-stimulation pathways. In peripheral lymphoid organs, T-cells interact with antigen-presenting cells (APCs). For $CD4^+$ T-cells, major histocompatibility complex type II presents antigen to the TCR/CD3 complex, stabilized by CD4 (center-left). If the TCR encounters its cognate antigen in this interaction, CD4 recruits LCK, which phosphorylates the two CD3ζ chains, recruiting ZAP70. ZAP70 is then phosphorylated by LCK, and ZAP70 then phosphorylates LAT. LAT serves to scaffold many interactions, importantly recruiting PLCγ1, which then converts PIP_2 to two intermediates: DAG, activating the RAS pathway, and IP_3, initiating calcium flux. This activation by itself is short-lived without contribution from the co-stimulatory pathway. B7-family ligands, primarily CD80 and CD86, are present on activated APCs, which monomerically bind to CD28 (right-center). Phosphorylation of the CD28 cytoplasmic tail allows for the recruitment of intermediates including GRB2, which complexes with VAV1 and PI3K. VAV1 is also activated by LAT (not pictured) and is important for maintaining calcium flux. PI3K recruits and activates AKT pathway by converting PIP_2 to PIP_3. Other B7 receptors, notably CTLA4, are co-inhibitory. CTLA4 binds B7 ligand with high affinity to prevent interaction with CD28. Upon ligation, CTLA4 also inhibits CD28 co-activation through several mechanisms. Figure created by Timothy McKeithan.

With the many different regions which may bind both membrane-bound and cytosolic proteins in the T-cell, GRB2 and VAV1 activate a plethora of other proteins, some of which will be cursorily mentioned here. Notably, GRB2 and VAV1 phosphorylate PLCG1, which in turn activates the calcium influx pathway via enzymatic cleavage of PIP_3 into inositol triphosphate (IP_3) and diacylglycerol (DAG).[57,58] DAG also activates FYN.[58] Activation of the calcium pathway also eventually phosphorylates NFAT which translocates to the nucleus and has widespread effects on transcription. The guanine exchange factor (GEF) function of VAV1 in particular is important for activation of Ras-superfamily kinases, including RHOA, which are together necessary for essentially all vital function of T-cell biology including actin polymerization, cell motility, global kinase pathway transduction, and global intracellular movement.[59]

Costimulation in T-cell activation[1]

As mentioned above, sustained T-cell activation requires two separate activation steps. The first is through the variable CD3/TCR which is antigen-specific. The other is through one of many invariant pathways. CD3/TCR activation without co-stimulation induces anergy, in which the T-cell is not able to respond to even high-affinity stimulus or proliferate.[60]

Classically, co-stimulation occurs through CD28, the prototypical costimulatory receptor and founding member of the B7 receptor family. *CD28* contains four exons: the first is a trafficking peptide which is cleaved off in final processing; the second contains the entire extracellular domain, which is how ligand interacts with CD28; the third is the transmembrane domain; and the fourth is the cytoplasmic domain. Activated APCs (via cytokine secretion from innate immune cells, among others) increase the expression of

[1] Some parts rely heavily on Rohr et al. 2015 (ref. 122)

B7 family ligands,[61] primarily CD80 (B7.1) and/or CD86 (B7.2). Thus, when activated APCs bind naïve T-cells, T-cells ligate both CD3/TCR and CD28 (see Figure 4).

The intracellular domain is necessary for signal transduction after ligand binding[62] and includes a YMNM motif, which, when phosphorylated, binds the SH2 domains of Src family kinases, PI3K regulatory subunits, and GADS/GRAP2 and GRB2. The CD28 intracellular tail also contains two proline-rich motifs that bind the SH3 domains of various signaling proteins, including ITK, GRAP2, and LCK.[63] The intermediates of CD28 activation further scaffold many of the interactions discussed under "T-cell activation." Together, CD28-mediated PI3K, GRB2, and VAV1 signaling increase NF-κB and NFAT nuclear translocation, augmenting T-cell survival, production of the proliferative cytokine IL-2, and cell cycling.

Activation of both CD3 and CD28 underlies the exquisite complexity of adaptive immunity. The various T-helper subtypes (see "Development and genetics" below) are only specified upon activation.

Members of the B7 receptor family, not just flagship member CD28, have important, overlapping, and competing roles in T-cell signaling. The prototypical competing member is cytotoxic T-lymphocyte antigen 4 (CTLA4) which, like CD28, forms heterodimers.[64] CTLA4 shares high protein homology with CD28 but has some differences that result in major changes of affinity and function.[64-68] First, CTLA4 also binds B7 ligands, but is able to do so at up to 100-fold greater affinity than CD28, both through greater affinity due to primary sequence differences but also because CTLA4 homodimers can bind two B7 ligands whereas CD28, due to steric restraints, can bind only one.[64] In binding ligand better than CD28, CTLA4 prevents the continued transduction of signal thorough CD28. CTLA4 also initiates transendocytosis,[69] in which it wrenches ligand out of the donating cell membrane and endocytoses the ligand/receptor complex for degradation, thereby forcibly preventing further CD28

activation. The inhibition is not only limited to the extracellular interactions; the CTLA4 intracellular domain is unable to bind important intermediates GRB2 and VAV1 and may directly activate or inhibit PI3K/AKT activation upon activation through poorly understood mechanisms.[70,71] CTLA4 can also inhibit CD28 from interacting with intermediates including LCK and FYN.[71,72] However, it is important to note that despite the 20 years that CTLA4 signaling has been studied, many articles directly contradict each other, such that most of these details still need to be fully verified.[73]

Interestingly, the profoundly anti-stimulatory effects of CTLA4 are known to be exploited by many solid tumors;[61] whereas neoantigens normally elicit an immune response, some cancers cause the activation of CTLA4, thereby inhibiting T-cell-mediated immunity against the tumor. Thus “releasing this break” via CTLA4-inhibitory antibodies has proven a powerful method to stimulate anti-cancer immunity.

Another B7 receptor, programmed death 1 (PD1), also has an overall negative effect on T-cell activation and has similarly been exploited for anti-tumor immunity. For PTCLs, PD-1 is of particular interest because it is important for identity and function of the T-follicular helper cell (T_{FH}) as discussed in the next section. Inducible co-stimulator (ICOS) and B- and T-lymphocyte attenuator (BTLA) are also B7 receptors similarly important for T_{FH} function.[61]

Development and genetics of AITL and PTCL, NOS

In order to consider modes of investigation and treatment of these different PTCLs, it is important to understand as much as possible the cellular basis for oncogenesis. Thus, identifying the cell of origin (COO) is a necessary component of further inquiry. Only with the advent of next-generation sequencing (NGS) techniques has the technology existed to accurately examine small, otherwise unidentifiable subpopulations within a heterogeneous lymphoma. Thus, the cell types of origin for various lymphomas, especially PTCLs, have only recently been described. Gene expression profiling (GEP) has been an integral tool to understand COO and biology of PTCLs; the technique is explained under "Next generation sequencing" below.

This section does not serve to review the entirety of our understanding of T-lymphocyte subtype function, but only to highlight the differences between the putative cells of origin of various PTCL entities.

COO: AITL

From extensive GEP analysis of histologically identified AITL cases performed by our group[74] and others[75], the evidence supports the T-follicular helper (T_{FH}) cell as the cell of origin for AITLs. AITLs tend to have a high expression many genes associated with TCR signaling, including subunits of the TCR, CD3 genes, CD4, costimulatory CD28, other B7-family receptors CTLA4, BTLA, and PD-1, as well as many T-cell signaling intermediates.[76] This supports the concept of strong TCR signals as required for T_{FH} differentiation as discussed below, and that continued activation of this pathway would

be necessary for T_{FH}-derived lymphoma to develop. This does not imply that TCR activation is a unique feature of AITLs, however.

T_{FH} cells are resident T-cells of the germinal center (GC) which are necessary for the formation and maintenance of the GC reaction, a hallmark of adaptive immunity in vertebrates. These cells are have surface expression of CD3 subunits and CD4, and are marked with expression of the master transcriptional regulator BCL6 and co-expression of CXCR5, PD1, and ICOS;[77-79] however, there is no universal agreement as to whether "true" T_{FH} cells express all or some combination of these markers, nor is it certain whether cells that express all of these markers are necessarily T_{FH} cells. Thus, for clarity, another requirement – presence in the GC – ensures that T-cells that are likely involved in the GC reaction are known as T_{FH} cells. Cells outside the germinal center are termed "pre-T_{FH} cells" depending on their expression of BCL6, CXCR5, PD1, and ICOS, but because they are not in the germinal center they cannot directly participate in the GC reaction.

Although there is no consensus on the step-wise mechanism of T_{FH} differentiation, there is strong experimental evidence that delineates a significant portion of the origin of the T_{FH} cell. First, antigen-experienced T-cells undergo priming. Naïve T-cells express *positive regulatory domain-containing protein 1* (*PRDM1*), whose product, known as both B-lymphocyte-induced maturation protein 1 (Blimp1) or PRDM1, is important for maintaining homeostasis in inactive T-cells[80,81] and for preventing the T_{FH} transcriptional program[78] (see Figure 5 and Table 3). Upon T-cell receptor (TCR) / cluster of differentiation 3 (CD3) activation, a $PRDM1^{+}CD4^{+}$ T-cell can be exposed to a variety of cytokine microenvironments within peripheral lymphoid tissues. Exposure to interleukins (IL)-21 and/or IL-6, both of which are elaborated by activated immune tissue but especially other T-cells,[82] can induce the expression of *BCL6* via their respective receptors IL-21R and IL-6R, which activate signal transducer and activator of

transcription 3 (STAT3).[83] There is conflicting evidence as to the exact contributions of each of these cytokines to T_{FH} identity, suggesting some or total functional redundancy; however, the loss of both significantly reduces T_{FH} differentiation.[84] It is also possible that T_{FH} cells are in fact first polarized towards the T_H2 or T_H1 lineages, then afterwards towards T_{FH}; see "T_H2" under "PTCL, NOS" below. Either way, in these primed, newly *BCL6*-expressing $CD4^+$ T-cells as in *BCL6*-expressing B-cells, mRNA does not necessarily lead to protein translation in B-cells,[85,86] likely indicating an additional, as-of-yet unidentified selection measure for determining T_{FH} identity versus other T_H subsets.

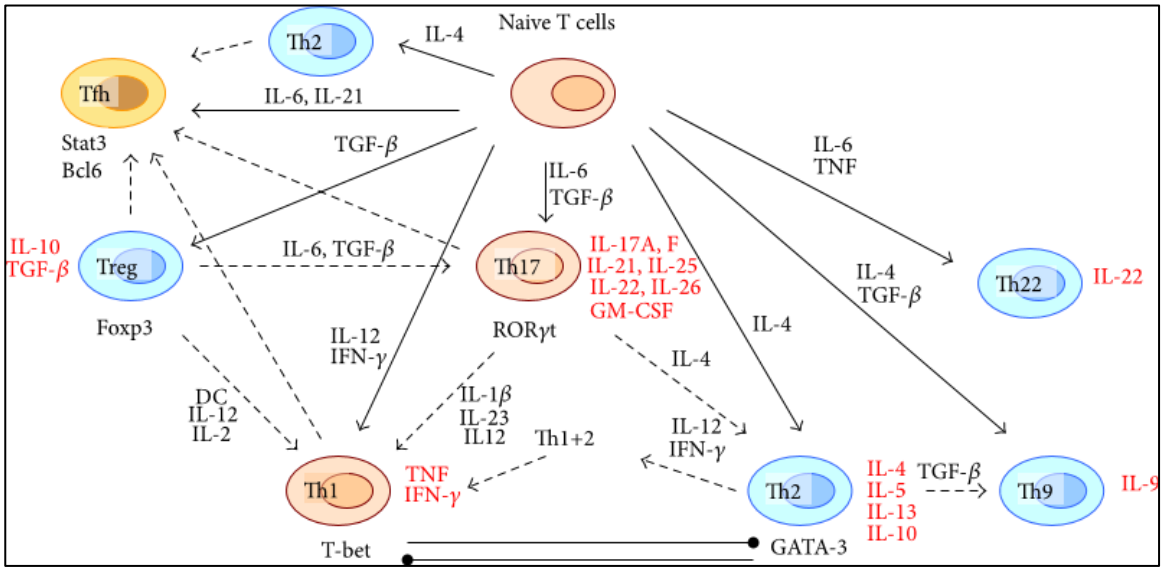

Figure 5. Simplified scheme of T-cell differentiation pathways and plasticity (dashed arrows). Secreted cytokines are listed in red.[87] Reprinted with permission.

Once translated, BCL6 in turn represses *PRDM1* and master regulators of other T_H subtype identity: *TBX21*, *GATA3*, *RORγT*, and *FOXP3*, which control T_H1, T_H2, T_H17, and Treg transcriptional identities, respectively.[78] BCL6 also leads to the upregulation of the chemokine receptor *CXCR5*, likely very early because BCL6 levels correlate well with CXCR5.[82,88,89] CXCR5, with concomitant loss of chemokine receptor CCR7, allows these "pre-T_{FH}" cells to home to follicles, where they can interact with antigen-presenting

dendritic cells (DCs) as well as B-cells.[90,91] Chemokine CXCL13 serves as the specific ligand for CXCR5 and is expressed primarily by professional antigen-presenting cells (APCs). Expression of inducible co-stimulator (ICOS), a B7-family co-stimulatory molecule, by the $BCL6^{+}CXCR5^{+}$ T-cells is required to at the time of DC priming to set the stage for germinal center formation, and DCs express the ICOS ligand, ICOS-L.[83,92] Although a DC-dependent phase is necessary for robust T_{FH} development, the T-DC interactions appear to be transient and must be replaced by T-B interactions for prolonged T_{FH} function.[77,93] High-affinity TCR interactions with APCs, especially dendritic cells, generate more T_{FH} cells as well.[94]

	T_H1	T_H2	T_{FH}
Cytokines to induce	IFNγ, IL-12	IL-4	IL-6, IL-21
Signal transduced through	STAT1, STAT4	STAT6	STAT3
Primary transcription factor	TBX21	GATA3	BCL6
Cytokines produced	IFNγ, TNFα	IL-4, IL-5, IL-13, IL-10	IL-21
Primary cellular cross-talk	NK cells, macrophages, CD8+ T-cells	B-cells, mast cells, eosinophils, basophils	B-cells, follicular DCs

Table 3. Relevant T-helper subtype characteristic identities. The prototypical inducing cytokines, signal-transducing intermediates, transcription factors, evolved cytokines, and primary cellular interactors are shown for the T-helper 1 (T_H1), T-helper 2 (T_H2), and T-follicular helper (T_{FH}) cells.

Other transmembrane proteins appear to be involved in early T_{FH} function but with a less clear mechanism. Expression of CD28, the canonical T-cell co-stimulatory molecule and member of the B7 family, is necessary for the formation of T_{FH} cells; CD28-null mice do not develop germinal centers,[95,96] likely because they lack T_{FH} cells. However, CD28 ligation has not been found to be necessary for T_{FH} development at any

specific stage. Because of its primacy in early signal transduction through the TCR/CD3 complex, it seems likely that CD28-null mice cannot have sufficiently high T-cell activation to generate T_{FH} cells. Similarly, OX40, a member of the tumor necrosis factor receptor family, is important for primed T-cell survival and can induce CXCR5 expression,[97] but OX40-null mice have near-normal GCs and normal T_{FH} cell populations,[98,99] suggesting a non-necessary role.

Once T_{FH} cells find their cognate B-cells, the germinal center takes shape. BCL6 is even more upregulated in T_{FH} cells during the GC reaction.[78] High levels of CXCL13 expressed by FDCs as well as ICOS-L in FDCs and B-cells are required to maintain the follicular localization of T-cells, and a lack of ICOS on the T-cells or ICOS-L on B-cells prevents these T-B interactions.[98] Robust ICOS stimulation leads T_{FH} cells to upregulate production of IL-21, which positively signals to the neighboring B-cells, creating a positive feedback loop.[76] This ICOS-mediated signaling can also be modulated downstream: mutations which decrease the activity of Roquin, an mRNA-binding protein which degrades ICOS mRNA, increase ICOS signaling and therefore T_{FH} differentiation and function as well as increase GC size.[100-102] T_{FH} cells are the major control for GC B-cell differentiation, through which B-cells undergo class switching and become long-term antibody-secreting plasma cells, via direct (OX40, CD40L) and indirect (IL-4, IL-21) mechanisms.[76]

Other transmembrane proteins also take on important roles at the germinal center stage, notably of the B7 family. In addition to CD28 and ICOS, PD1 is upregulated dramatically as T-B interactions increase in strength and both T and B compartments continue to expand clonally. PD-1/PD ligand 1 interactions between T and B cells are required for GC B-cell differentiation and activity as well as T_{FH} activity.[103] T-cells co-expressing PD-1 and CXCR5 are the prime representatives of active germinal center T_{FH} cells. Another B7 family member, B- and T-lymphocyte attenuator (BTLA), is

upregulated on T_{FH} cells during the germinal center reaction and is probably involved in decreasing co-stimulation through overall negative regulation on CD28,[104] although what exactly it does has not been completely assessed in relation to T_{FH} cells specifically. The strongest ligand of BTLA, herpes virus entry mediator (HVEM), mediates a multifactorial inhibition[105] of unclear significance in T_{FH} function.

It is important to note that despite the fairly detailed understanding of how T_{FH} cells are generated, there exists no model which generates T_{FH} in vitro that can retain their function. By the same note, there is not an AITL model available that recapitulates the unique architecture of the disease or even is a phenotypic T_{FH} cell. This has 1) hindered research in T_{FH} function, and 2) hindered research in AITL specifically.

COO: PTCL, NOS

GEP studies have also suggested that PTCL, NOS are also derived from T-helper subsets.[74,106] Our group has shown that expression of the T_H1-specific signature associated with TBX21 (historically known also as T-bet) or the T_H2-specific signature associated with GATA3 transcription factors delineate distinct groupings of PTCLs by prognosis and active genes. The canonical T-helper subset functions have been explored for the better part of 30 years, and as such it is much more convenient to consider the current understanding in review rather than by the multitude of original studies.[76,87,107,108]

T_H1 polarization is induced by exposure to interferon gamma (IFNγ) and IL-12, both of which are elaborated primarily by dendritic cells as well as natural killer (NK) cells. Signaling through IFNγ and IL-12 receptors activates STAT1 and STAT4, which induce the expression of *TBX21*. TBX21 upregulates the production of IFNγ and tumor necrosis factor (TNF)α, leading to a Type I-polarized positive feedback loop through both

autocrine and paracrine mechanisms, as well as supporting its own transcription. TBX21 also suppresses *GATA3*, *RORγT*, *FOXP3*, and *BCL6*, thereby inhibiting polarization towards the other T-helper lineages. The Type I response increases the proliferation and function of $CD8^+$ cytotoxic T-cells, macrophages, and natural killer cells, among others, thereby preventing the spread of primarily intracellular pathogens, e.g. viruses, as well as bacterial infection. IFNγ is also directly implicated in stimulating the release of immunoglobulin (Ig)G antibodies from B-cells, which increases macrophage function via pathogen opsonization.

T_H2 polarization, however, is induced by exposure to IL-4, which initially is released from other activated T-cells, eosinophils, basophils, mast cells, and dendritic cells. The IL-4 receptor phosphorylates STAT6, which then upregulates *IL4* as well as a number of other genes, including the master transcription factor of T_H2 identity, *GATA3*. With IL-4 inducing a feed-forward loop, GATA3 suppresses the other T-helper transcription factors, further upregulates itself and *IL4*, and upregulates *MAF* (whose product, c-MAF, is another, but less lineage-specific, transcription factor). Upon interaction with other Type II effector cells – the aforementioned basophils, eosinophils, and mast cells – T_H2 cells elaborate IL-5 and IL-13, migratory, maturational and proliferative signals for the Type II cells. Also elaborated is IL-10, a potent suppressor of T_H1 activity and a mild attenuator of all T-cell function. This response is associated with multicellular infections such as helminths, and is necessary for sustained B-cell stimulation, antibody production, and antibody class switching. Because of the necessity of T_H2 function for antibody-mediated immune function, the Type II response is of particular interest in autoimmune disease and allergy.

Because of the T_H2 activity on B-cells, it has been hypothesized that T_{FH} cells may be derived from T_H2 cells.[76] This is supported by the relative high levels of IL-4 within peripheral lymph organs, a result of resident dendritic cells as well as activated migratory

T-cells. Further, T_H2 cells are already primed to interact with B-cells whereas T_H1 cells are not, also supporting the notion of a close relationship between the T_{FH} and T_H2 phenotypes. Therefore, activated T-cells in lymph organs may be first polarized towards T_H2, and only with the addition of IL-21 and/or IL-6 stimulation at the appropriate time is *BCL6* upregulated and the T_{FH} program activated. This could also partially explain why some *BCL6*$^+$ cells do not become T_{FH} cells; they are already T_H2-polarized, and the exposure to T_{FH} cytokines cannot overcome this effect, so *BCL6* is thereafter downregulated. However, others have found that although T_{FH} cells may elaborate and respond to IL-4, the increase in IL-4 production is independent of the known T_H2 mechanism,[89] suggesting T_H2 independence. At the same time, a recent study has found that murine activated T-cells in T_H1-polarizing growth conditions *in vitro* express both *Bcl6* and *Tbx21* in an IL-12-dependent manner, and only after prolonged culture is the T_H1 identity set and *Bcl6* downregulated,[109,110] suggesting a T_H1-T_{FH} intermediate that only afterwards is specified; this was replicated *in vivo* by exposure to toxoplasma. Either way, it is likely that the "traditional" cytokine-mediated T-helper subtype specification in Table 3 and Figure 5 misses very important complexities.

One other T_H subset, the regulatory T cell (Treg), deserves special mention here because of its canonical function. Identified by expression of the transcription factor FOXP3, Tregs profoundly suppress other T-cell function through expression of suppressive cytokines IL-10 and TGFβ, and through direct interaction.[107,108] Tregs are present throughout the peripheral lymph system and are often found adjacent to active lymph tissue. Thus, in order to develop into cancer, T-cells likely somehow escape the suppression caused by Treg cells. This mechanism is unclear, but both AITL and PTCL, NOS have perturbed Treg compartments. AITL cases tend to have fewer intranodal Tregs than normal tissues, and those cells that are there show a resting, e.g. inactive, phenotype.[111] In fact, there is an example of a FOXP3-high PTCL, NOS which was

quickly fatal.[112] Therefore, T-cell lymphoma cells must be altering other T-cell compartments, but how is not yet understood.

Type I and Type II immune activation (mediated by T_H1 and T_H2 cells, respectively) have historically been discussed as mutually exclusive. The last fifteen years of work, however, has demonstrated not only many more transcriptionally and phenotypically distinct helper-T classes, including T_{FH} cells as discussed above plus T_H17, T_H9, and T_H22, which all interact to create the classically described types of activation.[87,107,108] There is great plasticity between the different subsets, though T_H1 and T_H2 identities are thought to be relatively stable because they have built-in positive feedback loops to maintain the current polarization and inhibit all other helper lineages (see Figure 5). This transcriptional flexibility has been found to be important for maintaining a variety of disease states and their animal models, suggesting that this plasticity may play further roles in T-cell lymphoma development that have not yet begun to be explored.

Next-generation sequencing: new frontiers in PTCL research

Only with the advent of next-generation sequencing (NGS) has the search for the genetic underpinnings of PTCLs begun to come to fruition. There are three significant bottlenecks in obtaining meaningful sequencing data, and we will discuss each in relation to PTCLs.

First chokepoint: the sample itself. The greatest initial challenge in searching for genetic events in PTCLs has been the rarity of samples. Pathologists and oncologists from multiple institutions working together to maximize sample collection, such as the members of the Leukemia/Lymphoma Molecular Profiling Project (LLMPP), has gone a long way to facilitating the sharing of samples and data.

Even then, collecting biopsies with enough residual tumor to get sufficient DNA has been problematic; as discussed in "Pathologic characteristics," T-cell lymphoma cells tend to not grow in easy-to-separate clumps but be infiltrative, surrounded by normal and reactive tissues including normal T-cells. Obtaining a 100% pure cancer sample, much less a 75% cancer sample, is therefore nigh on impossible, unlike in solid tumors or even some B-cell lymphomas which grow in sheets.[4] In sequencing studies, these samples are considered to have low "tumor content." Consider that it is relatively simple to obtain a high-purity population of neoplastic cells from solid tumors or different types of leukemia, either by excising part of the tumor or by collecting circulating neoplastic cells from blood. For these, a relatively high proportion of the assayed nucleic acids will come from the neoplasms; one refers to these samples as having high tumor content. In the case of almost every PTCL subtype, neoplastic cells and normal cells exist side-by-side in affected organs, and it is difficult to effectively distinguish them by histology. Excised tissues, therefore, may have extremely varied, but often quite low, neoplastic contributions. Further, PTCLs generally do not have a leukemic phase in which large numbers of neoplastic cells are released into the blood,[4] so harvesting peripheral blood mononuclear cells (PBMCs) has even a lower likelihood of collecting neoplastic cells for analysis.

Tissue processing is the next complication. Biopsies for routine pathologic practice are formalin-fixed and paraffin-embedded (FFPE) before sectioning and staining; the fixation process leads to severe DNA fragmentation and damage and therefore sequencing artifacts, mostly C>T|G>A, thought to be due to cytosine deamination during formaldehyde removal.[113] Storing biopsies "fresh frozen," by flash freezing and embedding in a polyethylene glycol / polyvinyl alcohol-based medium (OCT; "optimal cutting temperature"), prevents this potential problem. However, this method is more labor-intensive, more expensive, less useful in standard pathology lab practice, and

requires long-term storage at -80 degrees Celsius or in liquid nitrogen, all of which put this method beyond what most lab practitioners and institutions are willing and able to do on a regular basis. In the past five years, technological developments including commercially available, kit-based techniques have been optimized for the extraction of FFPE DNA or RNA, significantly decreasing artifactual reads and increasing overall quality of sequencing output.[114] This not only increases the use of new cases, but also opens up archival tissue to sequencing examination. Other storage-related problems can arise, e.g. if the sample has become too oxidized, DNA quality may be too low to use,[114] but many archival tissues will still be able to be extracted for sequencing.

It is important to note that PTCLs as opposed to other cancers have additional issues raised during sequencing. When performing sequencing studies, usually a normal, non-cancerous tissue from the same patient is sequenced as a control to determine whether any variants found are germline, e.g. not cancer-specific, or somatic, mutations in the cancer. For historic PTCL cases, no normal was ever taken, and even in the sequencing era cases often do not have corresponding normal tissues. Thus, it is harder to call a variant somatic without something to which it can directly compare. Prospectively, normal tissue, in the form of swab of unaffected skin or nucleic acid extracted from peripheral blood, can be collected, but it is difficult to ensure that standard collection practices are followed when the samples come from all over the world. In this study, no cases have corresponding normal tissues to which mutant calls can be compared, but variant frequency can serve as a partial surrogate; if the variant frequencies (VF; described below) approximate 50% or 100%, the variant is likely to be in all of a single or both alleles, and is possibly germline. However, for most of these cases, VF is much less than 50%, indicating a heterogeneous population, some of which contain a mutant allele; the most likely cause is if the mutation is somatic.

Having obtained tumor samples of high quality, either DNA or RNA (or both), the next bottleneck has been in the actual sequencing techniques. Consider the time and cost of sequencing an entire human genome in 2000, when the first genome was completed: 10 years, nearly $100,000,000. This cost was from using Sanger sequencing, and from paying all the man-hours to sequence and analyze.[115] The Sanger method uses serial addition of dideoxynucleic acids which can be incorporated into a growing DNA strand but cannot serve as a substrate for elongation.[116] Four reactions were performed, one for each of the dNTPs, resulting in four tubes each with a multitude of chains of different lengths. The chain-terminated sequences were sequentially loaded into a polyacrylamide-urea gel and separated by electrophoresis. Thus, a user could quickly read through short segments when developed, e.g. by radiography. This method is for the most part accurate, but has several problems, including that it only sequences any given base one time, it is problematic in repetitive sequences, resolution of single bases may be difficult depending on the imaging platform, and it is incredibly labor-intensive. Capillary-based Sanger sequencing machines allowed unattended sequencing while ensuring multiple rounds of coverage over the same bases, increasing accuracy dramatically and bringing the maximum number of bases sequenced per day up to approximately 115 kilobase pairs (kbp; 115,000 base pairs), which is what was in use by the end of the completion of the Human Genome Project.

To combat the problems that Sanger sequencing could not overcome, as well as increase the throughput of sequencing studies, massively parallel sequencing (MPS) / next-generation sequencing (NGS) techniques were developed in the first decade of the 21st century. Several commercially available machines exist but they all have many similarities.[115,117] This study uses whole-transcriptome sequencing (WTS)/RNASeq and targeted sequencing, so these two modalities will be discussed here. Simultaneous

reading allows for much greater depth, or number of times a given base is read, decreasing error. It also allows for a greater number of base pairs to be read with no bias – the Illumina HiSeq X10 can read up to $1.8x10^6$ kbp,[118] an approximate 15 million-fold increase over what was in use in the year 2000. Sequencers also include a quality value for every base, which is the sequencer's estimate in confidence of the read given the values of the other bases not called.

For most WTS analyses[117] including the one used here, "library preparation" occurs first, in which polyadenylated mRNAs are isolated and converted to complementary DNA (cDNA), and broken into small fragments with an approximate median of 50-150bp. During library preparation, adaptors are ligated, and cDNA with adaptors are selected. An additional "barcode" may be ligated between the adaptor sequences and the target to run multiple sequences together. Adaptor-ligated fragments are then bound in solid state, e.g. to a plate or flow cell, and the cDNA may be amplified by a high-fidelity polymerase. Finally, the fragments are sequenced, though by what mechanism is dependent upon the machine.

The WTS in this study was performed on an Illumina GIIx machine, which uses the standard Illumina library preparation as described in the preceding paragraph. The amplification step, called "bridge amplification," ensures that there is enough substrate to allow the optical system to "see" each base when added and relies on segments complementary to the adaptors already adhered to the flow cell. This innovation allows less input (as low theoretically as a few nanograms) of sample, and increases the likelihood of accurately identifying rare sequences, but also introduces potential false reads due to polymerase error. The bridge amplification process creates "clusters" of identical sequences physically close together on the flow cell. The clusters are then repeatedly run and detected by the machine, completely eliminating humans from the actual sequencing steps. When run, the flow cell is flooded with fluorescently labeled

DNA bases which have a blocking group on the 3' end of the base, preventing additional incorporation of other bases. Once bound, the clusters are read by the fluorescent tag on the newly-incorporated base. The tag is then cleaved, and the blocking group is chemically substituted with a hydroxyl group, allowing each strand to incorporate a new base on the next run.

We also perform targeted exome sequencing,[119-121] which employs a different capture technique than WTS. For this study, cDNA was PCR-amplified by multiple primers targeting each exon, and the amplicons were sequenced as described above. This method allows incredible depth of the targets of interest, but can introduce PCR errors which are then amplified during processing.

The ability to generate all these sequences has been a boon to PTCL research (and all genetics), but it has also generated problems with copious volumes of data. Raw sequencing files vary wildly in size due to the type of sequencing performed, the amount of primary sample input, and the depth of sequencing. Quality data are also included within the file and can double or triple the file size. And one does not usually sequence a single case by itself when looking for cancer-causing changes; dozens to hundreds of cases are included in a single run. For many, sheer storage can become a problem. Further problematic is the amount of space required to analyze data as described below. Processing can tie up even good computers for extended periods of time, which is decreased by the use of cloud computing so that many of the calculations can be done on a separate server.

Sequencing data must go through several steps before meaningful results are available, and each step of processing can employ one or more of dozens of available algorithms, which may lead to discrepancies even when different groups use identical sequencing data. For PTCLs, our group has developed its own analysis

pipeline,[74,106,122-124] which specifically is used for our high- and low tumor-content samples.

First, low-quality reads are eliminated from further processing to decrease strain and time. Then, the raw reads must be aligned to the reference sequence: for humans, the most recent public version of the Human Genome Project is usually used. Once aligned, differences from references are then called; in cancer, these are putative mutation sites. However, it is important to note that single nucleotide polymorphisms (SNPs), which are classified as differences from reference in 1% of the population or greater, will be found in mutation calling because they differ from reference. Considering their high frequency, most sequencing studies looking for novel mutations, including the present work, filter out SNPs at this stage using the dbSNP database maintained as part of the Human Genome Project.

Once mutations are called, further analysis can be performed to help decide whether the putative mutations have significant effect on the product. That is, for proteins, the putative substitution can be assessed automatically for likelihood to be functional, deleterious, or neutral. For non-coding RNAs assessed through cDNA, mutations which affect seed site or other binding site can potentially be assessed, though the tools to do this well are still in development.

Finally, though, the end user has to decide whether a mutation is likely relevant by themselves, and to verify some of the mutations by separately performing PCR and Sanger sequencing.

One major use of RNASeq that is not for mutational analysis is gene expression profiling (GEP)[74,106,117] when cDNA is used as the input. GEP can be performed by array, wherein unique probes are bound to individual microwells of a chip, cDNA is loaded onto the whole chip, and the probes hybridize to their specific complementary cDNA segments during processing. The binding is read by degree of fluorescent or

chemiluminescent output, and therefore is a semi-quantitative measure of each individual target. NGS can do the same thing *in silico*: numbers of reads of any transcript can be found and therefore compared proportionally to other samples. Unlike an array-based GEP, sequencing does not rely on pre-made probes, making RNASeq able to find any transcript, not just what is pre-loaded into the array. However, amplification procedures can artificially alter the ultimate expression levels due to bias in the amplification or sequencing process.

Known mutations in PTCL, NOS and AITL

The first discovered set of mutations, and among the most frequent in PTCLs, affect genes which alter epigenetic stability. These are primarily loss-of-function mutations in TET2 and DNMT3A, and a gain-of function mutation of IDH2.

Ten-eleven translocase 2 (a.k.a. Tet methylcytosine dioxygenase 2; TET2) has at least one loss-of-function (LOF) mutation in approximately 80% of PTCL cases[122,123,125-129] and catalyzes the conversion of 5-methycytosine (5mC) to 5-hydroxymethylcytosine (5hmC), the first step in cytosine demethylation. In promoter regions, methylated cytosines in CpG islands (CG dinucleotides) repress transcription; TET2 catalyzes, therefore, the first and rate-limiting step in preventing an abnormal global accumulation of 5mC. Mutations found in PTCLs usually lead to a loss of TET2 function, either by premature translational arrest and nonsense-mediated decay or loss of catalytic activity. Either event is expected to prevent demethylation and thus effect global hypermethylation. This has indeed been found to be true in TET2-mutated murine leukemia models[130] as well as in primary TET-mutated glioblastoma[131] and acute myeloid leukemias (AML).[132] Unfortunately, it has been difficult to assess the contributions of TET2 mutation in PTCL for several reasons. First, as described above,

the incidence of PTCLs is overall much lower than that of either glioblastoma or AML, leading to a lack of primary tissues. Even more importantly, PTCLs often have much lower tumor content than samples of the other cancers, likely masking less striking specific epigenetic changes. TET2 mutations are particularly interesting because homologs with the same function, TET1 and TET3, are also mutated in myeloid leukemias[133] and gliomas[131] and often mutually exclusively from TET2, but never in PTCLs. Why exactly this is the case is unclear.

One additional layer of complexity with TET2 is that it is mutated fairly frequently in the general population without hematologic malignancy as well, with approximately 2.0%-3.5% carrying at least one hematologic malignancy-related somatic mutation including TET2.[134,135] This suggests that TET2 mutations may serve as the founding changes for a wide variety of malignancies. In reference to lymphopoiesis, it suggests that the thymocytes may already have TET2 mutations; therefore, even PTCLs may have predisposing mutations before maturation.

DNA methyltransferase 3A (DNMT3A) is mutated in about 30-40% of PTCL, NOS and AITL, but usually only in cases that have TET2 mutations as well.[123,129,136] It catalyzes *de novo* CpG methylation, thereby decreasing transcription of affected genes. Its mutations almost exclusively occur in the methyltransferase domain and lead to a loss of methyltransferase function.[137] Thus, its mutations would be expected to lead to global hypomethylation, or at least hypomethylation of genes that should be silenced. DNMT3B, a family member with unique functions, is not found to be mutated in PTCLs, nor is it mutated in other malignancies either.

Isocitrate dehydrogenase 2 (IDH2) is found to be mutated in approximately 30% of AITLs and only rarely in PTCL, NOS.[123,138] It is an enzyme of the Krebs cycle which converts isocitrate to α-ketoglutarate (α-KG). Unlike the other enzymes above, IDH2 is mitochondrial. Also unlike the other enzymes, IDH2 mutations occur at a single codon,

arginine 172, mutated usually to either serine or lysine, and these mutations are gain-of-function (GOF), rather than LOF. Mutant IDH2 gains additional catalytic activity, converting isocitrate to 2-hydroxyglutarate (2-HG) in addition to α-KG. 2-HG cannot be used in subsequent steps of the Krebs cycle, so it diffuses out of the mitochondria and into the nucleus, where it directly interferes with 5mC-5hmC conversion by TET2 by competing with α-KG, a cosubstrate in the enzymatic reaction. It similarly inhibits several other dioxygenases, including a number of lysine demethylases.[139,140]

Interestingly, IDH2 mutations in AITL occur almost exclusively in the background of TET2 mutations, whereas in AML[132] and gliomas,[141] IDH2 mutations are mutually exclusive from TET2 mutations. Similarly, both AML and glioma may have IDH1 or IDH2 mutations, and they are mutually exclusive, whereas in AITL, only IDH2 is mutated. Further, leukemias and gliomas have two hotspots for IDH2 mutations – R140 and R172 – whereas PTCLs only appear to have the latter. Our group has recently attempted to delve into the specific mechanisms of IDH2 mutation on T-cell function and found epigenetic alterations on several T-cell-specific genes[123] that may contribute to the pathogenesis of AITL.

The most unexpected recent addition to the PTCL mutation spectrum is in RHOA, the flagship member of the RHO GTPase superfamily. Approximately 53-70% of AITL cases and 20% of PTCL cases have identical mutations at glycine 17, mutated to valine or less frequently glutamate.[123,125,127,128] These mutations appear to occur exclusively in the background of TET2 mutation. RHOA and its close family members are central to a host of cellular processes, including signal transduction, cellular migration, calcium homeostasis, and mitosis, among others. The G17V mutation has been studied *in vitro* and in non-T cells.[125,127,128] The substitution of glycine 17 prevents the G-box, the domain responsible for stabilizing guanine nucleotide, from binding guanine. Therefore, RHOA G17V cannot bind GTP or GDP and therefore cannot perform any of its effector

functions. Further, through mechanisms not entirely clear (though there are some hypotheses: see “Discussion”), the RHOA mutant prevents WT RHOA from its effector functions, including binding of GTP and formation of stress fibers. RHOA G17V mildly augmented Jurkat T-cell proliferation as well.

Considering the importance of the TCR pathway to PTCL maintenance from the GEPs, it follows that mutation of members of this pathway which could be relevant to lymphomagenesis and cancer progression. Interestingly, few mutations have been reported. One study shows a few mutations in FYN,[125] which have not been reported since; another shows a mutation in VAV1, and a few in CD28;[128,142] and yet a third study finds single case of a fusion between *ITK* and *SYK*,[143] two kinases important in early TCR transduction (see “CD4+ T-cell activation cascade”). However, none are well-characterized. Other studies have also found high expression platelet-derived growth factor receptor α (PDGRFA) without mutation,[144] and relatively frequent mutation of phospholipase C γ-1 (PLCG1),[145,146] both of which can increase TCR/CD3 activation responsiveness, though these findings have not yet been replicated in any other patient population or sequencing dataset.

With this understanding of the current state of research in peripheral cell lymphomagenesis, this thesis delves into mutation and activation of the CD28 co-stimulatory pathway in PTCL, NOS and AITL.

CHAPTER 1: MATERIALS AND METHODS

Patient specimens

The clinical and pathological characteristics of the patients included in the study have been published[106,122,123] and are included in Table 4 below. We included 20 molecularly diagnosed AITL lymphomas for transcriptome sequencing in our study and 85 additional cases of molecularly and/or histologically diagnosed AITL, PTCL-NOS, and ALK-negative ALCL. This study was approved by the Institutional Review Boards of the University of Nebraska Medical Center and City of Hope National Medical Center.

Case	Disease	Sex	Age	Time	Status	CD28.call	CD28mut	TET2	RHOA
001	AITL	Female	76.51	2.90	1	0		0	1
002	AITL	Male	76.68	4.66	0	0		1	1
003	PTCL	Female	66.52	5.81	1	0		0	0
004	PTCL	Male	49.73	0.46	1	0		1	1
005	PTCL	Male	97.36	0.04	1	0		0	0
006	PTCL	Male	64.55	0.04	1	0		0	0
007	PTCL	Female	70.28	3.12	1	0		1	1
008	PTCL	Male	68.67	1.46	1	0		0	0
009	ALCL.neg	Male	64.11	0.84	1	0		0	0
010	AITL	Male	58.03	0.66	1	1	T195P	1	1
011	PTCL	Female	75.26	8.70	0	0		0	0
012	PTCL	Female	78.89	1.33	1	0		0	0
013	PTCL	Male	66.25	4.28	0	0		0	0
014	PTCL	Male	80.92	0.59	1	0		1	0
015	AITL	Male	40.34	14.96	0	0		0	0
016	AITL	Male	40.46	3.85	0	0		1	1
017	PTCL	Female	74.52	0.09	1	0		0	0
018	AITL	Female	74.76	6.92	0	0		1	1
019	AITL	Male	66.63	2.21	0	1	D124E	1	1
020	AITL	Female	65.99	1.17	0	0		0	0
021	AITL	Female	64.39	1.02	0	0		1	1
022	PTCL	Female	54.67	2.88	0	0		1	1
023	AITL	Male	65.49			0		1	1
024	AITL	Male	68.07	6.34	0	0		1	0
025	AITL	Male	63.00			0		1	0

026	PTCL	Male	19.37			0		0	0
027	AITL	Female	52.19	3.83	0	0		1	0
028	AITL	Female	74.54			0		1	0
029	AITL	Male	45.44			0		1	0
030	PTCL	Female	72.14	4.31	0	0		1	0
031	AITL	Female	73.58	0.07	1	0		1	0
032	AITL	Female	69.31	0.20	0	0		1	0
033	AITL	Male	33.30			0		1	0
034	AITL	Male	59.22			0		0	0
035	PTCL	Male	33.77			0		1	1
036	AITL	Female	79.95	0.01	0	0		1	0
037	AITL	Male	63.43	0.44	1	0		1	1
038	AITL	Male	52.90			0		1	0
039	AITL	Male	66.95			0		0	1
040	PTCL	Female	68.70			0		1	1
041	AITL	Male	60.84	0.74	0	0		1	1
042	AITL	Female	67.93			0		1	0
043	AITL	Female	47.50	0.52	0	0		1	1
044	PTCL	Male	65.23			0		0	0
045	PTCL	Male	65.23			0		0	0
046	PTCL	Male	27.92			0		0	0
047	AITL	Male	69.33	2.25	1	0		1	1
048	PTCL	Female	73.52	7.92	1	0		1	1
049	AITL	Male	68.07	0.32	1	1	T195P	1	1
050	AITL	Female	57.83	0.77	1	0		1	1
051	AITL	Male	44.10	3.06	0	0		1	1
052	AITL	Female	58.86	0.25	1	0		1	1
053	PTCL	Male	51.05	0.92	1	0		0	0
054	PTCL	Male	76.02	1.26	1	0		1	1
055	PTCL	Male	69.52	2.30	1	0		1	1
056	PTCL	Male	63.72	4.52	1	0		1	0
057	AITL	Male	82.13	0.62	1	0		0	1
058	AITL	Female	51.55	11.85	0	0		1	0
059	ALCL.neg	Male	58.72	0.03	1	0		0	0
060	ALCL.neg	Male	39.94	0.10	1	0		0	0
061	ALCL.neg	Male	48.66	3.04	1	0		0	0
062	ALCL.neg	Male	48.66			0		0	0
063	ALCL.neg	Male	30.86	0.08	1	0		0	0
064	ALCL.neg	Female	89.45	0.07	1	0		1	0
065	ALCL.neg	Male	77.84	2.47	1	0		1	1
066	ALCL.neg	Male	78.27	0.09	1	0		1	0
067	ALCL.neg	Male	59.82	0.79	1	0		0	0
068	ALCL.neg	Male	77.01	3.57	0	0		0	0

069	PTCL	Male	58.33	2.11	1	0		0	0
070	PTCL	Male	75.00	10.48	0	0		1	0
071	PTCL	Male	61.40	6.33	0	0		0	1
072	PTCL	Female	46.51	0.97	1	0		1	0
073	PTCL	Female	62.38	8.66	0	0		0	0
074	PTCL	Female	59.26	5.19	0	0		0	0
075	PTCL	Male	29.42	1.08	1	0		1	1
076	PTCL	Male	63.09	2.45	1	0		0	0
077	PTCL	Male	54.50	5.57	0	0		0	0
078	PTCL	Female	55.90	0.57	1	0		1	0
079	PTCL	Male	74.28	0.62	1	0		0	0
080	PTCL	Female	67.55	18.40	1	1	T195I	1	1
081	PTCL	Male	83.69	0.29	1	0		1	0
082	PTCL	Male	66.76	0.52	1	0		0	0
083	PTCL	Male	75.29	1.49	1	0		0	0
084	PTCL	Female	88.08	2.55	0	0		1	1
085	PTCL	Female	62.86	0.75	1	0		1	0
086	AITL	Female	87.23	0.06	1	1	D124E;T195P	1	1
087	AITL	Male	51.00	0.20	1	1	D124V	1	1
088	AITL	Female	55.00	1.85	1	0		1	1
089	AITL	Female	69.82	2.15	1	1	T195P	1	1
090	PTCL	Female	81.71	14.79	1	0		**0**	1
091	ALCL.neg	Female	78.00	0.60	1	0		1	0
092	AITL	Male	78.00	0.07	1	0		1	1
093	AITL	Female	68.00	2.21	0	0		1	1
094	AITL	Male	48.00	0.27	1	0		1	0
095	AITL	Male	72.00	2.40	1	0		0	1
096	PTCL	Male	53.00	2.03	1	0		0	1
097	AITL	Male	69.03	2.29	1	0		0	0
098	AITL	Female	73.20	5.93	1	0		0	0
099	AITL	Female	72.96			0		0	1
100	AITL	Female	63.00			0		1	0
101	AITL	Female	77.00			0		0	0
102	AITL	Male	49.00			0		0	0
103	AITL	Female	59.00			0		1	0
104	AITL					0		1	1
105	AITL					0		0	0

Table 4. Clinical characteristics of patients in this study. Legend on next page.

Table 4. Clinical characteristics of patients in this study. Gender, age at diagnosis, follow-up information, and CD28, TET2 and RHOA mutation status are indicated for the 105 cases of AITL, PTCL-NOS, and ALK-ALCL in this study. For follow-up status, 1 = deceased. For mutation status, 1 = present.

Patient RNA and targeted exome sequencing

RNAs were extracted from the AITLs using the QIAgen RNEasy kit and analyzed by high-throughput RNAseq using the Illumina GIIx sequencer. TopHat[147] was used for alignment, and Cufflinks[148] was used for gene expression analysis. TopHat-Fusion[149] was used to analyze aberrant transcripts. TopHat uses Bowtie[150] as an alignment engineer. Gene expression levels were calculated by Cufflinks/Cuffnorm v2.2.1 relative to the median of all samples. To normalize to the T-cell signature,[74,106] the mean FPKM values for the nine T-cell-specific genes CD2, CD3D, CD3E, CD3G, CD3Z (CD247), CD5, CD7, ZAP70, and LAT were calculated for each cancer sample and normal control. Then, the CD28 FPKM value was divided by the mean nine-gene normalization factor and multiplied by 100%. For targeted sequencing, we used the TruSeq Custom Amplicon (TSCA) platform (Illumina, Inc.) to interrogate all four exons of CD28, all eleven exons of TET2, and all five exons of RHOA in PTCL specimens. The TSCA approach allows sequences >600kb and up to 1,536 amplicons in a single multiplex reaction. The integrated indices support sequencing up to 96 samples per MiSeq run (Illumina). Alignment was performed with Mutascope,[151] which takes advantage of the fixed start/end coordinates in amplicon sequencing to improve alignment. VarScan2[152] was used to call variants.

Gene expression profiling (GEP) and gene set enrichment analysis (GSEA) were performed as described comparing CD28 WT AITL cases to AITL cases with high-variant frequency D124 or T195 mutations. There were 178 differentially expressed genes found. Gene sets are described in Figure 15.

Fusion transcript validation and sequencing

The ICOS-CD28 and VAV1-HNRNPM fusion mRNAs discovered on whole transcriptome sequencing were verified by PCR and Sanger sequencing on patient cDNA using the following primers: ICOS (forward): 5'-TGAACACTGAACGCGAGGAC-3'; CD28 (reverse): 5'-CATTGGTGGCCCAACAGG-3'; VAV1 (forward): 5'- GATGCAGCAGAATT-TGCCATCAGC-3'; HNRNPM (reverse): TTGCATTGCTCTCCTGGCATGTTC.

Survival analysis

The Kaplan-Meier curve was constructed, and difference in survival was tested by the log-rank method, using the survival package in R.[153]

Surface plasmon resonance (SPR) spectrometry

Binding experiments were carried out using surface plasmon resonance as implemented in the BiacoreTM T200 (GE Healthcare). All analyses were performed at 37 °C. Analyses of the interaction between CD28 and its ligands were performed in HBS-EP buffer (0.01M HEPES, pH 7.4, 0.15M NaCl, 0.05% sodium azide, 0.005% (v/v)

Surfactant P20). Analyses of the interaction between the tyrosyl phosphopeptides of CD28 and SH2 domain-containing proteins were performed in a “Cytoplasmic Buffer” (0.01M HEPES, pH 7.4, 0.146 M KCl, 0.05% sodium azide, 0.005% (v/v) Surfactant P20). For determining the binding affinity of CD28 for their ligands, a blank flow cell was used as the control, and CD28 Fc fusion protein at 0.1 mg/ml, 10mM sodium acetate, pH 5.0, was directly immobilized to the dextran matrix of Research Grade CM5 sensor chips (GE Healthcare) by amine coupling using the manufacturer’s kit (GE Healthcare) and an activation time of 5 min, resulting in immobilization levels of approximately 2500 RU. For determining the binding affinity of tyrosyl phosphopeptides of CD28 for SH2 domain-containing proteins, biotinylated tyrosyl phosphopeptides or the universal control peptide (a 15-residue neutral peptide with the sequence of GSGSGSGSGSGSGSG, G = Glycine, S = Serine) were indirectly immobilized to the sensor surface of SA sensor chips (GE Healthcare) via streptavidin to levels of approximately 250 RU as previously described.[154] Equilibrium binding analysis was undertaken as described.[64,65] Briefly, 2-fold serial dilutions of analytes were injected simultaneously over flow cells containing the immobilized proteins or peptides. Injections were of 30s duration, at a buffer flow rate of 20µl/min, which was sufficient for binding to reach equilibrium. The binding data were examined using Biacore T200 Evaluation Software (GE Healthcare), and affinities were derived using the curve fitting tools of Origin version 5.0 (MicroCal Software Inc., Northampton, MA) and Microsoft Excel.

Digital Droplet PCR for putative CD28 F51L mutations

To determine the absolute numbers of copies of CD28-F51L and CD28-WT within our samples, the Bio-Rad QX200 system (Bio-Rad, Hercules, CA) was used to perform

digital droplet PCR in a duplex assay. Two hundred ng of genomic DNA were used as input, and the reaction mix was prepared according to the manufacturer's guidelines (Droplet Digital PCR Applications Guide, Bio-Rad). Following droplet generation, samples were amplified on a Bio-Rad CFX384 Thermal Cycler with the following primer combination (CD28 Forward Primer: 5'-ACAATGCGGTCAACCTTAG-3', CD28 Reverse Primer: 5'-CAGACTTCCACAGCACTATC-3') in the presence of two differentially labeled oligonucleotide probes (WT: HEX-labeled 5'- CCCGG+A+A+CTC+CC-3'; F51L: FAM-labeled 5'-CGG+A+G+CTC+CC-3', where "+" indicates that the following nucleotide is a locked nucleic acid). Probe signals were quenched with 3' Black Hole Quencher. The primers and probes were purchased from Integrated DNA Technologies (San Diego, CA). Data were analyzed using QuantaSoft analysis software (version 1.6.6, Bio-Rad). On average, 32,640 copies (range 11640 – 100200) of the CD28-WT allele were present in a single 20 µL reaction, whereas no copies of the mutant allele were detected. Five samples with a putative CD28 F51L mutation were analyzed together with one negative template control, three reactive lymph node specimens, and seven cases with unknown CD28 mutation status.

Molecular modeling of novel CD28 mutants

The following PDB files were used to analyze the effects of the D124V mutation in CD28: 1YJD (CD28),[155] 1I85 (CD86 and CTLA4),[156] and 1I8L (CD80 and CTLA4).[157] The amino acid change in CD28 was made in Coot[158] and was modeled in each of the three preferred rotamers. Each rotamer was analyzed for steric clashes with Molprobity[159] and the Val rotamer with only one clash was selected. The wild-type and mutant CD28 structures were aligned with CTLA4 in the CD86-CTLA4 structure using

LSQKAB[160] in CCP4i[161] (residues 60-118 of CTLA4 were used for the alignment). The aligned CD28 structures were combined with CD86 using PHENIX.[162] Interactions between CTLA4, CD28, and CD28 D124V and CD86 were analyzed with LigPlot+.[163] These interacting residues were used to guide the docking program HADDOCK[164] to create docked structures of CD86 or CD80 with CTLA4, CD28, and CD28 D124V. After initial rigid-body energy minimization and semi-flexible refinement in torsion angle space, HADDOCK performs a final refinement in explicit solvent. This was done to more accurately predict the interface between CD86 and CD28 over simple rigid-body alignment in the absence of an experimental structure of the complex. The docking of CTLA4 with CD86 demonstrated that the program could accurately recapitulate the experimental structure of the complex (data not shown). Each of these docking results as well as the CD86-CTLA4 complex from structure 1I85 and the CD80-CTLA4 complex from structure 1I8L were split into the individual structures using PDBSET in CCP4i and the electrostatic surface potentials were analyzed with APBS[165] and PDB2PQR[166] using the APBS plugin[167] in PyMOL.[168] To analyze the effects of the T195P mutation in CD28, the crystal structure of DpYMNMT from CD28 bound to the GRB2 SH2 domain was used (PDB 3WA4).[169] Residues Pro-Arg-Arg were added to the C-terminal end of the CD28 peptide and Thr195 was mutated to Pro with Coot. The water molecules, Cd ion, and acetic acid molecule were removed from the PDB file and the three letter code for phosphotyrosine was changed from PTR to TYP, which is the code required by HADDOCK. The interactions between the CD28 peptide and the GRB2 SH2 domain were analyzed with LigPlot+. This revealed that the phosphotyrosine interacts with R67, R86, S88, S90, and S96 of GRB2, and the N193 residue of the CD28 peptide interacts with K109 and K120. These residues were then used to guide docking of the DpYMNMTPRR and DpYMNMPPRR CD28 peptides to the GRB2 SH2 domain using HADDOCK.

Cell lines and transduction

CD28 constructs

The entirety of CD28 with or without D124V or T195P mutations was cloned into GFP-containing pMIG-2B vectors (Promega). Retrovirus was produced in 293T cells essentially as described previously.[170] Briefly, $2x10^6$ 293T cells were transfected with 8μg pMIG-CD28 plasmid and 9.4μg pCL3-Ampho viral packaging plasmid by the calcium chloride method. Transfected 293T cells were cultured in Jurkat media (RPMI-1640, 10% FBS, 1% 1M HEPES buffer, 1% penicillin/streptomycin) and retrovirus-containing supernatant was collected and filtered (0.45μm). Virus and polybrene (10μg/mL, Sigma-Aldrich, St. Louis, MO) were used to infect ~500,000 Jurkat cells, clone E6.1 (ATCC). Cells were centrifuged at 300 *g* for 75 minutes at 32°C. Transfected cells stably maintaining GFP expression after one week were sorted using flow cytometry. Cells were then cultured and frozen or used in the activation assay. All cell culture reagents were obtained from Life Technologies unless otherwise stated.

VAV1 constructs

VAV1-variant-2 was purchased in the pOTB7 vector, and HNRNPM was purchased in the pCMV-Sport6 vector (Harvard Medical School, Clones HsCD00326560 and HsCD00321972, respectively).

A single FLAG-tagged VAV1-standard was created using the following primers: forward: 5'- GTTTTTGGATCCGCCATGGACTACAAGGACGACGATGACAAGGGTG-GAGGTATGGAGCTGTGGCGCCAATG-3'; reverse: 5'-TCACAGCAGGTGGACAGG-

AAGG-3'. pOTB7-VAV1 and the PCR product were digested with BamHI and AflII. The resultant 4352bp and 258 bp fragments were ligated, generating pOTB7-flagVAV1.

To generate the VAV1-HNRNPM junction, patient cDNA was amplified using the following primers: forward: 5'- GTTTTTCGGTCCGGATCCCTTGTAACAGGGTGAAGC-CCTATG-3'; reverse: 5'- GCAGCTTTTTTCATGCTCTCTTC-3', producing a 502bp fragment. This fragment and pCMV-Sport6-HNRNPM were digested with RsrII and EcoRI, and the fragment was ligated into the pCMV-Sport6-HNRNPM vector to produce a 6963bp pCMV-Sport6-fusionHNRNPM intermediate.

To create VAV1-HNRNPM, the pOTB7-flagVAV1 and pCMV-Sport6-fusionHNRNPM vectors were both digested with BamHI and Bsu36I, and the appropriate 2032bp and 6894bp fragments, respectively, were ligated to produce pCMV-Sport6-flagVav1-HNRNPM. This served as the basis for the rest of the construct design.

To create the final construct used in this study, VAV1-HNRNPM, VAV1-front, and VAV1-whole were all cloned with a triple FLAG tag on the N-terminus, and back-HNRNPM was cloned with a triple FLAG tag on the C-terminus. They were all inserted at the SalI and BamHI sites of either the pBABE-puro (gift from Hartmut Land, Jay Morgenstern & Bob Weinberg (Addgene plasmid # 1764)[171] or the pMIT retroviral vector (gift of T. Mitchell)[172] which has the murine Thy1.1 coding sequence downstream of the IRES. Accuracy of the cloning was confirmed by Sanger sequencing.

For pBABE-puro-based vectors, pCL3-ampho virus was packaged in 293T cells transfected with Lipofectamine (Thermo Scientific) per the manufacturer's protocol, and the resultant virus was used to infect VAV1-null Jurkat cells (J.vav1; gift of D. Billadeau).[173] Resistance to puromycin was selected over four weeks.

For pMIT-based vectors, ecotropic receptor-encoding retrovirus (pBABE zeo Ecotropic Receptor was a gift from William Hahn, Addgene plasmid # 10687) was packaged in pCL3-ampho in 293T cells transfected with Lipofectamine, which was then

used to infect J.vav1 cells. Resistance to Zeocin was selected over a period of four weeks. Then, vectors encoding each of the four VAV constructs or empty pMIT were transfected by Lipofectamine into PLAT-E cells (gift of Zuoming Sun, City of Hope), and the resultant ecotropic virus was used to transfect J.vav1-EcR cells. After one week, cells were sorted for positive Thy1.1 expression by anti-Thy1.1 antibody (APC-conjugated, clone OX7; Biolegend), and they were sorted three more times for equivalent Thy1.1 levels before being frozen or used in experiments.

T-cell stimulation and luciferase assay

To prepare the stimulatory beads, anti-CD3 antibody UCHT1 (BioLegend, San Diego, CA) and either CD80-Ig or CD86-Ig (Sino Biological, Beijing, China) were ligated to M450 tosylated beads (Life Technologies) per the manufacturer's instructions at a ratio of 1:1. In some experiments, human CD3/CD28 beads (Life Technologies) were used. For the NF-κB reporter assay, $6x10^6$ Jurkat cells stably transduced with the CD28 mutants or WT were electroporated with Photinus luciferase NF-κB reporter vector pGL4.32 (Promega) and the Renilla pRL-TK control vector (ratio 10:1) using the Amaxa Nucleofector® (program X-001). Twenty-four hours post-electroporation, the cell number was determined and cells were stimulated with the indicated beads at a ratio of 1:1 for four hours and then harvested and lysed. The dual luciferase assay from Promega was performed according to the manufacturer's instructions, and luciferase activity was measured using the POLARstar Omega plate reader (BMG Labtech, Offenburg, Germany).

Nanostring nCounter assay

To measure gene expression over time,[174] one million Jurkat cells stably transduced with either CD28 mutants or WT, or each of the VAV-fusion-containing pMIT vectors, were stimulated with one million of the indicated beads for the indicated time, then immediately washed in PBS, lysed in Qiagen buffer RLT, and placed at -80°C until use. Aliquots were thawed, and 10,000 cells per reaction were prepared for nCounter expression analysis per the manufacturer's instructions (NanoString Technologies, Inc. Seattle, WA). We designed a customized codeset panel for 29 genes and two housekeeping genes (Table 5). Cell lysate was hybridized to the custom codeset at 65° overnight. The reaction was processed on the nCounter prepstation and gene expression data were acquired on the nCounter Digital Analyzer on the "high resolution" setting. Standard quality control by the nSolver analysis software was employed.

Immunofluorescence

Transduced J.vav1 cells were counted and washed with PBS, then spun against slides using a Cytospin in 2.5% bovine serum albumin (Sigma-Aldrich, St. Louis, MO; medium acceleration, 5 minutes), then fixed for 20 minutes in 4% paraformaldehyde (PFA; Sigma) in PBS, washed three times for with PBS. Cells were then permeabilized for 1 hour in 0.3% Triton-X100 (Sigma) / 0.5% BSA in PBS (TB-PBS), washed with fresh TB-PBS, then incubated overnight at 4 degrees in the dark with rabbit anti-FLAG (Cell Signaling Technology, clone 2368) 1:800 in 0.5% BSA-PBS. The next day, cells were washed three times in TB-PBS, then incubated for 90 minutes at room temperature in the dark with PE donkey anti-rabbit 1:1500 in 0.5% BSA-PBS (BioLegend,

Catalog#406421). After incubation cells were washed three times in PBS then sealed with Prolong Gold anti-fade with DAPI (Life Technologies) and a cover slip. Twenty-four hours later, slides were imaged on a Zeiss LSM-710 confocal microscope for emissions at 555nm and 410nm.

Gene	Accession	Target Sequence
CCL4	NM_002984.2	TTCTGCAGCCTCACCTCTGAGAAAACCTCTTTGCCACCAATACCATGAAGCTCTGCGTGACTGTCCTGTCTCTCCTCATGCTAGTAGCTGCCTTCTGCTC
CCL9	NM_031200.1	CCCTGTTCTCTATGTTTTTGTGGGTGAGAGATTCCGCCGGGATCTCGTGAAAACCCTGAAGAACTTGGGTTGCATCAGCCAGGCCCAGTGGGTTTCATTT
CD226	NM_006566.2	TTAAGCTTTGGGCAAGGGCTATTTACCAGGGCTTAAATGTTGTGTCTAGAATTAAGTATGGGCATAAACTGGCTTCTGAATCCCTTTCCAGAGTGTTGGA
CD69	NM_001781.1	AGGACATGAACTTTCTAAAACGATACGCAGGTAGAGAGGAACACTGGGTTGGACTGAAAAAGGAACCTGGTCACCCATGGAAGTGGTCAAATGGCAAAGA
CD83	NM_004233.3	CTGTTCTTGAAGCAGTAGCCTAACACACTCCAAGATATGGACACACGGGAGCCGCTGGCAGAAGGGACTTCACGAAGTGTTGCATGGATGTTTTAGCCAT
CDH5	NM_001795.3	TCTCCCCTTCTCTGCCTCACCTGGTCGCCAATCCATGCTCTCTTTCTTTTCTCTGTCTACTCCTTATCCCTTGGTTTAGAGGAACCCAAGATGTGGCCTT
CNN3	NM_001839.4	TGATCCCAAATACTGTGCTGCTCCTACAGAACCTGTCATTCACAACGGAAGCCAAGGAACAGGAACAAATGGTTCGGAAATCAGTGATAGTGATTATCAG
DUSP2	NM_004418.3	CTGGCCCTCATTCGGGGTCGGGAACCAAGGGTGTGTCTGCTCTTTCCCTCCCCATCCTCTGGCAGAAATCAGCTAGACGCTATACCGTGGACTCTCCCTG
DUSP5	NM_004419.3	GTGGATGTAAAACCCATTTCACAAGAGAAGATTGAGAGTGAGAGAGCCCTCATCAGCCAGTGTGGAAAACCAGTGGTAAATGTCAGCTACAGGCCAGCTT
EGR1	NM_001964.2	GAGGCATACCAAGATCCACTTGCGGCAGAAGGACAAGAAAGCAGACAAAAGTGTTGTGGCCTCTTCGGCCACCTCCTCTCTCTCTTCCTACCCGTCCCCG
EGR2	NM_000399.3	GGTGGAGCTAGCACTGCCCCCTTTCCACCTAGAAGCAGGTTCTTCCTAAAACTTAGCCCATTCTAGTCTCTCTTAGGTGAGTTGACTATCAACCCAAGGC
EGR3	NM_004430.2	CGTACAGGGTGGCTCCTTTGAAGTGGAGTAATAGGGAAGGTTGCTCTCTGCCACAGCTTGCAGCATGGTCTTGACTGAATGTACTGTTCCTGTTAGCGTT
EGR4	NM_001965.3	GACAGTTCCCGCGGTCCAGGCGCTGTCACCCTTGTCAGCCGCGCTTTGGGGGAAGTCTTCTGAGACCACCCAGTGAATAGGCACTACCCTGGGATTCAAG
FTH1	NM_002032.2	CCAAATACTTTCTTCACCAATCTCATGAGGAGAGGGAACATGCTGAGAAACTGATGAAGCTGCAGAACCAACGAGGTGGCCGAATCTTCCTTCAGGATAT
GUSB	NM_000181.1	CGGTCGTGATGTGGTCTGTGGCCAACGAGCCTGCGTCCCACCTAGAATCTGCTGGCTACTACTTGAAGATGGTGATCGCTCACACCAAATCCTTGGACCC
IER3	NM_003897.2	TCAACTCCGTCTGTCTACTGTGTGAGACTTCGGCGGACCATTAGGAATGAGATCCGTGAGATCCTTCCATCTTCTTGAAGTCGCCTTTAGGGTGGCTACG
IL2	NM_000586.2	AGGATGCAACTCCTGTCTTGCATTGCACTAAGTCTTGCACTTGTCACAAACAGTGCACCTACTTCAAGTTCTACAAAGAAAACACAGCTACAACTGGAGC
IL2Ra	NM_000417.1	CTTGGTAAGAAGCCGGGAACAGACAACAGAAGTCATGAAGCCCAAGTGAAATCAAAGGTGCTAAATGGTCGCCCAGGAGACATCCGTTGTGCTTGCCTGC
IL3	NM_000588.3	GCCCTTGAAGACAAGCTGGGTTAACTGCTCTAACATGATCGATGAAATTATAACACACTTAAAGCAGCCACCTTTGCCTTTGCTGGACTTCAACAACCTC
IL9	NM_000590.1	AAGTACTAAAGAACAACAAGTGTCCATATTTTTCCTGTGAACAGCCATGCAACCAAACCACGGCAGGCAACGCGCTGACATTTCTGAAGAGTCTTCTGGA
TIEG	NM_005655.3	TTTCAATGTGATTCTTCTAAAGCACTGGTTTCAAGAATATGGAGGCTGGAAGGAAATAAACATTACGGTACAGACATGGAGATGTAAAATGAGTTTGTAT
LTB	NM_002341.1	AGGAACAGGCGTTTCTGACGAGCGGGACGCAGTTCTCGGACGCCGAGGGGCTGGCGCTCCCGCAGGACGGCCTCTATTACCTCTACTGTCTCGTCGGCTA
MYO1F	NM_012335.3	GCCCGACCAGTACCAGATGGGGAGCACCAAGGTCTTTGTCAAGAACCCAGAGTCGCTTTTCCTCCTGGAGGAGGTGCGAGAGCGAAAGTTCGATGGCTTT
NR4A1	NM_173157.1	ACCGGCTGCAGTGTGCCCGTGGCTTCGGGGACTGGATTGACAGTATCCTGGCCTTCTCAAGGTCCCTGCACAGCTTGCTTGTCGATGTCCCTGCCTTCGC
NR4A3	NM_173198.1	GTCGTCTGCCTTCCAAACCAAAGAGCCCATTACAACAGGAACCTTCTCAGCCCTCTCCACCTTCTCCTCCAATCTGCATGATGAATGCCCTTGTCCGAGC
PCK1	NM_002591.2	GGGCACATCAACATGATGGAGCTTTTCAGCATCTCCAAGGAATTCTGGGAGAAGGAGGTGGAAGACATCGAGAAGTATCTGGAGGATCAAGTCAATGCCG
PDCD1	NM_005018.1	CTTCTTCCCAGCCCTGCTCGTGGTGACCGAAGGGGACAACGCCACCTTCACCTGCAGCTTCTCCAACACATCGGAGAGCTTCGTGCTAAACTGGTACCGC
PDGFA	NM_002607.5	TCCACCACCGCAGCGTCAAGGTGGCCAAGGTGGAATACGTCAGGAAGAAGCCAAAATTAAAAGAAGTCCAGGTGAGGTTAGAGGAGCATTTGGAGTGCGC
POLA1	NM_016937.3	GTCAGTTGGTGTAAAGTTGAGGCAATGGCTTTGAAACCAGACCTGGTGAATGTAATTAAGGATGTCAGTCCACCACCGCTTGTCGTGATGGCTTTCAGCA
TNFa	NM_000594.2	AGCAACAAGACCACCACTTCGAAACCTGGGATTCAGGAATGTGTGGCCTGCACAGTGAAGTGCTGGCAACCACTAAGAATTCAAACTGGGGCCTCCAGAA
TNFAIP3	NM_006290.2	CAAAGCCCTCATCGACAGAAACATCCAGGCCACCCTGGAAAGCCAGAAGAAACTCAACTGGTGTCGAGAAGTCCGGAAGCTTGTGGCGCTGAAAACGAAC

Table 5: Nanostring Codeset. The genes with accession number and targeted regions are listed, along with sequence and comments for each probe, if applicable. Target design was performed and validated by Nanostring Technologies, Inc.

Flow cytometric analyses

All flow analyses employed standard gating on forward- and side scatter profiles to ensure only data for single cells of the appropriate size were analyzed.

For Thy1.1 expression, cells were stained for 30 minutes at 37 degrees with 1µg/mL AlexaFluor 647 anti-Thy1.1 (BioLegend, clone OX-7), then washed with PBS.

For proliferation, one million cells of each cell line were incubated with CFSE (Life Technologies) 1:1500 for 30 minutes at 37 degrees per the manufacturer's instructions, then 10,000 gated events were assessed every day for one week on an Accuri C6 (BD Biosciences) for emission in FL-1.

For CD69 expression, 80,000 cells of each cell line were plated in a 96-well plate and stimulated for 8 hours with CD3/CD28 beads (Invitrogen) or not. Cells were washed, beads removed by a magnet, then cells were stained 1:500 with anti-CD69-PE (BioLegend, clone FN50) for 30 minutes at 37 degrees in the dark. Cells were then washed with PBS and 30,000 gated events assessed on an Accuri C6 for emission in FL-2.

For VAV1 expression, one million cells were rinsed with PBS and fixed with 4% PFA for 10 minutes at 37 degrees, then chilled, and rinsed with PBS. Cells were then permeabilized in methanol (Macron Chemicals, Central Valley, PA) for one hour on ice. After washing with PBS, cells were incubated with rabbit anti-VAV1 (Cell Signaling Technologies, #2502) 1:25 in 0.5% BSA-PBS for one hour at room temperature with occasional mixing. After washing, cells were then incubated with Alexa647 goat anti-rabbit Ig (Cell Signaling Technologies, clone 4414) 1:800 in 0.5% BSA-PBS for 30 minutes at room temperature in the dark, then washed in PBS-2% FBS and analyzed on an Accuri C6 for emission in FL-4.

Calcium flux was analyzed essentially as described previously. Five million cells of each cell line were incubated with Indo1-AM (Life Technologies) 1:1000 in 100µL HBSS (Life Technologies) for 30 minutes at 37 degrees in the dark, then washed in PBS and incubated another 30 minutes at 37 degrees in the dark to cleave AM esters. After washing again, cells were kept on ice until use. Cells were collected on a BD LSR Fortessa using the recommended filter sets for Indo1 acquisition. Cells were collected for 90 seconds to establish baseline, then stimulated for 12 minutes with 1ug/mL anti-CD3 (BioLegend, clone UCHT1) and 1µg/mL anti-CD28 (BioLegend, clone CD28.2) cross-linked with rabbit anti-mouse Ig (BioLegend, clone Poly4053). Data were binned for each second, and the ratio of emission at 515nm (“violet”)/395nm (“blue”) was plotted against time in Microsoft Excel.

CHAPTER 2: RESULTS[2]

Detection of CD28- and VAV1-containing fusion transcripts, and mutations in CD28 and VAV1, through whole transcriptome sequencing

Our analysis of WTS data from 20 AITL cases revealed a single case showing an in-frame *ICOS-CD28* fusion transcript. This fusion transcript was confirmed by Sanger sequencing of cDNA from the case showing a fusion of *ICOS* exon 1 (forward) with *CD28* exon 2 (Figure 6A). *ICOS* exon 1 encodes the membrane signal sequence, but this is cleaved from the protein; thus, *ICOS* promoter-mediated expression of the transcript would be expected but with no change in the final product. ICOS is highly expressed in AITL and in T_{FH} cells.[74] The fusion transcript was found to contain a mutation of aspartate 124 of CD28 to valine (D124V; Fig. 6B). This AITL case was found to express *CD28* at a level higher than most other cases in this study; additionally, the AITL cases expressed *CD28* at a level higher than normal T-cell subsets when normalized for T-cell content[175] (Figure 7A). Three cases with the CD28 residue threonine 195 mutated to proline (T195P) with varying variant frequencies (VFs) were also identified. Additionally, we also found *TET2* single-nucleotide variants and indels as reported previously[126] as well as *RHOA* mutations.[123] Based on these findings, we performed targeted whole-exon sequencing for *CD28*, *TET2*, and *RHOA* on 90 T-cell lymphoma cases (38 AITL – including five also having WTS, 40 PTCL-NOS, and 12 ALK- ALCL). In 88 cases, subtype was assigned molecularly.[74] For PTCL-NOS cases,

[2] Used with permission from Rohr et al. 2015 (reference 122)

GEP previously performed[106] classified the cases into TBX21 or GATA3 subtypes; cases that did not fit into either category were considered “unclassified” (Table 6). Clinical information for all cases in this study is available in Table 4.

We also found a single *VAV1-HNRNPM* fusion transcript; the junction occurred

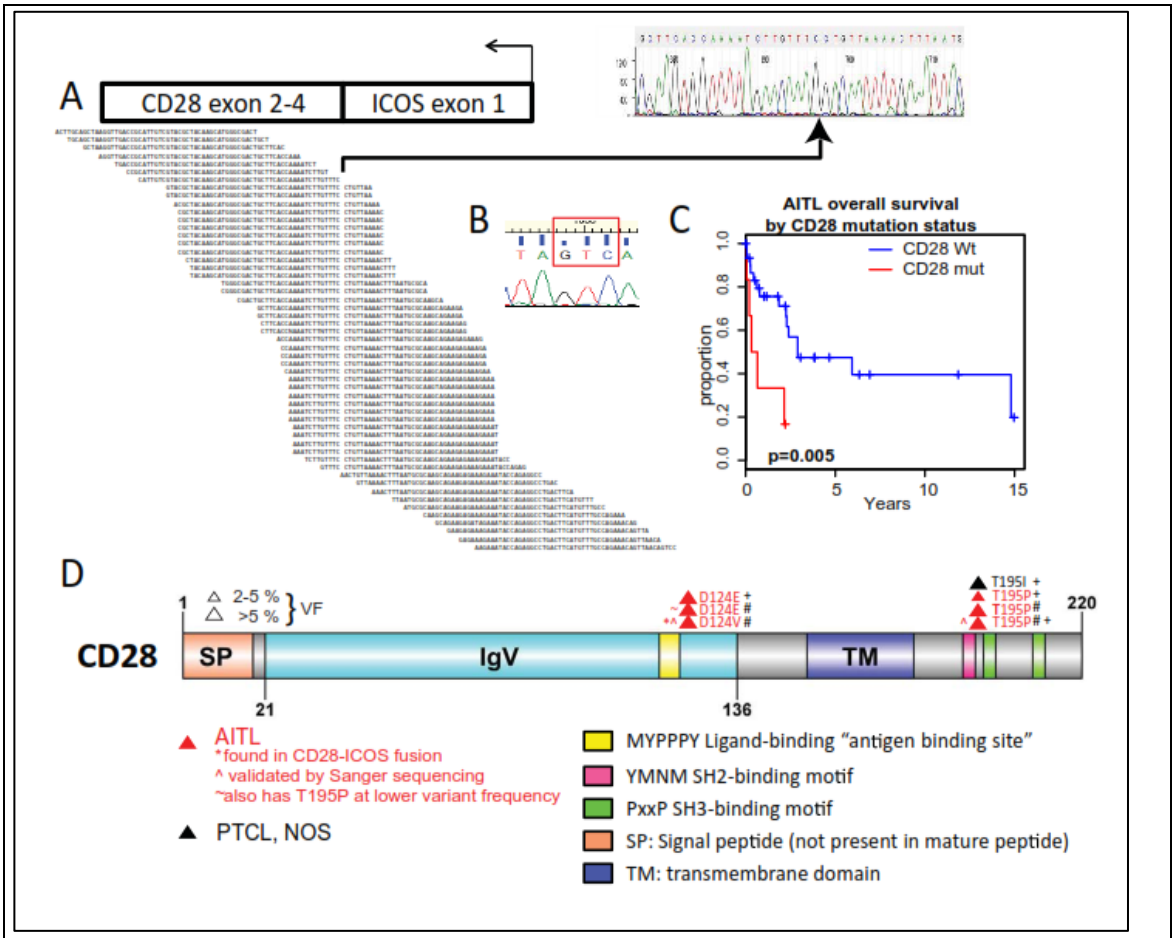

Figure 6: Distribution of CD28 mutations discovered on transcriptome and targeted sequencing in T-cell lymphoma subtypes. A: Alignment of ICOS-CD28 fusion transcript and identification of breakpoint, verified by Sanger sequencing. B: Demonstration by Sanger sequencing of D124V mutant in ICOS-CD28 transcript, GAC>GTC (red box). C: Kaplan-Meier survival analysis of AITL cases with CD28 mutations (red) versus AITL cases with no CD28 mutations (black). CD28-mutant cases had inferior survival after diagnosis (p=0.005). D: CD28 map and mutations found in 20 AITL cases with whole transcriptome sequencing plus 38 AITL (including five cases overlapping with transcriptome sequencing; red), 40 PTCL-NOS (black), and 12 ALK-ALCL cases. SP: signal peptide; IgV: Ig variable region-like domain CD28 and CTLA4; TM: transmembrane domain. Yellow: “antigen-binding” site required for interaction with ligand within IgV domain; pink: SH2-binding motif; green: SH3-binding motifs. #: identified in whole-transcriptome sequencing; +: identified in targeted sequencing platform. The diagram was built using DOG, version 2.0.[176]

between *VAV1* exon 24 (forward) and *HNRNPM* exon 2. The two genes are present on chromosome 19 in the same orientation; an approximately 1.66Mb deletion may have generated the fusion. This was validated by PCR and Sanger sequencing (Figure 8A,B). Other putative fusions were also identified from the WTS data (Figure 7C).

		Number (% of screened)		
		T195	D124	Total by diagnosis (%)
AITL (n=53)°		3 (5.7)	3 (5.7)*	6 (11.3)
PTCL, NOS (n=40)	TBX21 (n=19)	1 (5.3)	0	1 (5.3)
	GATA3 (n=12)	0	0	0
	Unclassified (n=9)°	0	0	0
ALCL, ALK- (n=12)		0	0	0
Total by residue		4	3	7 (6.7)

Table 6: Recurrent mutations in *CD28* in screened T-cell lymphoma cases. Summary of mutations in *CD28* found on targeted sequencing of PTCL cases, grouped by resultant mutated residue and diagnosis. Seven of 105 total cases (6.7%) had mutations at recurrent residues within CD28. *: this D124E case also has a T195P mutation at lower variant frequency; this case is only tabulated in the D124 column. °: one case of AITL and one case of PTCL-Unclassified has only a histological diagnosis.

CD28 mutations are relatively frequent in AITL and correlate with poor survival

The frequencies of CD28 mutations are presented in Table 6 and Fig. 6D, and the *TET2* and *RHOA* mutation status and molecular diagnosis for individual cases are in Table 7. Several of the mutations were verified by PCR and Sanger sequencing as somatic (Figure 9). The average depth in our targeted sequencing platform was >1000-fold, and variant frequencies for a single nucleotide polymorphism (SNP; rs3116496)

within the targeted region reveal a SNP proportion of approximately fifty percent (Table 8). Paired-end reads filtered out likely misreads, and only recurrent mutations affecting the same codon were identified to reduce the possibility of artifact or random calls. Mutations at D124 and T195 were identified by these criteria, and seven of 105 (6.7%) PTCL cases had a mutation at one of these residues, including 6/53 (11.3%) AITLs. Two mutations, both at residue T195, had VFs greater than 10% in the targeted platform data, and one mutation at D124 had a VF greater than 5%.

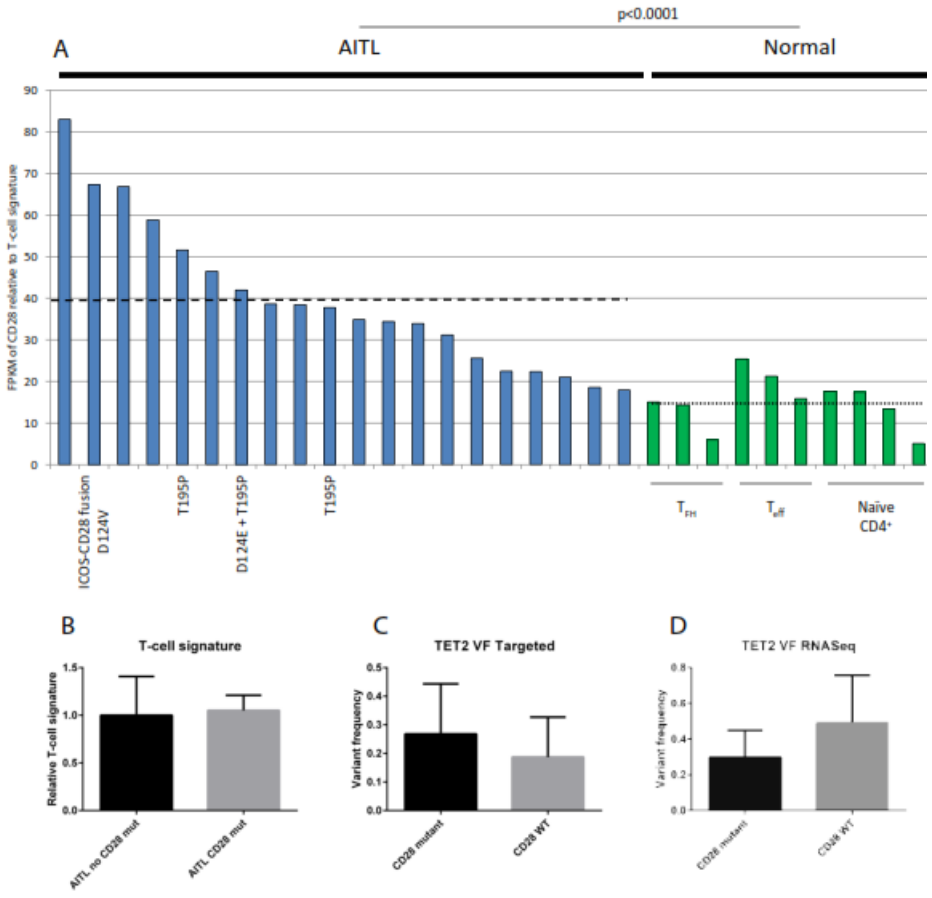

Figure 7: FPKM of CD28 in AITL compared to non-neoplastic T-cell subtypes, and comparison of CD28-mutant and –WT case T-cell signature and TET2 frequency. A: The FPKM for CD28 was calculated in each sample, and then samples were normalized to the T-cell signature26,32 to account for low tumor content in AITL. Data for normal T-cells were publicly available33. The average FPKM ratio for cancer samples was 31.21 (dashed line), whereas for the normal subtypes combined the average was 11.61 (dotted line; $p<0.0001$, Mann-Whitney test). These values are likely underestimations of the true CD28 FPKM values in the tumor because the normalization method cannot distinguish the neoplastic from non-neoplastic contribution to the T-cell signature. B: CD28 mutation status did not alter T-cell signature ($p>0.61$). C-D: CD28 mutation status was independent of TET2 mutant call variant frequency in both the targeted (C; $p>0.32$) and RNA sequencing platforms (D; $p=0.40$) and E-F: CD28 mutation status was independent of RHOA mutant call variant frequency in both the targeted (E; $p>0.99$) and RNA sequencing platforms (F; $p>0.31$).

There was no difference in relative expression of the T-cell signature[106] (Figure 7B) between CD28 wild-type and mutant cases in the transcriptome data. There was also no significant difference in average *TET2* or *RHOA* VF based on *CD28* mutation status in either the RNAseq or the targeted sequencing platforms (Figure 7B-D). AITL cases with CD28 mutations have inferior survival to CD28-WT cases (p=0.005; Fig. 6C). We also found apparent mutations at residue phenylalanine 51 (F51) as previously reported in T-cell lymphomas,[128] but these were all found at extremely low apparent VF (<2%) and could not be verified by droplet digital PCR (ddPCR).[177]

Codon	Disease	Residue change	Variant frequency	TET2 mutation variant frequency	RHOA mutation variant frequency
D124	AITL	D124V	21.9 (Tr)	16.0 (Tr)	11.9 (Tr)
		D124E*	49.1 (Tr)	45.6 (Tr)	28.5 (Tr)
		D124E	5.9	11.57	9.75
T195	AITL	T195P	64.2 (Tr)	50.0 (Tr)	11.2 (Tr)
			10.58	17.73	3.72
		T195P	42.7 (Tr)	28.12 (Tr)	20.6 (Tr)
		T195P	2.17	44.98	21.1
	PTCL-TBX21	T195I	12.3	13.09	14.4

Table 7: Mutated residue in CD28 by diagnosis, variant frequency, and TET2 and RHOA mutation status and frequency. The CD28 mutation reads are grouped by diagnosis. Because TET2 mutations are varied, and individual cases often have more than one single-nucleotide variant (SNV) or indel, only the presence of SNVs or indels and the highest variant frequency is shown. Variant frequencies are either from transcriptome (Tr) or targeted sequencing data as indicated. *: this case with D124E also had a T195P mutation at 6.6% variant frequency.

We also subjected published PTCL sequencing datasets[125,127,128] to the same analysis pipeline and found two T195P and three F51 mutations, ranging from 2.29% to 41.12% variant frequency (Table 9). Cases of a fusion of *CD28* with family member

CTLA4 have recently been reported in Sézary syndrome,[178,179] and a recent report on adult T-cell leukemia/lymphoma[180] shows several mutations and fusions of *CD28.* We examined our WTS data for additional *CD28* fusion transcripts but none were found. We also examined our NK/γδTCL data[181] and found no *CD28* mutations.

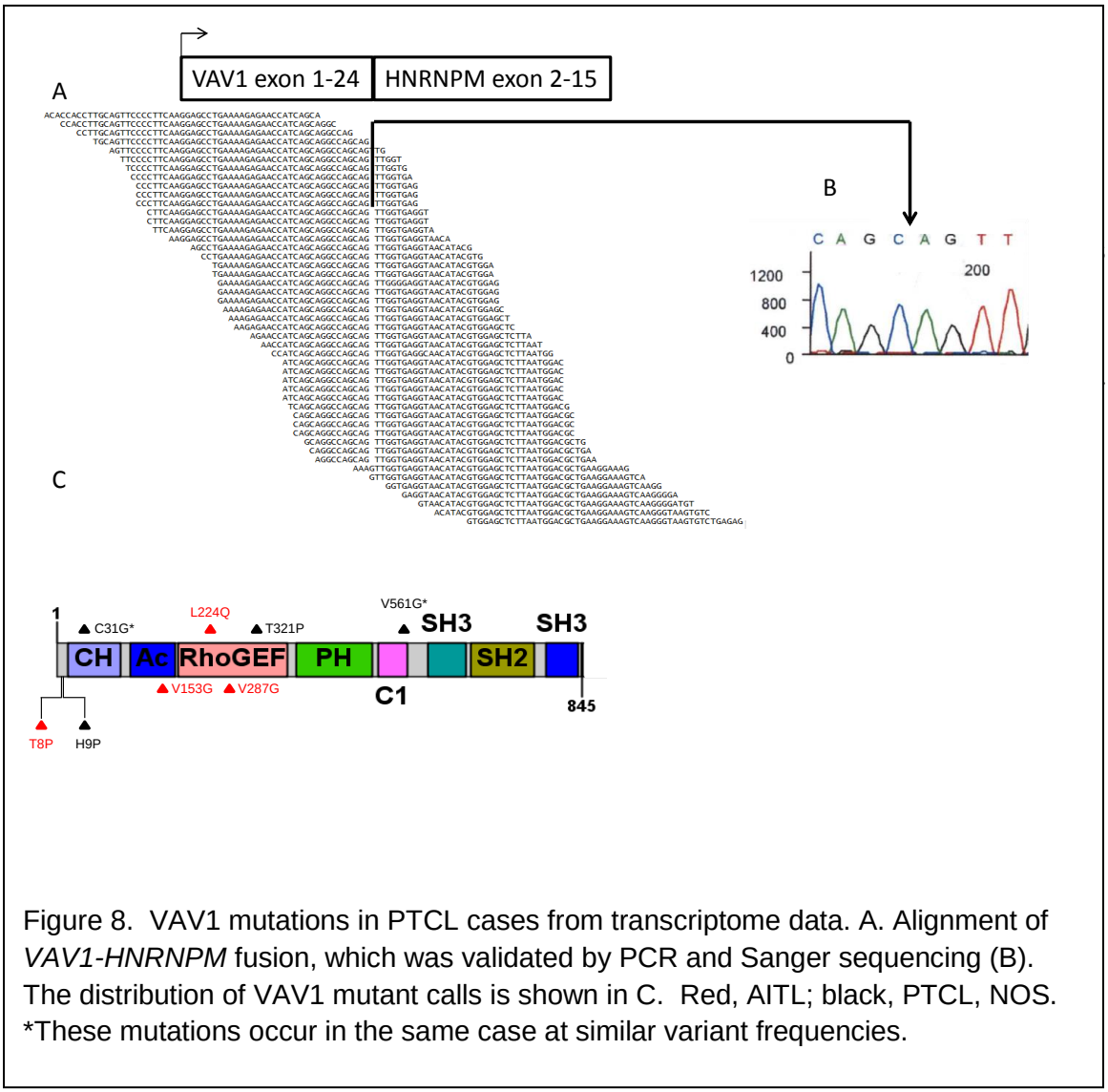

Figure 8. VAV1 mutations in PTCL cases from transcriptome data. A. Alignment of *VAV1-HNRNPM* fusion, which was validated by PCR and Sanger sequencing (B). The distribution of VAV1 mutant calls is shown in C. Red, AITL; black, PTCL, NOS. *These mutations occur in the same case at similar variant frequencies.

Case	Call location		Ref	Call	SNP VF	Ref_F	Ref_R	SNP_F	SNP_R
2	chr2	204594512	T	C	50.16%	310	316	315	315
8	chr2	204594512	T	C	56.84%	306	303	404	398
10	chr2	204594512	T	C	48.73%	421	425	400	404
13	chr2	204594512	T	C	49.53%	486	487	469	486
16	chr2	204594512	T	C	1.06%	558	562	6	6
17	chr2	204594512	T	C	52.50%	401	408	447	447
18	chr2	204594512	T	C	48.48%	595	593	556	562
20	chr2	204594512	T	C	49.45%	567	572	561	553
21	chr2	204594512	T	C	82.21%	582	581	2677	2696
23	chr2	204594512	T	C	52.47%	550	556	610	611
25	chr2	204594512	T	C	46.02%	610	603	518	516
27	chr2	204594512	T	C	99.83%	4	4	2334	2350
31	chr2	204594512	T	C	48.30%	840	859	788	799
33	chr2	204594512	T	C	52.87%	545	539	605	611
36	chr2	204594512	T	C	57.89%	519	519	703	724
40	chr2	204594512	T	C	55.23%	505	501	620	621
41	chr2	204594512	T	C	55.30%	506	519	634	634
42	chr2	204594512	T	C	51.41%	677	688	721	723
48	chr2	204594512	T	C	59.95%	522	526	786	783
51	chr2	204594512	T	C	99.83%	6	4	2993	3008
63	chr2	204594512	T	C	43.16%	1803	1800	1368	1368
65	chr2	204594512	T	C	97.69%	3	3	124	130
66	chr2	204594512	T	C	51.62%	616	620	654	665
67	chr2	204594512	T	C	46.52%	1197	1200	1040	1045
73	chr2	204594512	T	C	99.42%	4	4	681	693
75	chr2	204594512	T	C	99.79%	3	4	1629	1630
76	chr2	204594512	T	C	13.69%	2246	2237	356	355
80	chr2	204594512	T	C	54.84%	305	311	373	375
83	chr2	204594512	T	C	72.20%	288	292	755	751
92	chr2	204594512	T	C	56.56%	392	399	517	513
93	chr2	204594512	T	C	50.93%	1075	1063	1106	1113
95	chr2	204594512	T	C	59.31%	271	269	394	393

Table 8: Targeted sequencing SNP calls. For the cases with SNP rs3116496 (which is within an intron of *CD28*; Chromosome 2, position 204594512, T>C), the variant frequencies for most SNP calls were at approximately 50% or 100%, likely indicating the presence of the SNP in either one or both alleles of *CD28*, respectively.

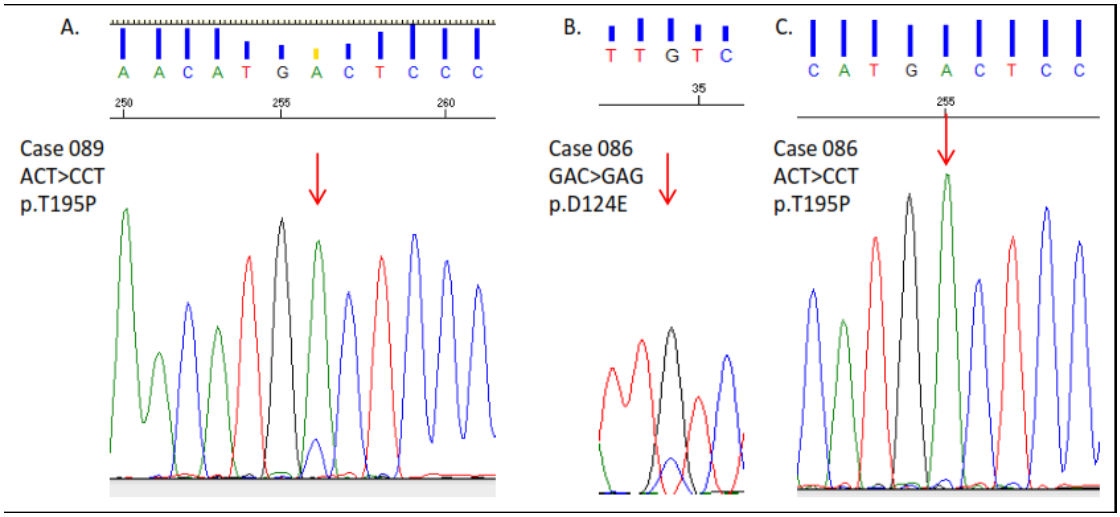

Figure 9. CD28 variants are somatic mutations. A-C: Three additional putative CD28 mutations were subjected to Sanger sequencing. T195P (A, C) and D124E (B) all had the expected mutant calls at a frequency <<50%, indicating that these variants are somatic in nature, rather than germline.

SampleID	Chr	Position	Gene	Ref	Var	Variant reads: tumor	WT reads: tumor	VarFreq Tumor	Variant reads: normal	WT reads: normal	VarFreq Normal	AA change
Yoo.Case5	2	204591454	CD28	T	G	17	277	5.78%	0	150	0%	F51V
Yoo.Case6	2	204591454	CD28	T	A	88	126	41.12%	9	135	6.25%	F51I
Palomero.AITL.35	2	204591454	CD28	T	G	15	59	9.74%	0	103	0%	F51V
Yoo.Case1	2	204599555	CD28	A	C	8	47	4.55%	0	52	0%	T195P
Yoo.Case4	2	204599555	CD28	A	C	4	171	2.29%	0	71	0%	T195P

Table 9: Reads supporting CD28 mutations from other PTCL datasets. We subjected the data from three PTCL studies29-31 to our pipeline and found five cases with mutations: two T195P and three at F51.

CD28 mutant D124V has a greater affinity for CD86 than CD28 WT

To assess whether D124 mutations affect the affinity of CD28 for its physiological ligands, we selected the CD28 D124V mutant for surface plasmon resonance (SPR)-based analysis of the binding affinity of CD28 for its ligands. Representative binding curves and Scatchard plots for determination of experimental K_d and K_a are shown in Figure 10A-D. The affinity of CD28 D124V for CD86 was an average 2.6-fold higher than that of CD28 WT (Fig. 10E; $p < 1x10^{-5}$ for 6 replicates), whereas CD80 binding affinity was not significantly different.

To understand why CD86 has a greater affinity for the CD28 D124V mutant than for CD28 WT, we modeled their interaction (Figure 11). Because a complete crystal structure of CD28 bound to ligand is not available, we used the crystal structures of the CD28 extracellular domain[155] and the complex between CD86 and CD28 family member CTLA4.[156] In this model, the protein surface in the vicinity of the D124V mutation has a more positive overall charge compared to CD28 WT and more closely resembles the surface charge of CTLA4 (Fig. 11C, F, I), which binds CD86 with a 20- to 100-fold greater affinity than CD28.[66-68] This is possibly because the negatively charged D124 counters any surrounding positive charges, leading to a neutral surface on CD28 WT. The D124V mutant is therefore expected to interact more strongly with the negatively charged pocket of CD86 (Fig. 11A, D, G, black dashed outline). Thus, the increased affinity of the mutant may result from improved charge complementarity. Furthermore, several residues, notably in the ligand-binding site, are rotated compared to CD28 WT. This is likely a result of the improved electrostatic interactions with the mutant CD28, leading to a better packing of the interface. We also performed molecular modeling on the CD80-CD28 interaction (Figure 12; Table 10) in the same manner using the crystal structure of CTLA4 in complex with CD80.[157]

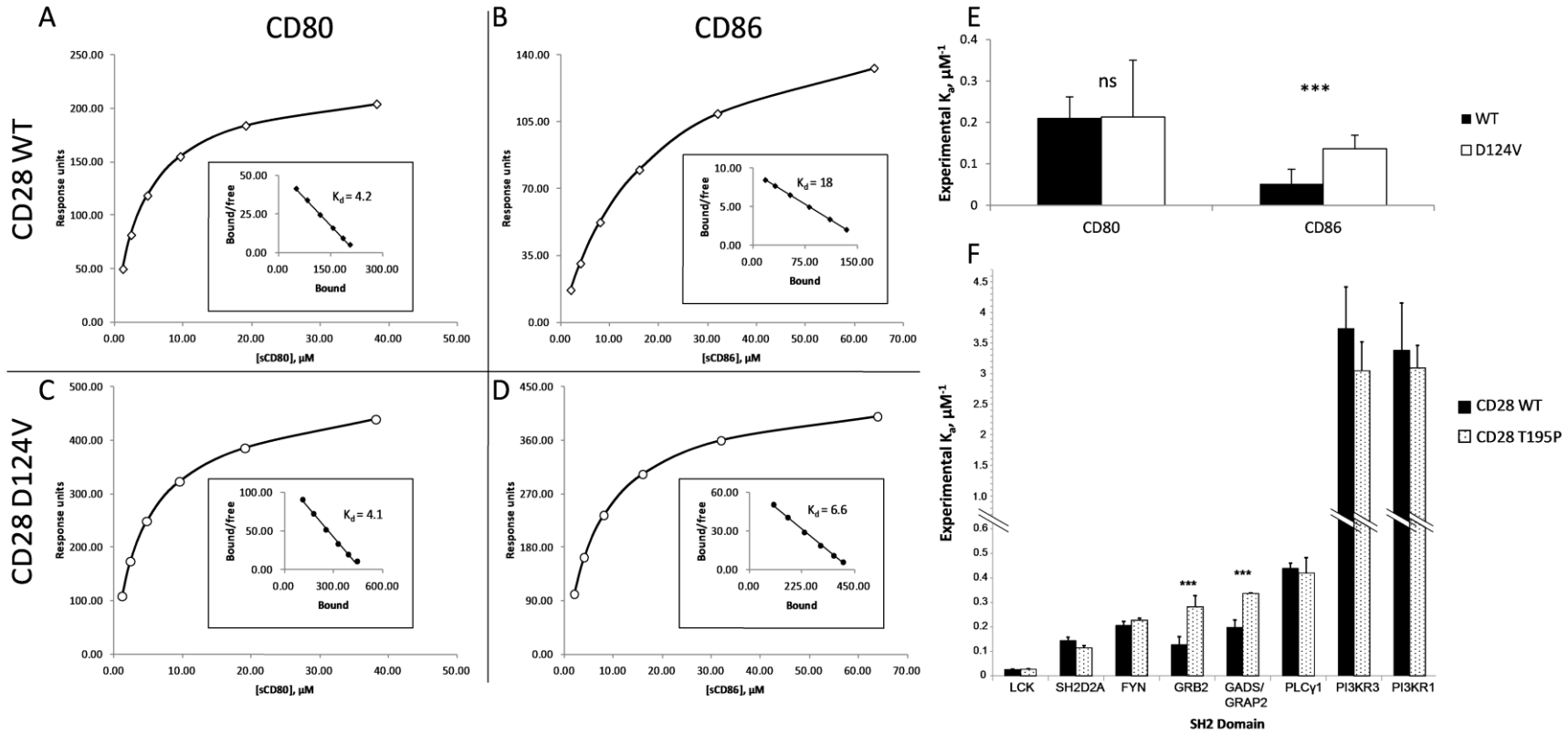

Figure 10. Differential binding affinities in CD28 WT and mutants. A-D: Binding affinities to B7 family ligands CD80 and CD86 were compared between CD28 WT and the D124V mutant. Representative curves of CD28 WT (A, B) and D124V (C, D) binding soluble CD80 (A, C) or CD86 (B, D). The inset Scatchard plot shows the regression for the dissociation constant K_d calculation. E: The values for the association constant K_a were experimentally determined six different times; the average and standard deviation are shown. ***: $p < 1x10^{-5}$ for 6 replicates; ns, not significant. F: CD28 tail motif phosphopeptides were indirectly immobilized in a flow cell and introduced to the SH2 domains of the indicated proteins. Relative affinities (mean ± standard deviation) for CD28 species experimentally determined for the SH2 domains from the indicated proteins. ***: $p < 1x10^{-5}$ for 8 replicates.

CD28 mutant T195P has a higher affinity for GRB2 and GADS/GRAP2 than the CD28 WT

The T195P mutation changes a polar amino acid to a hydrophobic one at the residue between the YMNM-containing SH2-binding motif and proximal PxxP-containing SH3-binding motif, essential mediators of adaptor protein binding during downstream signaling.[182] This mutant of CD28 is predicted to have a higher affinity for GRB2 than WT according to ScanSite.[183] To examine experimentally whether T195P alters the affinity of CD28 for adaptor proteins, we determined the affinity of this form of CD28 for several SH2 domains in known binding partners (Fig. 9). For two replicates, only GADS/GRAP2 and GRB2 showed significant differences, so each was assayed six more times. The CD28 T195P mutant had an average 1.7-fold greater affinity for GADS/GRAP2 and a 2.0-fold greater affinity for GRB2 than the CD28 WT ($p < 1x10^{-5}$ for both).

No complete crystal structure of the CD28 cytoplasmic domain is available, and it is likely intrinsically disordered. However, there is one model of a synthesized (non-native) CD28 phosphotyrosine motif interacting with the SH2 domain of the adaptor protein GRB2,[169] which we employed to build our model. The CD28 T195P mutation, which alters the lone residue between the SH2- and proximal SH3-binding motifs, was predicted to modify the conformation of the cytoplasmic tail C-terminal to the mutation (Fig. 10J-L). Interestingly, the HADDOCK model[164] predicts that the interaction with GRB2's SH2 domain is not directly altered. Rather, P196, within the adjacent SH3-binding motif, contorts significantly, potentially increasing the interaction between the CD28 P196 C_β and C_δ atoms and the side chains of GRB2 R142 and N143, respectively. Comparing wild-type CD28 to the T195P mutant, the distance between P196 C_β and the closest guanidino [-NHC(=NH)NH_2] group of GRB2 R142 is essentially unchanged (4.5 vs. 4.7Å). However, the distance between P196 C_δ and the closest amino group on

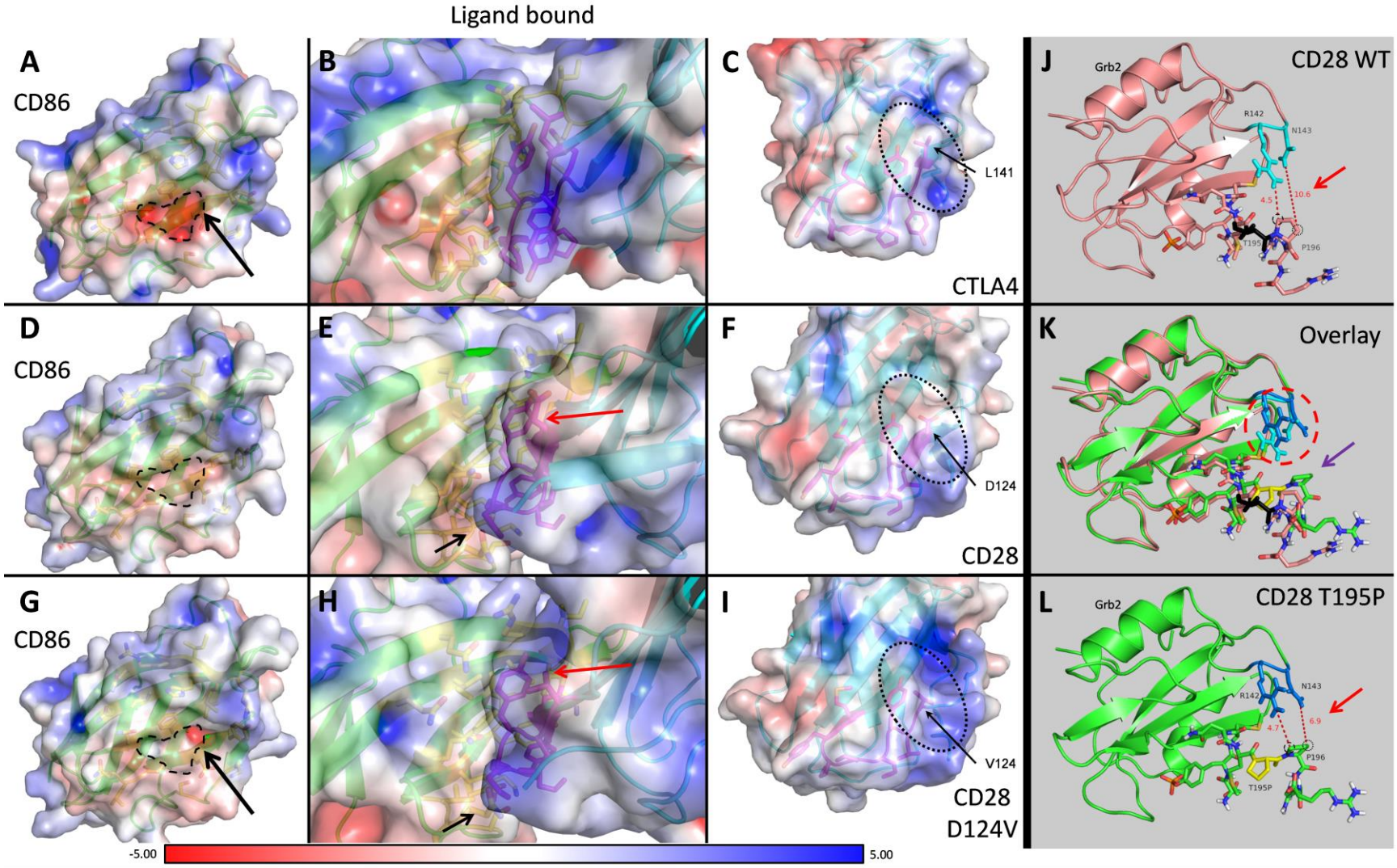

Figure 11. Protein modeling of CD28 WT and D124V interacting with CD86, and CD28 WT and T195P interacting with GRB2. Legend on following page.

Figure 11: Protein modeling of CD28 WT and D124V interacting with CD86, and CD28 WT and T195P interacting with GRB2. A-I: PyMOL models of CD86 bound to receptor CTLA4, CD28 WT, or CD28 D124V with APBS-generated electrostatic surfaces. A-C: CD86-CTLA4 interaction. The residue corresponding to D124 in CD28 (L141) is indicated in C and the protein surface in the vicinity of this residue has an overall positive charge (also apparent in B). The negatively charged binding surface of CD86 can be seen in A (dashed line and surrounding area). D-F: CD86-CD28 WT interaction. The surface around D124 is more neutral compared to CTLA4. G-I: CD86-CD28 D124V interaction. Replacement of the negatively charged aspartate residue leads to a more positively charged surface, similar to CTLA4. The orientation of several residues is changed (Y118 – red arrow, P121 – black arrow) between CD28 WT and CD28 D124V in these models. J-L: PyMOL models of the CD28 cytoplasmic tail with or without the T195P mutant binding adaptor protein GRB2. J, L: CD28 WT (J) and T195P (L) cytoplasmic tail binding GRB2 (J, salmon; L, chartreuse). T195 is colored black (J); T195P is colored yellow (L). Note the distances between CD28 P196 carbons C_β (black dotted circle) or C_δ (black dashed circle) and the closest non-hydrogen atoms on GRB2 (red arrows). CD28 P196 C_β moves from 10.6Å away from GRB2 N143 in the CD28 WT to 6.9Å in CD28 T195P. K: Overlay of CD28 WT versus T195P mutant binding of GRB2. There is a significant change in orientation of several CD28 residues: proximal SH3-domain P196 (purple arrow) rotates and approaches GRB2 N143 in the CD28 T195P mutant. GRB2 R142 and N143 have a strikingly different rotation in the CD28 T195P mutant compared to WT (red dashed circle).

GRB2 N143 decreases from 10.6 to 6.9Å, drawing it close enough to interact. Given the lack of constraints in this model that would be imposed by the remainder of the CD28 tail, these results must be interpreted with caution; however, they do provide a plausible explanation for the altered affinity.

VAV1 mutations: predicted affinity differences

The various apparent VAV1 point mutations (see Fig. 8) were not predicted to have any differential binding by ScanSite.[183] However, the VAV1-HNRNPM fusion was predicted to have an additional, high-affinity site for binding PLCG1, suggesting that the mutant may have a novel mechanism of activating PLCG1. This interaction could not be modeled because HNRNPM has no solved structure, and even by homology its structure could not be predicted due to its large, repetitive regions which do not appear to be

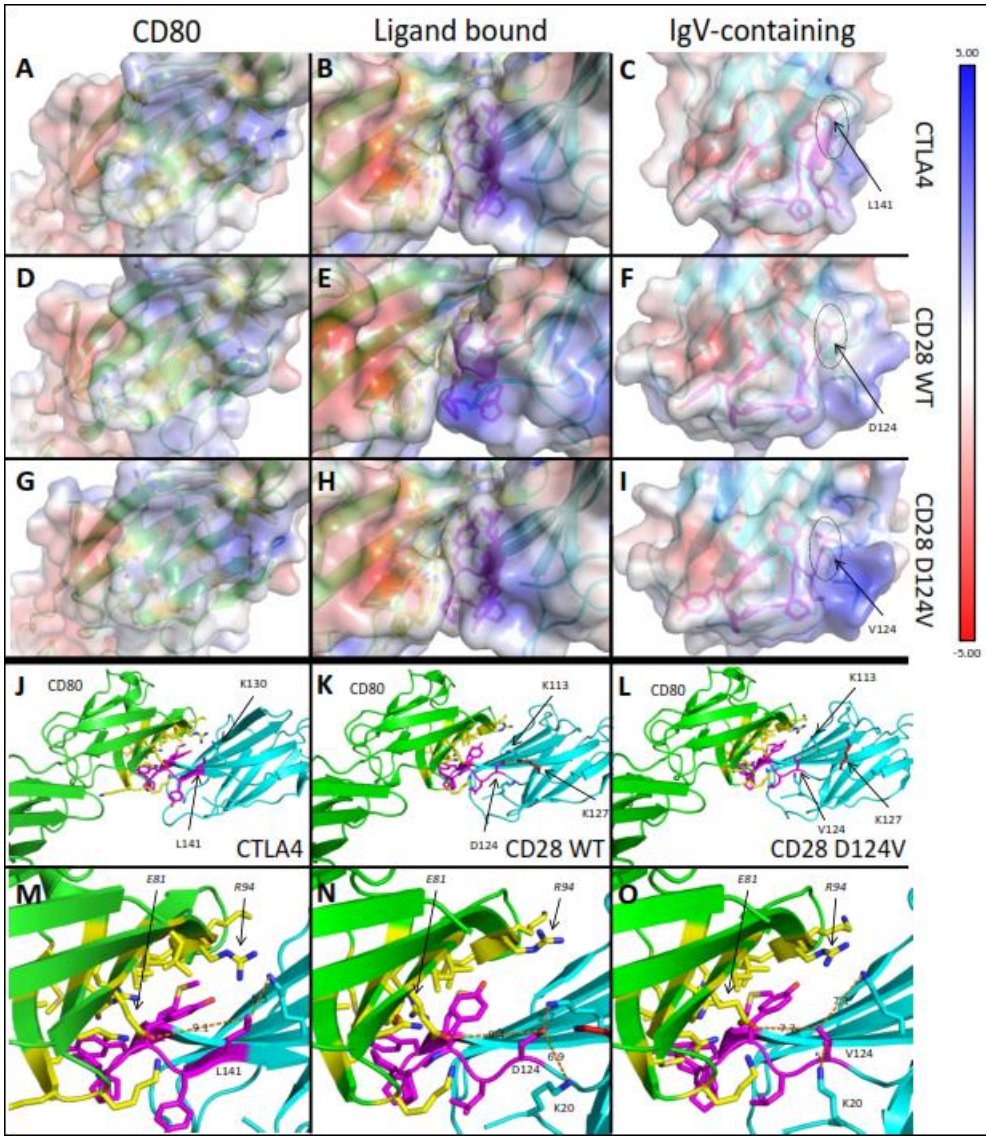

Figure 12. Molecular modeling of CD80 interacting with CTLA4, CD28 WT, and CD28 D124V. Legend on next page.

Figure 12: Molecular modeling of CD80 interacting with CTLA4, CD28 WT, and CD28 D124V. A-I: Surface diagrams of modeled interactions between CD80 and B7 family members as in Fig. 11. J-O: Cartoons of the same interactions; italicized and non-italicized labels indicate residues in CD28 or in the B7 family member, respectively. There are several notable differences between the CD80-CD28 WT interaction and that of CD80 and CD28 D124V. First, the surface of CD28 D124V near the mutated residue (Fig. 12I) is remarkably positively charged (bottom right), whereas in CD28 WT, the corresponding surface near residue D124 is more neutral (Fig. 12F). Upon examination of the residues interacting with D124 in CD28, the closest nitrogen (Nζ) of lysine 127 was found to be 2.1Å away from the oxygen group in D124 (Fig. 12K), likely due to electrostatic interaction and hydrogen bonding between the two side chains. The positive lysine approaching the negative aspartate cancels out both charges, leading to the neutral surface seen in the model. In CD28 D124V, the Nζ of K127 is 12.7Å from the closest carbon in V124 (Fig. 12L); as valine is hydrophobic, the positively charged lysine is repelled. This represents another significant difference. In CD28 WT, the amino nitrogen of K20 is 6.9Å from the closest oxygen of D124, whereas it is 5Å from the closest carbon atom in D124V despite the loss of electric attraction in the hydrophobic valine. This appears to be due to the electrostatic repulsion and/or steric hindrance from the attracted K127 in CD28 WT. Thus, K20 contributes to the positive surface charge in CD28 D124V described above, whereas in CD28 the charge is mitigated by D124. Additionally, this movement of K20 makes it closer to E81 in CD80 in the CD28 D124V mutant compared to the WT (6.0 vs. 9.8Å), suggesting additional electrostatic stabilization in the interaction of the mutant. CTLA-4 does not have a positively charged residue in the equivalent location. Comparing the interacting residues near and within the MYPPPY “antigen-binding” site of CD28 WT, CD28 D124V, and CTLA4 interacting with CD80, CTLA4 and CD28 D124V are more similar in distance from CD80 than CD28 WT (Table 1; Fig. 12M-O). Also of note, compared to the most negatively charged interaction surface of CD86 (Fig. 11), the corresponding surface of CD80 is notably more neutral or tending toward positively charged (Fig. 12A, D, G). This suggests a different mechanism for the improved activation of CD28 D124V, as delineated above.

anchored intrinsically. It is possible that HNRNPM is largely intrinsically disordered and can only hold a structure when in complex with nucleic acid through its RNA recognition motifs (RRMs).

Considering that the VAV1 point mutations only occurred in one case each, there are wide potential differences in affinities for binding partner through each unique site. These have not so far been modeled because they have not yet been confirmed as true mutations.

Intermolecular measurements

			Distance (Å) from CD80 atom		
CD28 (CTLA4) atom	**CD80 atom**	**Interaction type**	**CTLA4**	**CD28 WT**	**CD28 D124V**
K20-Nζ	E81-O	Hydrogen bond		9.8	6.0
M117(134)-Sδ	R92-NH	Hydrogen bond	4.4	3.8	3.4
P121(138)-Cγ	K36-Cγ	Dispersion forces	5.1	6.2	4.6
P121(138)-Cγ	K36-Cδ	Dispersion forces	4.6	5.7	3.7
Y122(139)-OH	R94-N1	Hydrogen bond	4.1	5.8	5.3
L123(Y140)-Cδ	K36-Cδ	Dispersion forces	4.5	7.2	3.2
L141-Cδ	E81-O	Dispersion forces	9.1		
D124-O		Hydrogen bond		9.4	
V124-Cγ		Dispersion forces			7.7

Intramolecular measurements

			Distance (Å) from Atom 2		
CD28 (CTLA4) atom 1	**Atom 2**	**Interaction type**	**CTLA4**	**CD28 WT**	**CD28 D124V**
K20-Nζ	D124-O	Hydrogen bond		6.9	
	V124-Cγ	Dispersion forces			5.0
K113(130)-Nζ	L141-Cδ	Dispersion forces	5.5		
	D124-O	Hydrogen bond		2.7	
	V124-Cγ	Dispersion forces			7.1
Y122(139)-Cε	L141-Cδ	Dispersion forces	5.1		
	D124-Cβ	Dispersion forces		4.8	
	V124-Cγ	Dispersion forces			3.7
K127-Nζ	D124-O	Hydrogen bond		2.1	
	V124-Cγ	Dispersion forces			12.7

Table 10: Inter- and intramolecular distances in the CD80-CTLA4, CD80-CD28WT, and CD80-CD28D124V interactions models. The distances between interacting atoms were calculated in PyMOL.

CD28 mutants alter transcription and induce higher NF-κB pathway activation than CD28 WT

To determine whether these mutations alter the kinetics or magnitude of CD28 signaling, we examined the expression of transcripts previously determined to be regulated upon CD28 ligand binding in Jurkat and/or $CD4^+$ T-cells.[184] Jurkat cells transduced with CD28 WT or mutants with similar levels of expression (Figure 13) were incubated for the indicated times with beads ligated with anti-CD3 antibody and CD86. CD28-positive Jurkat cells were chosen instead of CD28-null for this experiment to best model the heterozygous-mutant tumor as only one allele in the tumor cells is expected to be mutated.

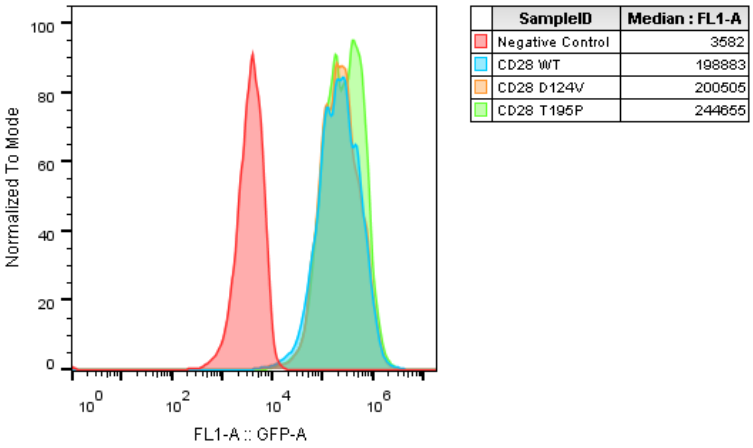

Figure 13: GFP expression in CD28 mutant- or WT-expressing Jurkat cell lines. Jurkat cells retrovirally transfected with pMIG-CD28 plasmids as described in the Materials and Methods were assessed for GFP expression by flow cytometry on an Accuri C6 cytometer.

Expression profiles were similar among the samples (Figure 14A); the Nanostring method, which directly counts the number of transcripts in a given sample, was chosen because it has greater reproducibility than qPCR.[174] Two of the assayed genes, *CD226* and *TNFA*, showed upregulation in CD28 T195P over WT (Fig. 14B, 14C). No assessed transcript was significantly different between CD28 D124V and WT.

An NF-κB reporter vector was transfected into these Jurkat cells, and the cells were exposed to beads coated with anti-CD3 and either CD80 or CD86 (Fig. 14D). Compared to Jurkat cells transduced with CD28 WT, D124V showed a 1.9-fold greater NF-κB induction in response to CD80 and a 1.7-fold greater induction to CD86. T195P showed 1.5-fold and 1.8-fold higher NF-κB induction to CD80 and CD86, respectively. The increase in activation by the D124V mutant did not significantly differ between CD80 and CD86, an unexpected finding given the difference seen in the SPR (Fig. 10). We also compared the GEPs of the six CD28-mutant AITL cases to those of CD28 WT AITL cases and found 178 differentially-regulated genes (Figure 15A). Gene set enrichment analysis (GSEA) showed several differentially regulated pathways, most notably an increased T-cell signal transduction signature in CD28 mutant cases and a higher B-cell development signature in CD28 WT cases (Fig. 15B-I).

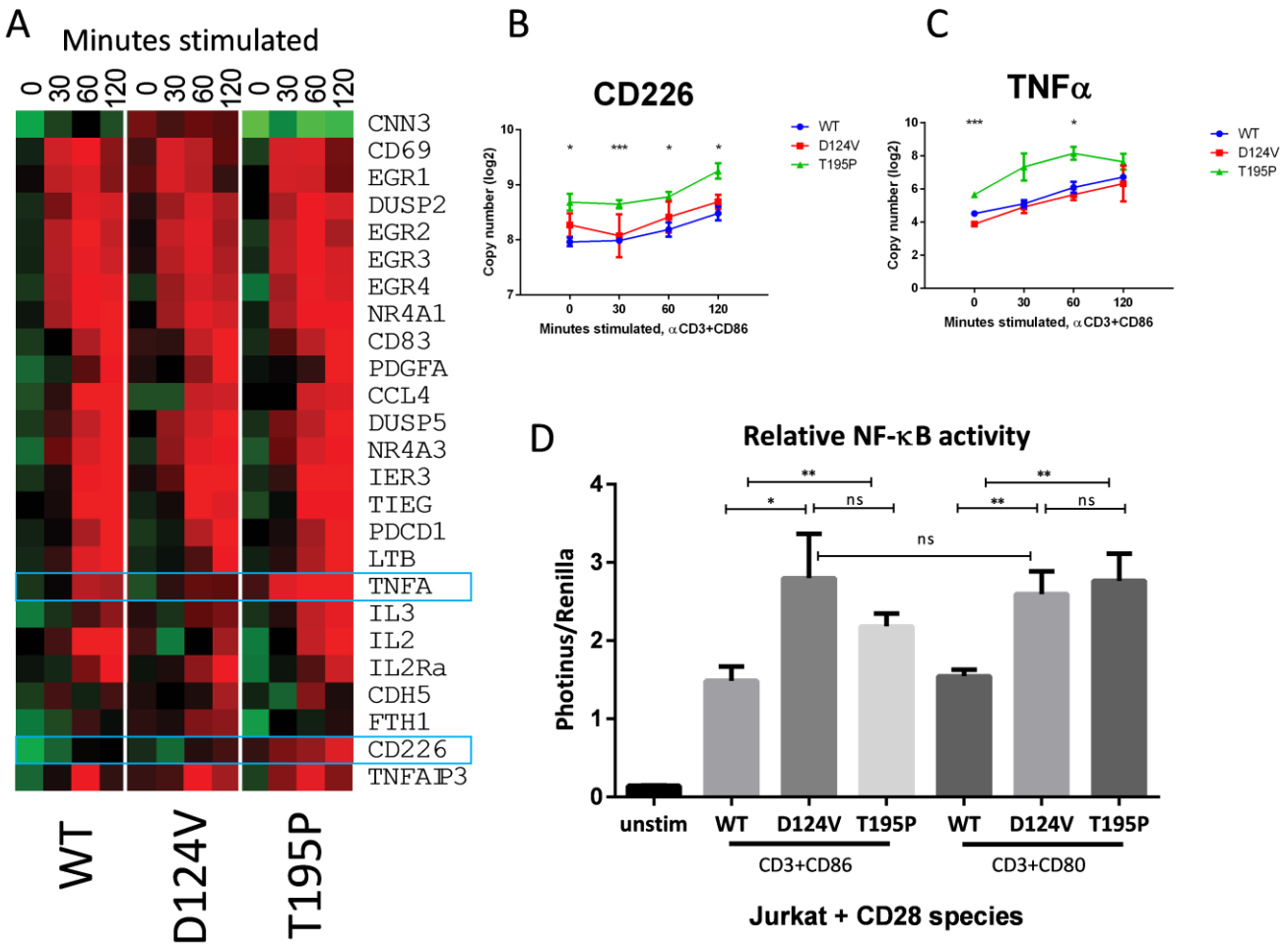

Figure 14. CD28 D124V and T195P mutants alter transcriptional profiles and increase NF-κB signaling in response to CD28 ligation. Legend on following page.

Figure 14. CD28 D124V and T195P mutants alter transcriptional profiles and increase NF-κB signaling in response to CD28 ligation. A: Jurkat cells stably transduced with GFP-containing retroviral constructs expressing CD28 WT or mutants were stimulated with beads ligated with anti-CD3+CD86 for the indicated time, and specific transcripts were quantitated using the Nanostring nCounter. The heat map was constructed from comparative expression profiling of the indicated genes. B-C: Two transcripts, *CD226* and *TNFA*, showed significantly increased expression in cells expressing the CD28 T195P mutant. *: $p<0.05$ between T195P and WT; ***: $p<0.005$ between T195P and WT. There is no significant difference between the D124V and WT. D: Luciferase reporters of NF-κB activation were transduced into Jurkat cells expressing the indicated CD28 transgene and stimulated with the indicated beads for four hours. Diagram averages three replicates. *, $p<0.05$; **, $p<0.01$; ns, not significant. Both CD28 mutants activated NF-κB more strongly than WT upon ligation of CD80 or CD86 with CD3 stimulation.

VAV1-HNRNPM fusion protein characterization

To understand the function of the VAV1-HNRNPM fusion protein, the entire fusion protein was cloned. For controls, VAV1 only N-terminal to the junction (Vav1-front), the entirety of VAV1 (VAV1-whole), or HNRNPM C-terminal to the junction (back-HNRNPM) were also cloned (Figure 16). The VAV1-containing constructs have a triple FLAG tag on the N-terminus; the HNRNPM-only construct has a triple FLAG tag on its C-terminus. The pBABE-based vectors were stably transfected into J.vav1 cells (a VAV1-null derivative of the Jurkat T-cell line), and cells were stained for the location of the FLAG tag (Figure 17). VAV1-HNRNPM showed mostly cytoplasmic staining with some nuclear puncta, suggesting primarily cytoplasmic localization.

The pBABE-puro constructs unfortunately progressively lost FLAG signal over several passages while retaining resistance to puromycin selection, so the constructs were recloned into the pMIT vector and selected based on quantity of murine Thy1.1 expression (Figure 18) for the remaining functional analyses. Each has only one or two replicates, so results must be interpreted cautiously.

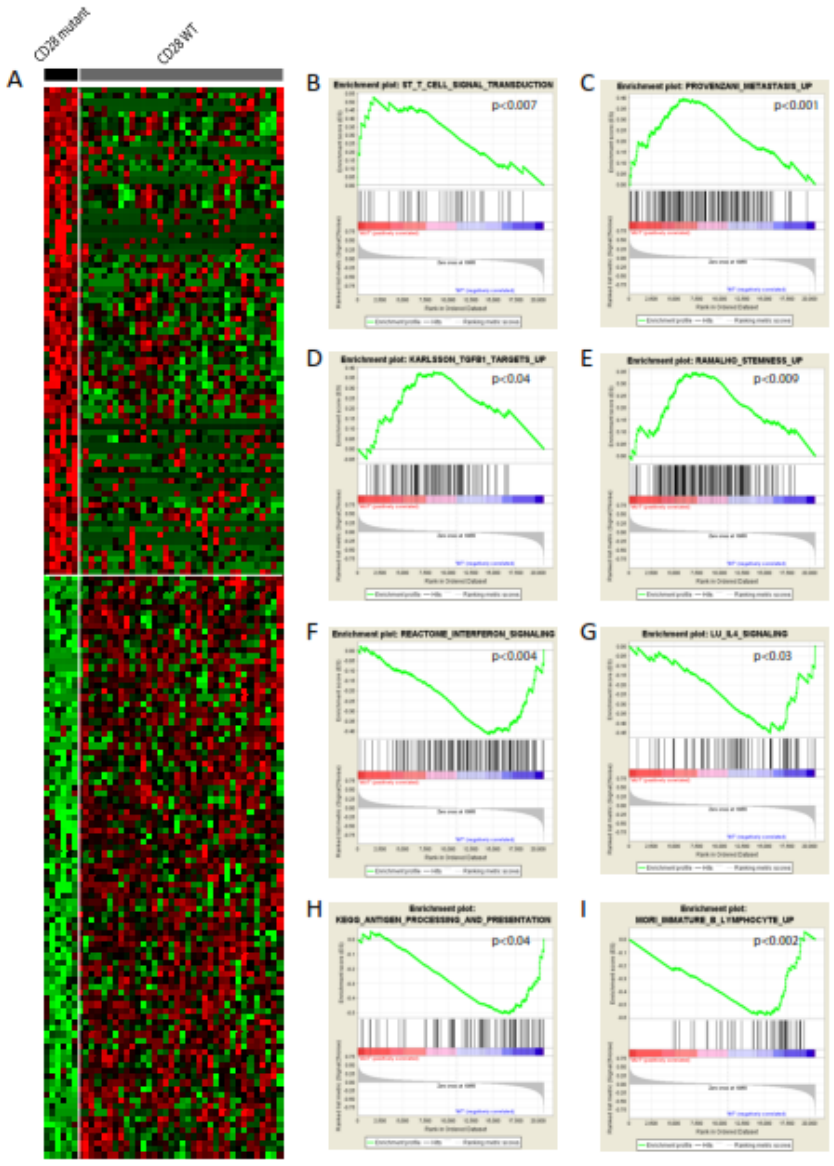

Figure 15: Gene expression profiling (GEP) and gene set enrichment analysis (GSEA) on CD28 mutant versus CD28 WT AITL cases. AITL cases with a high expression of D124 or T195 mutations (6 total) were compared to CD28-WT AITL cases. A: There were 178 genes with significant differential expression, $p<0.005$. B-G: GSEA on the expression profiles of CD28-mutant versus CD28-WT cases. Notably, the T-cell signal transduction signature (B) was overexpressed in the CD28 mutant group, as was the metastatic signature (C), the TGFβ pathway (D), and the stem cell signature (E). F-I: CD28 mutant cases underexpressed the IFNγ signaling, IL4 signaling, antigen processing, and pre-B lymphoma pathways, respectively.

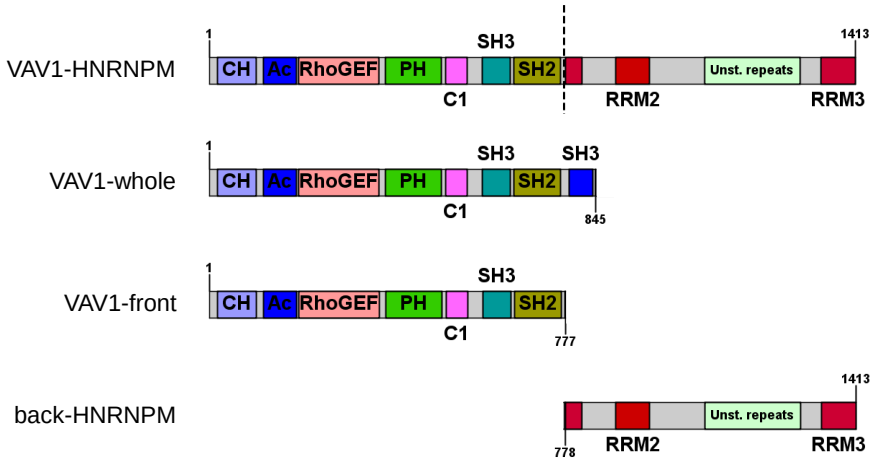

Figure 16. VAV1-HNRNPM construct and controls. Domain names and amino acid positions are indicated. The three VAV1-containing constructs have a triple FLAG tag on the N'-terminus; the back-HNRNPM construct has a triple FLAG on the C-terminus.

J.vav1 cells transfected with constructs or empty control, or the WT Jurkat, were assessed for proliferative capacity by carboxyfluorescein succinimidyl ester (CFSE) dye dilution (Figure 19). The fusion-containing cells have slightly higher fluorescence levels at later timepoints, suggesting a slightly lower proliferation level, and all J.vav1 cell lines had lower proliferative capacity than Jurkat. Notably, expression of WT VAV1 in J.vav1 cells did not reconstitute the proliferation seen in Jurkat.

These cells were also assessed for capacity to upregulate CD69, a marker of activation, during stimulation. The fusion-containing cells had lower CD69 expression at 24 hours of stimulation than cells expressing the other constructs (Figure 20).

Expression of VAV1 was assessed by intracellular flow cytometry. VAV1 was seen in all expected samples (Figure 21). However, the Jurkat cell did not show particularly good staining.

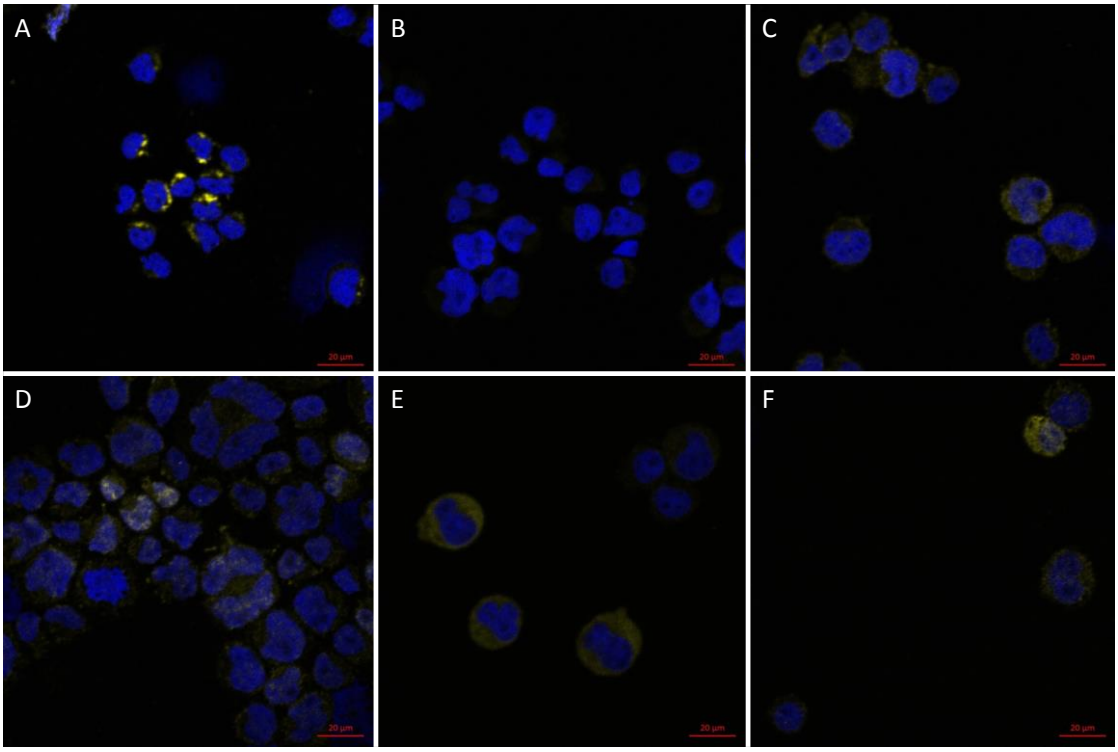

Figure 17. Cellular localization of VAV1-HNRNPM and related constructs using the FLAG tag. A-B. IDH2-FLAG Jurkat cells (A) stain in their mitochondria, and J.vav1 cells (B) have no staining. C. VAV1-HNRNPM cells have mostly cytoplasmic FLAG expression with distinct nuclear puncta. VAV1-front cells (D) and back-HNRNPM cells (F) have pancellular expression, whereas VAV1-whole cells have the expected exclusively cytoplasmic expression.

The importance of VAV1 in the initiation of calcium flux in T-cell activation is well-described, and the VAV1-HNRNPM fusion has a high predicted affinity for PLCG1 via a site on HNRNPM (see "VAV1 mutations – predicted affinity differences). Therefore, calcium flux in stimulation was assessed by flow cytometry. For two replicates, very little difference was seen, with the fusion-containing cells fluxing faster than empty vector but slower than other transfected cells (Figure 22).

To assess the effects of the fusion on transcription, cells were stimulated for 8 hours then interrogated using the Nanostring codeset described above. For one replicate, several genes were significantly upregulated compared to controls (Figure 23). Notably,

CCL4, CD69, CD83, IER3, LTB, TIEG, TNFAIP3, and TNFA, all of which are early activation response genes, have a large number of reads in the VAV1-HNRNPM sample, higher than the Jurkat Vav1^{+} control. The VAV1-whole and VAV1-front control-expressing cells also have higher expression of many of these than Jurkat, and usually higher than the VAV1-HNRNPM-expressing cells.

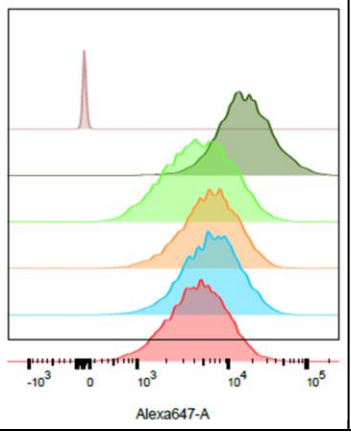

Figure 18. Thy1.1 expression of VAV1 constructs. Each transfected J.vav1 line has similar Thy1.1 levels. Untransfected cells have no Thy1.1 expression.

	Sample Name	Subset Name	Count
	Controls_Jvav1.fcs	Single Cells	9563
	Transfected_MP-low.fcs	Single Cells	9585
	Transfected_TP-low.fcs	Single Cells	9587
	Transfected_3P-low.fcs	Single Cells	9564
	Transfected_RP-low.fcs	Single Cells	9600
	Transfected_QP-low.fcs	Single Cells	9594

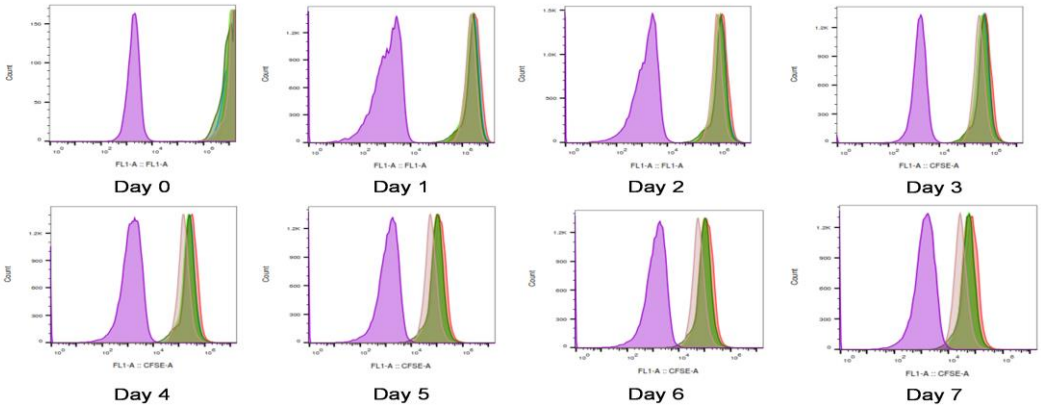

	Sample Name
	A08 DMSO only (M).fcs
	A07 Jurkat.fcs
	A06 Empty-pMIT.fcs
	A05 back-HNRNPM.fcs
	A04 Vav1-whole.fcs
	A03 Vav1-front.fcs
	A02 Vav1-HNRNPM.fcs

Figure 19. CFSE proliferation assay. Cells of each line indicated in the legend were analyzed over one week for proliferation capacity.

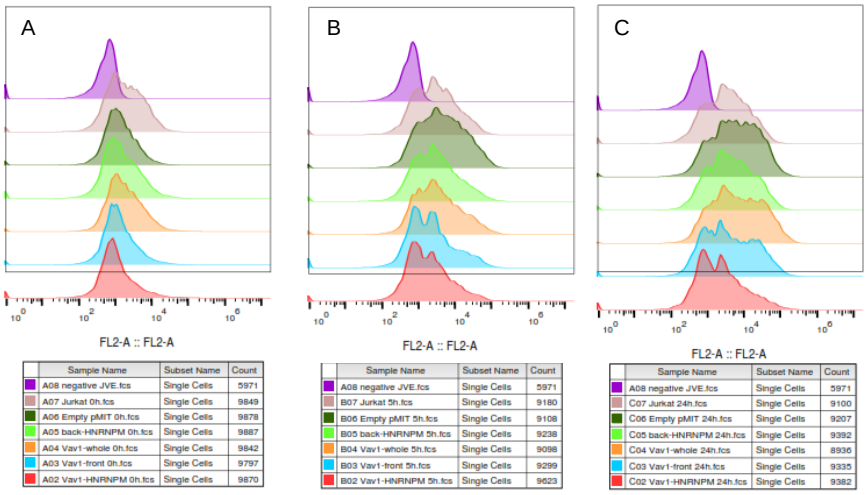

Sample Name	Subset Name	Count
A08 negative JVE.fcs	Single Cells	5971
A07 Jurkat 0h.fcs	Single Cells	9849
A06 Empty pMIT 0h.fcs	Single Cells	9878
A05 back-HNRNPM 0h.fcs	Single Cells	9887
A04 Vav1-whole 0h.fcs	Single Cells	9842
A03 Vav1-front 0h.fcs	Single Cells	9797
A02 Vav1-HNRNPM 0h.fcs	Single Cells	9870

Sample Name	Subset Name	Count
A08 negative JVE.fcs	Single Cells	5971
B07 Jurkat 5h.fcs	Single Cells	9180
B06 Empty pMIT 5h.fcs	Single Cells	9108
B05 back-HNRNPM 5h.fcs	Single Cells	9238
B04 Vav1-whole 5h.fcs	Single Cells	9098
B03 Vav1-front 5h.fcs	Single Cells	9299
B02 Vav1-HNRNPM 5h.fcs	Single Cells	9623

Sample Name	Subset Name	Count
A08 negative JVE.fcs	Single Cells	5971
C07 Jurkat 24h.fcs	Single Cells	9100
C06 Empty pMIT 24h.fcs	Single Cells	9207
C05 back-HNRNPM 24h.fcs	Single Cells	9392
C04 Vav1-whole 24h.fcs	Single Cells	8936
C03 Vav1-front 24h.fcs	Single Cells	9335
C02 Vav1-HNRNPM 24h.fcs	Single Cells	9382

Figure 20. Increased expression of CD69 in response to stimulation. Transfected cells plus wild-type Jurkat were stimulated for zero (A), 5 (B) or 24 (C) hours with CD3/CD28 beads, and surface expression of CD69 was assessed by flow cytometry.

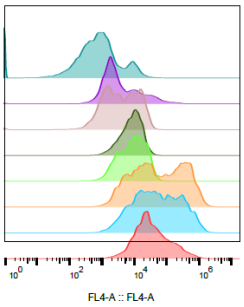

Sample Name	Subset Name	Count
A09 Jurkat no primary.fcs	Ungated	11384
A08 Jurkat.fcs	Single Cells	4761
A07 J.vav1-EcR.fcs	Single Cells	4685
A06 pMIT-empty Thy1-high.fcs	Single Cells	4809
A05 back-HNRNPM Thy1-high.fcs	Single Cells	4785
A04 Vav1-whole Thy1-high.fcs	Single Cells	4594
A03 Vav1-front Thy1-high.fcs	Single Cells	4748
A02 Vav1-HNRNPM Thy1-high.fcs	Single Cells	4748

Figure 21. Intracellular expression of VAV1. Cells were permeabilized and stained for VAV1, then assessed by flow cytometry.

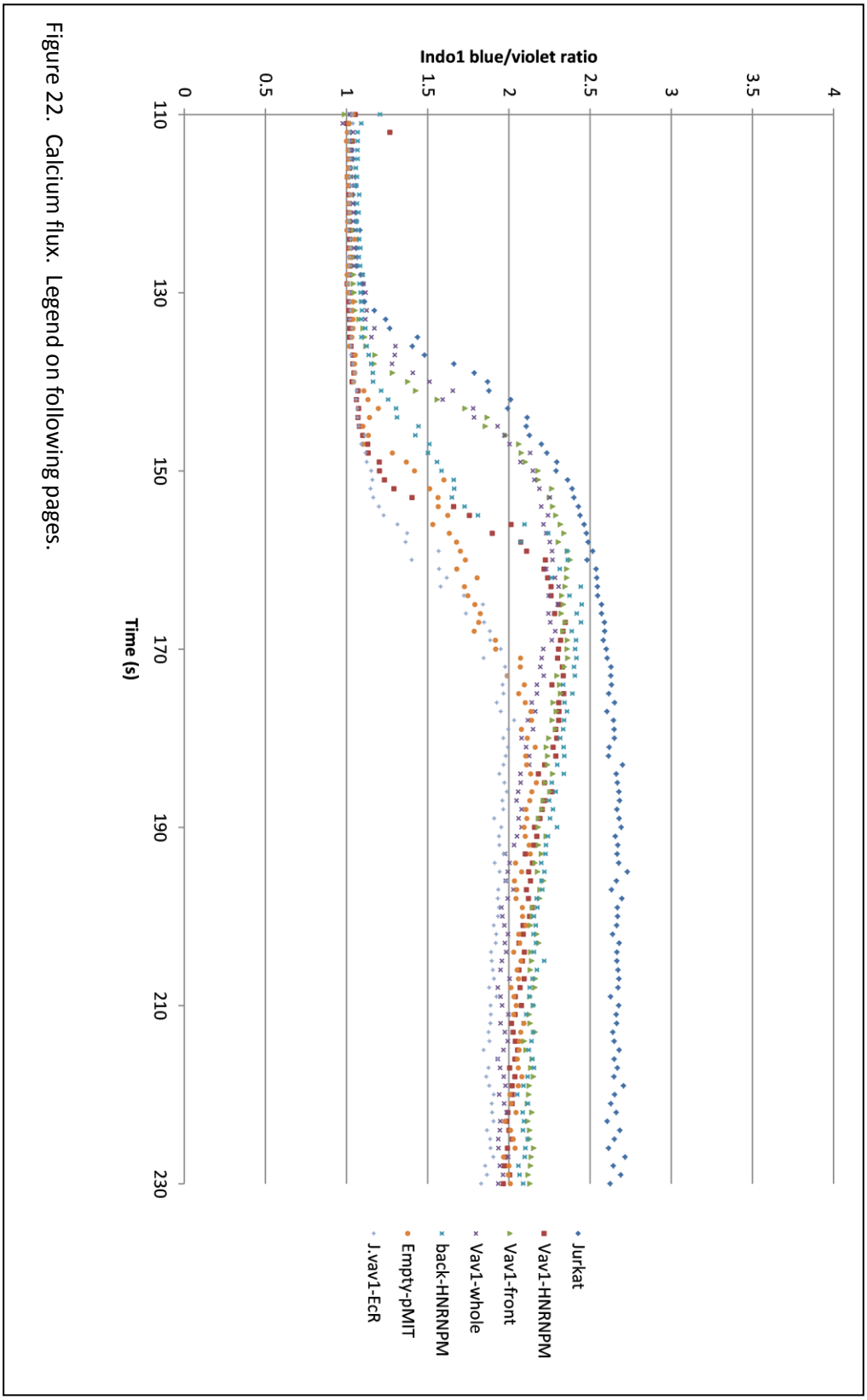

Figure 22. Calcium flux. Legend on following pages.

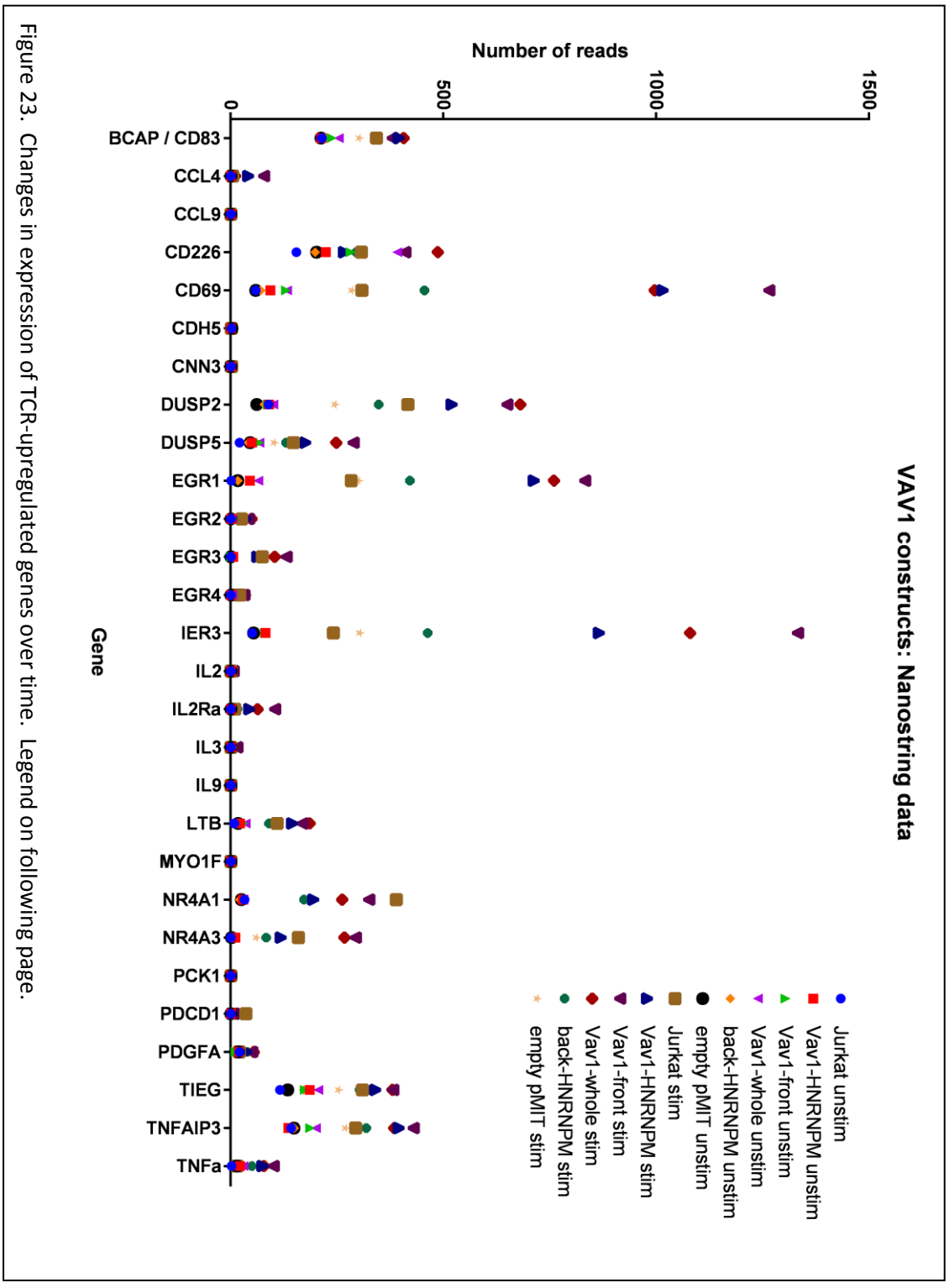

Figure 23. Changes in expression of TCR-upregulated genes over time. Legend on following page.

Figure 22. Changes in expression of TCR-upregulated genes over time. Transfected cells or wild-type Jurkat were stimulated or not for 8 hours with CD3/CD28 beads, and RNA levels were directly assessed. The VAV1-HNRNPM cells (red square and upright blue triangle) notably upregulated many targets higher than Jurkat (blue circle and brown square), including CD69, and IER3. The VAV1-whole and VAV1-front controls, however, upregulated most of the targets greater than Jurkat as well.

Figure 23. Calcium flux. Transfected cells or wild-type Jurkat were stimulated and degree of calcium flux was measured. Jurkat cells (top blue line) show the expected kinetics and degree of flux. Empty vector and EcR-transfected J.vav1 cells (bottom orange circle and gray crosses, respectively) show characteristic delay of influx and lower maximum levels, plus low sustainability. Cells with VAV1-front and VAV1-whole (green triangle and purple "X", respectively) have a similar early kinetic profile to Jurkat cells but cannot sustain the influx. Cells with VAV1-HNRNPM and back-HNRNPM display an intermediate kinetic profiles. Average of two replicates, normalized to baseline values.

CHAPTER 3: DISCUSSION AND DIRECTIONS FOR FUTURE STUDY[3]

CD28 and VAV1 mutations

Gene expression profiling analysis has pointed to a strong T-cell receptor signal in peripheral T-cell lymphomas, both for AITL and PTCL, NOS. This work explores the outcomes of mechanisms by which increased or constitutive activation of the T-cell receptor pathway may occur: mutation of proximal signal molecules. Sequencing data on 105 PTCL, NOS and AITL cases showed a fusion and recurrent mutations in CD28, the canonical T-cell co-stimulatory receptor, as well as several mutations and a fusion in VAV1. These molecules sit at the earliest stages of signal transduction through the TCR, and in both cases, their proper function is necessary to propagate and sustain T-cell activation. Recent sequencing studies on PTCLs, particularly AITL, have shown frequent mutations in RHOA and in the epigenetic modifiers TET2, DNMT3A, and IDH2, as well as less frequent mutations affecting TCR signaling proteins, including FYN. Our study finds similar frequencies and locations of TET2 mutations in AITL and other types of PTCL as previously determined, and we show that the less frequent CD28 mutations may play a role in promoting TCR and NF-κB signaling.

CD28 is the canonical co-stimulatory receptor which is activated by B7-family ligand while MHC binds the CD3/TCR complex with co-receptor CD4 (or CD8, though for the purpose of the diseases discussed in this thesis, CD4 is the operative molecule). Upon ligation, the CD28 intracellular domain's SH2- and SH3-binding motifs bind and a

[3] Sections of the discussion are based on Rohr et al. 2015 (ref. 122)

multitude of signaling proteins, notably, GRB2, PI3K, ITK, LCK, PKCθ, and FYN. These activated intermediates initiate major shifts in cellular metabolism, motility, and transcription status in concert with CD3/TCR activation. Although the TCR provides the major stimulatory signal, co-stimulator activation is required to maintain activation and allow the T-cell to assume its effector function. Co-inhibitory B7 family receptors, including CTLA4 and PD1, among others, compete with CD28. In addition to directly competing for ligand, the B7 family co-inhibitors can decrease CD3/CD28 signaling through direct and indirect interaction with signaling intermediates.

The cancer samples in this study show recurrent mutations of CD28 at two residues: aspartate 124, which is immediately adjacent to the six-amino acid MYPPPY "antigen-binding" motif, and threonine 195, which is between the SH2- and N-terminal SH3-binding motifs. One mutation at each residue (D124V and T195P) was found to have a higher affinity for binding partner by SPR and each was found to induce higher NF-κB activation than CD28 WT when stimulated. For T195P, there were also notable transcriptional differences upon activation. The interactions were modeled to identify the potential mechanism by which the increased affinity may occur.

The fusion transcript between ICOS and CD28 is driven by the ICOS promoter, most likely as a result of partial tandem duplication of the *CD28-ICOS-CTLA4* locus. Because ICOS is highly expressed in AITL, it is expected that this fusion can drive higher CD28 expression (Figure 7). However, the signal peptide, encoded by the first exon of ICOS, is cleaved from the final protein, such that the product only contains CD28 with the mutation. Recently reported cases of Sézary syndrome had a CTLA4-CD28 fusion, whose expression is expected to be driven by CTLA4; in this case, the extracellular domain of CD28 is replaced by CTLA4, which augments CD28 intracellular signaling through the higher-affinity CTLA4 extracellular domain.[178,179] A study on adult T-cell leukemia/lymphoma found rare CD28 D124, T195, and F51 mutations, *ICOS-CD28* and

CTLA4-CD28 fusion transcripts, and copy number increases of *CD28*.[180] Although we found no CTLA4-CD28 fusions, we show that enhanced CD28 pathway activation can be achieved also through mutation. The D124V mutant, which occurs adjacent to the extracellular ligand-binding site, has an increased affinity for ligand CD86 shown by modeling and SPR analysis (Figures 10 and 11). Our modeling of the interaction between CD86 and CD28 indicates that the increased affinity of the D124V mutant is likely due to improved electrostatic interactions as opposed to steric or hydrophobic factors. There is also evidence of enhanced downstream target activation. The fact that the D124V mutant has the same NF-κB activation with either CD80 or CD86 stimulation is unexpected based on the binding analysis (Fig. 14) which shows CD86, but not CD80, having a higher affinity for the D124V mutant. The model of the CD80-CD28 interaction shows several interactions that could explain these findings (Fig. 12). On the cell surface, the orientation of CD28 homodimers is highly constrained, whereas in the SPR flow cell, they are three-dimensionally unconstrained. Three-dimensional K_a measurements by SPR of TCR/MHC interactions are approximately 1000-fold lower than the same analysis in two dimensions. Thus, it is possible that a difference in affinity for CD80 between WT and mutant CD28 when confined to the plasma membrane may not be apparent by SPR analysis. Also, crystal structures of the modeled complexes would be useful, as they may reveal changes not predicted by the molecular modeling.

Interestingly, CD28 expression in multiple myeloma has been shown to alter myeloma proliferation and survival,[185] and to be predictive of disease progression and relapse in conjunction with CD86, but not CD80, expression.[186,187]

There are several possible mechanisms by which increased ligand affinity may augment CD28 signaling. First, the increased affinity for SH2-containing adaptor proteins may directly increase CD28 signaling. Another possibility is through reduced receptor-mediated endocytosis. The PI3K regulatory subunit's SH2 domain binds to the

phosphotyrosine motif of the CD28 cytoplasmic tail and effects a wide range of changes, including CD28 receptor internalization. Our binding assays show no significant difference between the CD28 WT and CD28 T195P binding of PI3K regulatory subunits (Fig. 10). Because GRB2 and GADS/GRAP2 have a significantly higher affinity for the T195P mutant tail over WT, perhaps these adaptor proteins outcompete PI3K for binding to the CD28 SH2-binding motif and thereby compromise CD28 endocytosis. A decreased downregulation of CD28 signaling would have the same effect as direct over-activation, e.g. to augment cell cycling, proliferation, and cytokine production.

Analysis of gene expression using nCounter (Fig. 14) showed enhanced upregulation of two CD28-responsive genes, CD226 and TNFA, by CD28 T195P compared to WT. CD226 is crucial for T_{FH} differentiation and can significantly modulate T-cell function by outcompeting its inhibitor TIGIT to bind receptor CD155.[188] TNFA is a potent cytokine that enhances proliferation, in part by inducing IκB-kinase phosphorylation and NF-κB activation.[189] It is also interesting that CD28-mutant AITL cases showed upregulation of the T-cell signal transduction signature over CD28 WT AITL cases (Fig. 7). One major consequence of TCR/CD28 signaling is the activation of the NF-κB signaling pathway, and both mutants demonstrate enhanced NF-κB activity using a luciferase reporter assay. Taken together, these data support the notion that the two CD28 mutations explored in this study may impart a functional advantage to CD28-mutant T-cells.

One other mutation hotspot in CD28 was identified in our screen, as found in previous studies: phenylalanine 51, which we found to be mutated to leucine or valine. However, these cases had extremely low variant frequency in the sequencing platform, and none of the mutations were able to be verified by digital droplet PCR. Other studies have also identified F51 mutations in PTCLs, including Sézary syndrome,[179] ATLL,[180] and AITL,[128] and we also found these mutations using our analysis pipeline (Table 9);

mutation of F51 was found to increase proliferation in a CTCL model.[179] Thus, despite the negative PCR data, it seems plausible that the F51 mutations are real but subclonal. Still, we cannot be certain.

The clonality or subclonality of various mutations in lymphoma is important for considering how cancers can become resistant to treatments. In the natural history of many cancers, including AITL and PTCL, NOS, there is often an initial response to chemotherapy resulting in decreased tumor size on imaging, but frequently cancers evolve to be resistant to treatment. As discussed in "Treatment and outcomes," PTCLs tend to relapse, often within the first few months after treatment begins. It is likely that relapse is caused by some subclone within a cancer which has a survival or proliferation advantage that allows it to grow even in the presence of the chemotherapy. We hypothesize that activating mutations of CD28 may give a clone a survival advantage, and thus be the population that survives chemotherapeutic insult. The only way to test this would be to have more samples. Ideally, there could be serial samples from the same patient to track mutational changes as has been done in diffuse large B-cell lymphoma[190] and others. A good start would be to get at least some samples that are known relapse after clinical remission. However, standard-of-care does not include rebiopsy for PTCLs unless there is clinical suspicion of a different malignancy or other concern, so there needs to be a concerted effort to collect and sequence relapsed PTCL cases in order to test whether CD28 or any other mutation is tied to risk of an event after treatment.

This study also finds and validates a gene fusion in which VAV1 participates, and identifies several putative mutations from WTS and WES data. GRB2, LCK, FYN, and other early TCR intermediates such as LAT and SLP76 directly or indirectly activate VAV1, a guanine exchange factor (GEF) that activates Rho family members including CDC42, RAC1, and RHOA, which regulate a multitude of intermediates in later signal transduction. Particularly, VAV1 is important in actin remodeling, calcium flux, and a

variety of pathways leading to transcriptional upregulation of activation-induced cytokines and other proteins via NFAT and NF-κB, among others. There are three VAV family proteins, but VAV1 is the most specific to, and most important for, the hematopoietic system.

Adult T-cell leukemia/lymphoma (ATLL), another PTCL subtype with fairly poor prognosis, has a well-defined, almost exclusive, association with infection by the human T-lymphotrophic retrovirus (HTLV-1). It is characterized by high TCR activation levels as well. As discussed above, a recent study examining an extremely large cohort (n=426) found great numbers of mutations throughout the genome.[180] Notably, ATLLs had a variety of mutations within TCR-associated proteins, many of which are or are predicted to be activating. There were also several fusion proteins involving the B7 family receptors CTLA4, CD28, and ICOS, all of which put the activating CD28 cytoplasmic domain under control of promotors of the inhibitory CTLA4, and increased copy number of *CD28*. There were also several recurrent mutations in VAV1 and PLCG1 which likely also function to positively regulate signaling. Why another AITL study in addition to this ATLL study found PLCG1 mutants whereas our samples had none is unclear. Possibly it has to do with the geographic and ethnic differences among the various populations as well as inherent differences between different subtypes of PTCLs. Further, one study found a high proportion (ten percent of their cohort) of CTLA4-CD28 fusions in various PTCL entities.[191] This number, frankly, seems too high considering that all other studies, including this dissertation, report no more than two percent of cases having *CD28* fusions; we have submitted a letter to the editor analyzing all available datasets and finding significantly fewer fusions than implied by that study.[192]

VAV1 was among the first GEFs identified, and its functional domains among the first assessed. VAV1 has a complex autoinhibitory mechanism by which its double

homology (DH) domain, a major catalyst for GEF activity, is inhibited by its neighboring acidic (Ac) domain, and phosphorylation of tyrosine 174 in the Ac domain in early TCR-mediated activation relieves this autoinhibition on the DH domain, eventually allowing the RhoGEF domain to exchange guanine. This autoinhibitory mechanism is augmented by interactions with the C-terminal SH3 domain, which is also relieved by indirect phosphorylation through TCR activation. Mutation or deletion of the C-terminal SH3 domain, therefore, prevents this secondary step of auto-inhibition thereby leading to increased activation. This indeed appears to be the case in ATLL, where the majority of VAV1 mutations are either within the Ac domain or clustered in the C-terminal SH3 domain, though there are other hotspots as well.

The VAV1-HNRNPM fusion found in this study eliminates the entire SH3 domain, and other putative mutations may have other effects on the various domains in which they take part. At the time of writing we are attempting to confirm the presence of these mutations by whole-exome sequencing. Should they prove to be real, their function will need to be assessed to determine whether they can alter downstream pathway activation and then lead to or propagate cancer. Preliminary work on the VAV1-HNRNPM mutation suggests that the fusion protein can translocate to the nucleus, likely via its somewhat cryptic nuclear localization sequence.[193] Although the effects on CD69 expression, a marker of activation, were minimal by flow cytometry (Fig. 19), there does indeed appear to be greater positive transcriptional effects of the mutant compared to the WT VAV1 in CD3/CD28 stimulation, including *CD69* specifically (Fig. 23). These each are, however, for a single biological replicate, so more data must be collected in order to assert whether the findings are true.

For the short-term future experiments, confirming and expanding the findings in the VAV1 fusion study will be necessary to decide whether the fusion is of consequence. In the longer term, the function of the putative VAV1 mutations needs to be assessed

should they prove to be true. Given the preponderance of mutations throughout VAV1 in ATLL, it follows that the apparent mutations in AITL and PTCL, NOS, if they are true, are likely relevant to the disease as well.

The mutations in AITL and PTCL, NOS must cooperate

TET2, IDH2, and DNMT3A mutations in AITL and PTCL, NOS are discussed at length in "Genetic origins." We found the expected overall and variant frequencies of TET2 mutations; IDH2 and DNMT3A mutations for these same cases are reported in Wang et al. 2015. Given that each of the other mutations exists nearly exclusively in the background of TET2 loss-of-function, there must be a degree of either cooperativity between the later mutations and TET2 LOF, or the loss of TET2 predisposes to other mutations. Either way, the global hypermethylation phenotype in TET2 mutant cells must create the environment required for T-cell lymphomagenesis, and exactly how the other mutations fit in is still a puzzle that must be solved.

The dominant negative G17V mutation in RHOA is particularly perplexing, though a variety of mutations in RHOA are known to occur in other cancers. For essentially all cell lineages including most hematopoietic cells, RHOA acts to polymerize actin and controls contraction on the trailing or lagging edge during cellular migration. RHOA was found to be a transforming factor in fibroblast culture,[194] and its activity is very important in metastasis of many solid tumors;[195,196] RHOA is frequently highly expressed in metastatic cancers. Several other mutant forms of RHOA have recently been identified in diffuse gastric carcinomas.[197] A plethora of RHOA mutations were also found in ATLL, some of which are activating and some inactivating.[180] Notably, the most common mutants in the gastric cancers – Y42C, R5Q/W, and G17E – are also expected to decrease GTP binding, though this has not been shown for R5 mutants. Pediatric Burkitt lymphomas also have relatively frequent R5Q/W mutations in RHOA.[180] Together, this suggests a common mechanism of RHOA GTP-binding inactivation that promotes cancer development, though what exactly this is remains mysterious,

particularly because no G17V mutations occurred in gastric disease or Burkitt lymphoma, and because RHOA-activating mutations can also occur in the same diseases. It would also be expected that if RHOA loss-of-function was oncogenic, then there would be examples of indels and nonsense mutations, and/or many more locations of mutation which would decrease RHOA activity. The fact that there are specific mutational hotspots suggests a mechanism beyond simple loss, and/or only a few mutations are not maladaptive.

Even the function of RHOA in lymphocytes has evidence somewhat difficult to reconcile. Early work on thymocyte development (the process summarized under "From stem cell to mature αβ T-cell") shows that RHOA activity is necessary for T-cells to mature, presumably because of 1) the intrathymic migration necessary for training, and 2) the importance of actin in stabilizing the immunologic synapse. Further, intercellular adhesion, which is initiated by transmembrane protein interactions but maintained by actin polymerization to keep adhesion proteins stable in the cell membrane, also requires RHOA function as specifically tested in Jurkat cells.[198] Thus, a loss of GTPase function would be expected to reduce actin polymerization, and this is indeed shown for the G17V mutant. Nevertheless, the total loss of functional RHOA in T-cells by transgenic expression of C3 exotoxin generates a T-acute lymphoblastic leukemia-like disease with thymic enlargement in mice.[199]

One possible explanation for this strange behavior of RHOA G17V may relate to its affinities for other proteins in the so-called GTPase cycle.[200] In order for GTPases like RHOA to function, they must be loaded with GTP. Inactive GTPases are stably bound to GDP, and in the case of the Rho family, most are complexed in the cytosol with any of a class of guanine dissociation inhibitors, or GDIs; the prototypical GDI for RHOA is RhoGDI. The GDI-bound fraction is in equilibrium with a small portion of membrane-bound, inactive protein that can potentially be activated by guanine exchange factors

(GEFs, of which VAV1 is one) which catalyze the exchange of GDP for GTP. The GTPase is now active. For the GTPase to become inactive, the GTP must be hydrolyzed; this is by the action of GTPase accelerating proteins (GAPs), prototypically RhoGAP for RHOA, which increases the intrinsic activity of the GTPase, hydrolyzing the terminal phosphate bond of the GTP to generate GDP. At this point, the GDP-bound GTPase can then re-complex with a GDI or be reactivated through the action of a GEF.

Not only is RHOA G17V unable to bind GTP and be active, it is unable to bind guanine nucleotide at all. Thus, it is hypothesized that the mutant RHOA may be "locked" in a conformation where it binds a GEF, but the GEF cannot dissociate because it cannot load GTP. If this were the case, there may be a preferential sequestration of some GEF or GEFs, allowing other GEFs or GAPs or GDIs to exert their pleiotropic effects on any number of cytosolic proteins. Our laboratory is actively working on discovering what the important interactions for RHOA G17V might be. One particularly interesting hypothesis (proposed by Timothy McKeithan) would be mostly lymphocyte-specific: because VAV1 is among the most important GEFs for RHOA in T-cells, perhaps membrane-bound RHOA G17V sequesters VAV1 close to the plasma membrane, preventing dissociation. VAV1 has many domains which can interact with many other proteins (see Figures 4 and 8) independent of its GEF function. Thus, if VAV1 is constitutively membrane-bound, it may be able to activate other early intermediates independent of TCR/CD28 activation.

Future directions: towards a model of PTCL, NOS and AITL

Research in PTCL, NOS and AITL pathogenesis is hindered for several reasons as mentioned above. Perhaps the most frustrating is a lack of PTCL models. Other T-cell-derived cancers such as T-cell leukemias and cutaneous T-cell lymphomas have several cancerous cell lines available publically from repositories such as the American Type Culture Collection (ATCC). The former includes the cellular model used for the majority of this study, Jurkat; besides the fact that is a leukemic line, it also is not the best representation for normal T-cells because it is missing the tumor suppressor PTEN, which exerts a variety of its own effects on cell cycle, activation, and migration; thus, it likely dos not faithfully represent the human mature T-cell.

AITL and PTCL, NOS, however, have never been successfully grown *in vitro*. This is partially due to the relative patient infrequency, such that there has been less available to attempt to grow, as well as the paucity of historical and even current data concerning primary tumor drivers. But the major reason is that both of these entities are strongly influenced by the micro-environment in which they develop. As discussed in "COO: AITL," the cells from which AITL are derived, T_{FH} cells, are able to mature and stay alive as a differentiated T_{FH} cell only in the presence of a germinal center, e.g. activated B-cells and FDCs. *In vitro* differentiation of T_{FH} cells, or at least T_{FH}-like cells, has been accomplished. However, long- or even medium-term expansion of a non-cancerous T_{FH} cell without B-cell and FDC interaction is as of yet impossible; our group has even tried to overexpress BCL6 in Jurkat cells, but to no avail (Jianbo Yu, unpublished data). This is further underscored by the fact that AITL only extremely rarely undergoes a leukemic transition, in which the cells are able to stay alive while circulating in the blood without the constant support of the meshwork of the peripheral lymphoid tissues. The only

foreseeable way truly generate a cell culture-based model of AITL is to develop a multi-cell-type co-culture in which dendritic cells present an antigen to which both $PRDM1^{lo}BCL6^{hi}CXCR5^{hi}CD4^{+}$ T-cells and mature B-cells are able to interact. Only in this complex system can the appropriate degree of activation through the TCR, along with OX40 co-stimulation from B-cells and CD28 co-stimulation from both B-cells and dendritic cells, be maintained. It is important to note that FDCs are important for T-cell training and do not normally take part in the GC reaction,[93] but there still needs to a consistent, controlled, physiologic activation measure for the T-cells to become T_{FH}.

Practically, the one way to possibly accomplish the model outlined above would be to generate mice in some way. We have generated mice with conditional loss of TET2 in T-cells to recapitulate what is found in human AITL and PTCL, NOS. Mice expressing Cre recombinase under control of the *Cd4* promoter (Jackson Laboratory, Tg(Cd4-cre)1Cwi/BfluJ, stock 017336) were crossed with mice which have the third exon of both their *Tet2* alleles bounded by LoxP sites.[133] Without Cre, cells have normal Tet2 expression because the LoxP sites are spliced with the introns in which they sit. However, in the presence of Cre, the third exon of *Tet2* is removed, such that all progeny of Cre-expressing cells, in this case CD4+ T-cells as well as perhaps some dendritic cells, will lose the third exon of Tet2 and not have a functional protein. Some mice were also crossed with the OTII line, expressing a transgenic T-cell receptor which encodes an ovalbumin-specific TCR for MHC Class II, thereby allowing selective activation with a known antigen (Jackson Laboratory, B6.Cg-Tg(TcraTcrb)425Cbn/J, stock 004194). These mice are currently aging and will be assessed over their life for development of lymphoma. Further, T-cells will be removed at various ages and assessed for functionality.

T-cells from the murine lines above could potentially be used as donors for *in vitro* or *in vivo* work. Another way to generate reactive T-cells could be through an acute

injection that would elicit an antibody reaction, such as sheep red blood cells; this will be less uniform, but would more appropriately generate a heterogeneous reaction more representative of the likely physiological reaction to antigenic challenge. There are still other agents that could generate a known response, e.g. murine viruses, but for these it would be too easy to contaminate the mice intended to be uninfected. This would be particularly problematic in a mouse facility at an academic institution that does not normally use biosafety level 2+ precautions or higher in routine handling and maintenance of mouse colonies.

Even once these T-cells are ready to be used in modeling, the major issue remains recapitulation of normal nodal architecture. For *in vivo* work, simple injection of potentially malignant T-cells should be enough to get them to home to peripheral lymphoid organs and divide as expected; only performing this experiment can decide. The *in vitro* modeling is even more complex. Peripheral lymphoid organs are three-dimensional structures, clearly, whereas tissue culture plates are two-dimensional. There do exist mesh inserts which adherent cells, FDCs in this particular model, could use as a scaffold and allowing multi-dimensional access for the potential interacting B and T cells, but it doesn't let B- and T-cells move around each other with the dendritic meshwork in place. Plus, gravity would pull non-adherent cells away from the insert towards the bottom of the well, and without moving lymph to keep cells in circulation, the lymphocytes would eventually not be able to interact with the FDCs anyway. A round-bottom plate would avoid the gravity issue but still not mimic the 3D structure of a lymph node. It is truly a conundrum.

Recent advances in bioengineering have generated organ-specific scaffolding which allows population by living, functional cells. In the functional cases (including heart,[201] liver,[202] and pancreas,[203] among others), the stated goal involves a single cell type (cardiomyocyte, hepatocyte, pancreatic β-cell, respectively) performing a cell-intrinsic

function in a position fixed in space. For peripheral lymphoid organs, these strategies would not work so well, because these organs need specific inflow and outflow with many different cell types interacting, and most of these interactions are not fixed in space anyway. Thus, a scaffold on which dendritic cells can grow would likely not be able to support a germinal center reaction or the migratory patterns of mature $CD4^+$ T-cells. Perhaps in many years, there will exist an artificial lymph node or spleen which is able to function in all organ capacities, but that certainly is not just around the corner.

One other possibility rests in the recent development of patient-derived xenograft (PDX) models, in which excisions of patient tumors are implanted in NOD/SCID/Il2rg-null (NSG) mice, and different potential chemotherapies are tried to assess the best response of the individual tumor. These findings then inform the choice of therapy in the patient. PDX models are fairly easy to generate for epithelial, solid tumors; in general, they can implant in almost any tissue. For the PTCLs, especially the stromal-dependent tumors like the two diseases assessed here, this does not work as well, but has been previously met with moderate success.[204] If PDXs can work consistently for biopsies of AITLs, then in addition to using the models to look at therapy, the tissue can propagate 1) to give more cells for sequencing, and 2) allow long-term monitoring of cancer progression in a way that has certainly not been possible up to this point, thereby generating an extrinsic model which uses human cells.

Conclusion: towards targeting co-stimulation for treatment of PTCLs

Here we have studied the effects of mutations in proximal molecules of the T-cell so-stimulatory pathway and found that they allow angioimmunoblastic T-cell lymphoma (AITL) and peripheral T-cell lymphoma, not otherwise specified (PTCL, NOS) to increase

activation through the TCR, thereby increasing downstream signaling. This signaling likely contributes to the survival of mutated cells, giving these cells the ability to contribute to lymphoma development and potentially resistance to therapy. It is clear, from this and from others' work, that the CD3/CD28 pathway is a central mechanism which prevents these cancerous cells from dying. Therefore the co-stimulatory pathway is a rational target for these diseases.

Altering CD28 biology, however, can have serious effects. In a Phase I trial of a CD28 superagonist used to stimulate immune reaction, all six healthy individuals experienced cytokine storm and progressed to various degrees of organ failure, consistent with systemic inflammatory response syndrome (SIRS).[205] Blocking of CD28 activity through an inhibitory antibody has recently been successful in preventing acute kidney allograft rejection in non-human primates[206] and is well-studied in rodents,[207] though titration for humans must be carefully done before clinical trial. Other inhibitors of co-inhibitory CD28-family receptors already exist and are used in patients:[208] anti-CTLA4 (ipilimumab), anti-PD1 (nivolumab), and anti-PDL1 (atezolizumab) are used to increase immunologic response to solid tumors in humans. More relevant to PTCLs, CTLA4-Ig (abatacept), which binds B7 ligand and prevents ligation with CD28, is already used successfully to treat many autoimmune diseases by preventing T-cell activation. With proven tolerability, we hold that abatacept or similar classes of immune modulators should be considered for trial in PTCLs. If a lymphoma is sequenced and has a TCR/CD28 activating mutation, then this drug may provide the key to prevent the signals which allow the cancer to persist.

Someday soon, there will be a successful treatment for PTCLs. It is only through hard work that we will find it.

REFERENCES

1 Vose, J., Armitage, J., Weisenburger, D. & International, T. C. L. P. International peripheral T-cell and natural killer/T-cell lymphoma study: pathology findings and clinical outcomes. *J Clin Oncol* **26**, 4124-4130, doi:10.1200/JCO.2008.16.4558 (2008).

2 Rudiger, T., Weisenburger, D. D., Anderson, J. R., Armitage, J. O., Diebold, J., MacLennan, K. A., Nathwani, B. N., Ullrich, F., Muller-Hermelink, H. K. & Non-Hodgkin's Lymphoma Classification, P. Peripheral T-cell lymphoma (excluding anaplastic large-cell lymphoma): results from the Non-Hodgkin's Lymphoma Classification Project. *Ann Oncol* **13**, 140-149 (2002).

3 Weisenburger, D. D., Savage, K. J., Harris, N. L., Gascoyne, R. D., Jaffe, E. S., MacLennan, K. A., Rudiger, T., Pileri, S., Nakamura, S., Nathwani, B., Campo, E., Berger, F., Coiffier, B., Kim, W. S., Holte, H., Federico, M., Au, W. Y., Tobinai, K., Armitage, J. O., Vose, J. M. *et al.* Peripheral T-cell lymphoma, not otherwise specified: a report of 340 cases from the International Peripheral T-cell Lymphoma Project. *Blood* **117**, 3402-3408, doi:10.1182/blood-2010-09-310342 (2011).

4 Swerdlow, S. H., Campo, E., Harris, N. L., Jaffe, E., Pileri, S., Stein, H., Thiele, J. & Vardiman, J. W. *WHO Classification of Tumours of Haematopoietic and Lymphoid Tissues*. (IARC Press, 2008).

5 Jaffe, E. S., Nicolae, A. & Pittaluga, S. Peripheral T-cell and NK-cell lymphomas in the WHO classification: pearls and pitfalls. *Mod Pathol* **26 Suppl 1**, S71-87, doi:10.1038/modpathol.2012.181 (2013).

6 Carbone, P. P., Kaplan, H. S., Musshoff, K., Smithers, D. W. & Tubiana, M. Report of the Committee on Hodgkin's Disease Staging Classification. *Cancer Res* **31**, 1860-1861 (1971).

7 A predictive model for aggressive non-Hodgkin's lymphoma. The International Non-Hodgkin's Lymphoma Prognostic Factors Project. *N Engl J Med* **329**, 987-994, doi:10.1056/NEJM199309303291402 (1993).

8 Gallamini, A., Stelitano, C., Calvi, R., Bellei, M., Mattei, D., Vitolo, U., Morabito, F., Martelli, M., Brusamolino, E., Iannitto, E., Zaja, F., Cortelazzo, S., Rigacci, L., Devizzi, L., Todeschini, G., Santini, G., Brugiatelli, M., Federico, M. & Intergruppo Italiano, L. Peripheral T-cell lymphoma unspecified (PTCL-U): a new prognostic model from a retrospective multicentric clinical study. *Blood* **103**, 2474-2479, doi:10.1182/blood-2003-09-3080 (2004).

9 Adams, S. V., Newcomb, P. A. & Shustov, A. R. Racial Patterns of Peripheral T-Cell Lymphoma Incidence and Survival in the United States. *J Clin Oncol* **34**, 963-971, doi:10.1200/JCO.2015.63.5540 (2016).

10 Federico, M., Rudiger, T., Bellei, M., Nathwani, B. N., Luminari, S., Coiffier, B., Harris, N. L., Jaffe, E. S., Pileri, S. A., Savage, K. J., Weisenburger, D. D., Armitage, J. O., Mounier, N. & Vose, J. M. Clinicopathologic characteristics of angioimmunoblastic T-cell lymphoma: analysis of the international peripheral T-cell lymphoma project. *J Clin Oncol* **31**, 240-246, doi:10.1200/JCO.2011.37.3647 (2013).

11 Baseggio, L., Traverse-Glehen, A., Berger, F., Ffrench, M., Jallades, L., Morel, D., Goedert, G., Magaud, J. P., Salles, G. & Felman, P. CD10 and ICOS

expression by multiparametric flow cytometry in angioimmunoblastic T-cell lymphoma. *Mod Pathol* **24**, 993-1003, doi:10.1038/modpathol.2011.53 (2011).

12 Yu, H., Shahsafaei, A. & Dorfman, D. M. Germinal-center T-helper-cell markers PD-1 and CXCL13 are both expressed by neoplastic cells in angioimmunoblastic T-cell lymphoma. *Am J Clin Pathol* **131**, 33-41, doi:10.1309/AJCP62WRKERPXDRT (2009).

13 Marafioti, T., Paterson, J. C., Ballabio, E., Chott, A., Natkunam, Y., Rodriguez-Justo, M., Plonquet, A., Rodriguez-Pinilla, S. M., Klapper, W., Hansmann, M. L., Pileri, S. A., Isaacson, P. G., Stein, H., Piris, M. A., Mason, D. Y. & Gaulard, P. The inducible T-cell co-stimulator molecule is expressed on subsets of T cells and is a new marker of lymphomas of T follicular helper cell-derivation. *Haematologica* **95**, 432-439, doi:10.3324/haematol.2009.010991 (2010).

14 Vose, J. M. Peripheral T-cell non-Hodgkin's lymphoma. *Hematol Oncol Clin North Am* **22**, 997-1005, x, doi:10.1016/j.hoc.2008.07.010 (2008).

15 *Peripheral T-cell Lymphoma, NOS*, <http://www.webpathology.com/case.asp?case=844> (

16 Jacobsen, E. & Freedman, A. S. *Initial treatment of peripheral T-cell lymphomas*, 2016).

17 Jacobsen, E. & Freedman, A. S. *Treatment of relapsed or refractory peripheral T-cell lymphoma*, 2016).

18 Dodero, A., Spina, F., Narni, F., Patriarca, F., Cavattoni, I., Benedetti, F., Ciceri, F., Baronciani, D., Scime, R., Pogliani, E., Rambaldi, A., Bonifazi, F., Dalto, S., Bruno, B. & Corradini, P. Allogeneic transplantation following a reduced-intensity conditioning regimen in relapsed/refractory peripheral T-cell lymphomas: long-term remissions and response to donor lymphocyte infusions support the role of a graft-versus-lymphoma effect. *Leukemia* **26**, 520-526, doi:10.1038/leu.2011.240 (2012).

19 Smith, S. M., Burns, L. J., van Besien, K., Lerademacher, J., He, W., Fenske, T. S., Suzuki, R., Hsu, J. W., Schouten, H. C., Hale, G. A., Holmberg, L. A., Sureda, A., Freytes, C. O., Maziarz, R. T., Inwards, D. J., Gale, R. P., Gross, T. G., Cairo, M. S., Costa, L. J., Lazarus, H. M. *et al.* Hematopoietic cell transplantation for systemic mature T-cell non-Hodgkin lymphoma. *J Clin Oncol* **31**, 3100-3109, doi:10.1200/JCO.2012.46.0188 (2013).

20 Shustov, A. R., Gooley, T. A., Sandmaier, B. M., Shizuru, J., Sorror, M. L., Sahebi, F., McSweeney, P., Niederwieser, D., Bruno, B., Storb, R. & Maloney, D. G. Allogeneic haematopoietic cell transplantation after nonmyeloablative conditioning in patients with T-cell and natural killer-cell lymphomas. *Br J Haematol* **150**, 170-178, doi:10.1111/j.1365-2141.2010.08210.x (2010).

21 O'Connor, O. A., Hamlin, P. A., Portlock, C., Moskowitz, C. H., Noy, A., Straus, D. J., Macgregor-Cortelli, B., Neylon, E., Sarasohn, D., Dumetrescu, O., Mould, D. R., Fleischer, M., Zelenetz, A. D., Sirotnak, F. & Horwitz, S. Pralatrexate, a novel class of antifol with high affinity for the reduced folate carrier-type 1, produces marked complete and durable remissions in a diversity of chemotherapy refractory cases of T-cell lymphoma. *Br J Haematol* **139**, 425-428, doi:10.1111/j.1365-2141.2007.06658.x (2007).

22 O'Connor, O. A., Horwitz, S., Hamlin, P., Portlock, C., Moskowitz, C. H., Sarasohn, D., Neylon, E., Mastrella, J., Hamelers, R., Macgregor-Cortelli, B., Patterson, M., Seshan, V. E., Sirotnak, F., Fleisher, M., Mould, D. R., Saunders, M. & Zelenetz, A. D. Phase II-I-II study of two different doses and schedules of pralatrexate, a high-affinity substrate for the reduced folate carrier, in patients with relapsed or refractory lymphoma reveals marked activity in T-cell

malignancies. *J Clin Oncol* **27**, 4357-4364, doi:10.1200/JCO.2008.20.8470 (2009).

23 O'Connor, O. A., Pro, B., Pinter-Brown, L., Bartlett, N., Popplewell, L., Coiffier, B., Lechowicz, M. J., Savage, K. J., Shustov, A. R., Gisselbrecht, C., Jacobsen, E., Zinzani, P. L., Furman, R., Goy, A., Haioun, C., Crump, M., Zain, J. M., Hsi, E., Boyd, A. & Horwitz, S. Pralatrexate in patients with relapsed or refractory peripheral T-cell lymphoma: results from the pivotal PROPEL study. *J Clin Oncol* **29**, 1182-1189, doi:10.1200/JCO.2010.29.9024 (2011).

24 *Pilot Study of Brentuximab Vedotin in Relapsed/Refractory Peripheral T-Cell Lymphoma Expressing CD30*, <https://ClinicalTrials.gov/show/NCT01841021> (

25 Fanale, M. A., Horwitz, S. M., Forero-Torres, A., Bartlett, N. L., Advani, R. H., Pro, B., Chen, R. W., Davies, A., Illidge, T., Huebner, D., Kennedy, D. A. & Shustov, A. R. Brentuximab vedotin in the front-line treatment of patients with CD30+ peripheral T-cell lymphomas: results of a phase I study. *J Clin Oncol* **32**, 3137-3143, doi:10.1200/JCO.2013.54.2456 (2014).

26 Horwitz, S. M., Advani, R. H., Bartlett, N. L., Jacobsen, E. D., Sharman, J. P., O'Connor, O. A., Siddiqi, T., Kennedy, D. A. & Oki, Y. Objective responses in relapsed T-cell lymphomas with single-agent brentuximab vedotin. *Blood* **123**, 3095-3100, doi:10.1182/blood-2013-12-542142 (2014).

27 Carson, K. R., Newsome, S. D., Kim, E. J., Wagner-Johnston, N. D., von Geldern, G., Moskowitz, C. H., Moskowitz, A. J., Rook, A. H., Jalan, P., Loren, A. W., Landsburg, D., Coyne, T., Tsai, D., Raisch, D. W., Norris, L. B., Bookstaver, P. B., Sartor, O. & Bennett, C. L. Progressive multifocal leukoencephalopathy associated with brentuximab vedotin therapy: a report of 5 cases from the Southern Network on Adverse Reactions (SONAR) project. *Cancer* **120**, 2464-2471, doi:10.1002/cncr.28712 (2014).

28 Coiffier, B., Pro, B., Prince, H. M., Foss, F., Sokol, L., Greenwood, M., Caballero, D., Borchmann, P., Morschhauser, F., Wilhelm, M., Pinter-Brown, L., Padmanabhan, S., Shustov, A., Nichols, J., Carroll, S., Balser, J., Balser, B. & Horwitz, S. Results from a pivotal, open-label, phase II study of romidepsin in relapsed or refractory peripheral T-cell lymphoma after prior systemic therapy. *J Clin Oncol* **30**, 631-636, doi:10.1200/JCO.2011.37.4223 (2012).

29 Whittaker, S. J., Demierre, M. F., Kim, E. J., Rook, A. H., Lerner, A., Duvic, M., Scarisbrick, J., Reddy, S., Robak, T., Becker, J. C., Samtsov, A., McCulloch, W. & Kim, Y. H. Final results from a multicenter, international, pivotal study of romidepsin in refractory cutaneous T-cell lymphoma. *J Clin Oncol* **28**, 4485-4491, doi:10.1200/JCO.2010.28.9066 (2010).

30 *Belinostat in Relapsed or Refractory Peripheral T-Cell Lymphoma*, <https://ClinicalTrials.gov/show/NCT00865969> (

31 O'Connor, O. A., Horwitz, S., Masszi, T., Van Hoof, A., Brown, P., Doorduijn, J., Hess, G., Jurczak, W., Knoblauch, P., Chawla, S., Bhat, G., Choi, M. R., Walewski, J., Savage, K., Foss, F., Allen, L. F. & Shustov, A. Belinostat in Patients With Relapsed or Refractory Peripheral T-Cell Lymphoma: Results of the Pivotal Phase II BELIEF (CLN-19) Study. *J Clin Oncol* **33**, 2492-2499, doi:10.1200/JCO.2014.59.2782 (2015).

32 *Study of KW-0761 (Mogamulizumab) in Subjects With Previously Treated Peripheral T-cell Lymphoma (PTCL)*, <https://ClinicalTrials.gov/show/NCT01611142> (

33 *Study of Tipifarnib in Subjects With Relapsed or Refractory Peripheral T-Cell Lymphoma*, <https://ClinicalTrials.gov/show/NCT02464228> (

34 *Efficacy & Safety Study of Selinexor in Relapsed/Refractory Peripheral T-cell Lymphoma & Cutaneous T-cell Lymphoma*, <https://ClinicalTrials.gov/show/NCT02314247> (

35 *CHO(E)P-14 Followed by Alemtuzumab Consolidation in Peripheral T Cell Lymphoma*, <https://ClinicalTrials.gov/show/NCT01806337> (

36 *Alemtuzumab and CHOP Chemotherapy for Aggressive Histological Peripheral T-Cell Lymphomas*, <https://ClinicalTrials.gov/show/NCT00453427> (

37 *A Phase I, Multicenter, Open-label, Dose-escalation Study to Assess the Safety of Lenalidomide in Patients With Advanced Adult T-cell Leukemia-lymphoma and Peripheral T-cell Lymphomaperipheral T-cell Lymphoma*, <https://ClinicalTrials.gov/show/NCT01169298> (

38 Toumishey, E., Prasad, A., Dueck, G., Chua, N., Finch, D., Johnston, J., van der Jagt, R., Stewart, D., White, D., Belch, A. & Reiman, T. Final report of a phase 2 clinical trial of lenalidomide monotherapy for patients with T-cell lymphoma. *Cancer* **121**, 716-723, doi:10.1002/cncr.29103 (2015).

39 *A Phase II Study With Bendamustine Plus Brentuximab Vedotin in Hodgkin's Lymphoma and CD30+ Peripheral T-cell Lymphoma in First Salvage Setting: the BBV Regimen*, <https://ClinicalTrials.gov/show/NCT02499627> (

40 Damaj, G., Gressin, R., Bouabdallah, K., Cartron, G., Choufi, B., Gyan, E., Banos, A., Jaccard, A., Park, S., Tournilhac, O., Schiano-de Collela, J. M., Voillat, L., Joly, B., Le Gouill, S., Saad, A., Cony-Makhoul, P., Vilque, J. P., Sanhes, L., Schmidt-Tanguy, A., Bubenheim, M. *et al.* Results from a prospective, open-label, phase II trial of bendamustine in refractory or relapsed T-cell lymphomas: the BENTLY trial. *J Clin Oncol* **31**, 104-110, doi:10.1200/JCO.2012.43.7285 (2013).

41 Leoni, L. M. & Hartley, J. A. Mechanism of action: the unique pattern of bendamustine-induced cytotoxicity. *Semin Hematol* **48 Suppl 1**, S12-23, doi:10.1053/j.seminhematol.2011.03.003 (2011).

42 Lee, J., Suh, C., Kang, H. J., Ryoo, B. Y., Huh, J., Ko, Y. H., Eom, H. S., Kim, K., Park, K. & Kim, W. S. Phase I study of proteasome inhibitor bortezomib plus CHOP in patients with advanced, aggressive T-cell or NK/T-cell lymphoma. *Ann Oncol* **19**, 2079-2083, doi:10.1093/annonc/mdn431 (2008).

43 Zinzani, P. L., Musuraca, G., Tani, M., Stefoni, V., Marchi, E., Fina, M., Pellegrini, C., Alinari, L., Derenzini, E., de Vivo, A., Sabattini, E., Pileri, S. & Baccarani, M. Phase II trial of proteasome inhibitor bortezomib in patients with relapsed or refractory cutaneous T-cell lymphoma. *J Clin Oncol* **25**, 4293-4297, doi:10.1200/JCO.2007.11.4207 (2007).

44 *Bortezomib and CHOP in Patients With Advanced Stage Aggressive T Cell or Natural Killer (NK)/T Cell Lymphomas*, <https://ClinicalTrials.gov/show/NCT00374699> (

45 *Carfilzomib in Treating Patients With Relapsed or Refractory T-Cell Lymphoma*, <https://ClinicalTrials.gov/show/NCT01336920> (

46 *Open-label, Phase II Study of MLN9708 in Patients With Relapsed/Refractory Cutaneous and Peripheral T-cell Lymphomas*, <https://ClinicalTrials.gov/show/NCT02158975> (

47 Pfreundschuh, M., Kuhnt, E., Trumper, L., Osterborg, A., Trneny, M., Shepherd, L., Gill, D. S., Walewski, J., Pettengell, R., Jaeger, U., Zinzani, P. L., Shpilberg, O., Kvaloy, S., de Nully Brown, P., Stahel, R., Milpied, N., Lopez-Guillermo, A., Poeschel, V., Grass, S., Loeffler, M. *et al.* CHOP-like chemotherapy with or without rituximab in young patients with good-prognosis diffuse large-B-cell lymphoma: 6-year results of an open-label randomised study of the MabThera

International Trial (MInT) Group. *Lancet Oncol* **12**, 1013-1022, doi:10.1016/S1470-2045(11)70235-2 (2011).

48 Feugier, P., Van Hoof, A., Sebban, C., Solal-Celigny, P., Bouabdallah, R., Ferme, C., Christian, B., Lepage, E., Tilly, H., Morschhauser, F., Gaulard, P., Salles, G., Bosly, A., Gisselbrecht, C., Reyes, F. & Coiffier, B. Long-term results of the R-CHOP study in the treatment of elderly patients with diffuse large B-cell lymphoma: a study by the Groupe d'Etude des Lymphomes de l'Adulte. *J Clin Oncol* **23**, 4117-4126, doi:10.1200/JCO.2005.09.131 (2005).

49 Sieburg, H. B., Cho, R. H., Dykstra, B., Uchida, N., Eaves, C. J. & Muller-Sieburg, C. E. The hematopoietic stem compartment consists of a limited number of discrete stem cell subsets. *Blood* **107**, 2311-2316, doi:10.1182/blood-2005-07-2970 (2006).

50 Lu, M., Kawamoto, H., Katsube, Y., Ikawa, T. & Katsura, Y. The common myelolymphoid progenitor: a key intermediate stage in hemopoiesis generating T and B cells. *J Immunol* **169**, 3519-3525 (2002).

51 Martin, C. H., Aifantis, I., Scimone, M. L., von Andrian, U. H., Reizis, B., von Boehmer, H. & Gounari, F. Efficient thymic immigration of B220+ lymphoid-restricted bone marrow cells with T precursor potential. *Nat Immunol* **4**, 866-873, doi:10.1038/ni965 (2003).

52 Gounari, F., Aifantis, I., Martin, C., Fehling, H. J., Hoeflinger, S., Leder, P., von Boehmer, H. & Reizis, B. Tracing lymphopoiesis with the aid of a pTalpha-controlled reporter gene. *Nat Immunol* **3**, 489-496, doi:10.1038/ni778 (2002).

53 Scimone, M. L., Aifantis, I., Apostolou, I., von Boehmer, H. & von Andrian, U. H. A multistep adhesion cascade for lymphoid progenitor cell homing to the thymus. *Proc Natl Acad Sci U S A* **103**, 7006-7011, doi:10.1073/pnas.0602024103 (2006).

54 Lind, E. F., Prockop, S. E., Porritt, H. E. & Petrie, H. T. Mapping precursor movement through the postnatal thymus reveals specific microenvironments supporting defined stages of early lymphoid development. *J Exp Med* **194**, 127-134 (2001).

55 Germain, R. N. T-cell development and the CD4-CD8 lineage decision. *Nat Rev Immunol* **2**, 309-322, doi:10.1038/nri798 (2002).

56 Tatarek, J., Cullion, K., Ashworth, T., Gerstein, R., Aster, J. C. & Kelliher, M. A. Notch1 inhibition targets the leukemia-initiating cells in a Tal1/Lmo2 mouse model of T-ALL. *Blood* **118**, 1579-1590, doi:10.1182/blood-2010-08-300343 (2011).

57 Roose, J. P., Mollenauer, M., Gupta, V. A., Stone, J. & Weiss, A. A diacylglycerol-protein kinase C-RasGRP1 pathway directs Ras activation upon antigen receptor stimulation of T cells. *Mol Cell Biol* **25**, 4426-4441, doi:10.1128/MCB.25.11.4426-4441.2005 (2005).

58 Lovatt, M., Filby, A., Parravicini, V., Werlen, G., Palmer, E. & Zamoyska, R. Lck regulates the threshold of activation in primary T cells, while both Lck and Fyn contribute to the magnitude of the extracellular signal-related kinase response. *Mol Cell Biol* **26**, 8655-8665, doi:10.1128/MCB.00168-06 (2006).

59 Rougerie, P. & Delon, J. Rho GTPases: masters of T lymphocyte migration and activation. *Immunol Lett* **142**, 1-13 (2012).

60 Gimmi, C. D., Freeman, G. J., Gribben, J. G., Gray, G. & Nadler, L. M. Human T-cell clonal anergy is induced by antigen presentation in the absence of B7 costimulation. *Proc Natl Acad Sci U S A* **90**, 6586-6590 (1993).

61 Greaves, P. & Gribben, J. G. The role of B7 family molecules in hematologic malignancy. *Blood* **121**, 734-744 (2013).

62 Rudd, C. E. & Schneider, H. Unifying concepts in CD28, ICOS and CTLA4 co-receptor signalling. *Nat Rev Immunol* **3**, 544-556 (2003).

63 Boomer, J. S. & Green, J. M. An enigmatic tail of CD28 signaling. *Cold Spring Harb Perspect Biol* **2**, a002436 (2010).

64 Collins, A. V., Brodie, D. W., Gilbert, R. J., Iaboni, A., Manso-Sancho, R., Walse, B., Stuart, D. I., van der Merwe, P. A. & Davis, S. J. The interaction properties of costimulatory molecules revisited. *Immunity* **17**, 201-210 (2002).

65 van der Merwe, P. A., Bodian, D. L., Daenke, S., Linsley, P. & Davis, S. J. CD80 (B7-1) binds both CD28 and CTLA-4 with a low affinity and very fast kinetics. *J Exp Med* **185**, 393-403 (1997).

66 Linsley, P. S., Brady, W., Grosmaire, L., Aruffo, A., Damle, N. K. & Ledbetter, J. A. Binding of the B cell activation antigen B7 to CD28 costimulates T cell proliferation and interleukin 2 mRNA accumulation. *J Exp Med* **173**, 721-730 (1991).

67 Linsley, P. S., Brady, W., Urnes, M., Grosmaire, L. S., Damle, N. K. & Ledbetter, J. A. CTLA-4 is a second receptor for the B cell activation antigen B7. *J Exp Med* **174**, 561-569 (1991).

68 Linsley, P. S., Greene, J. L., Brady, W., Bajorath, J., Ledbetter, J. A. & Peach, R. Human B7-1 (CD80) and B7-2 (CD86) bind with similar avidities but distinct kinetics to CD28 and CTLA-4 receptors. *Immunity* **1**, 793-801 (1994).

69 Qureshi, O. S., Zheng, Y., Nakamura, K., Attridge, K., Manzotti, C., Schmidt, E. M., Baker, J., Jeffery, L. E., Kaur, S., Briggs, Z., Hou, T. Z., Futter, C. E., Anderson, G., Walker, L. S. & Sansom, D. M. Trans-endocytosis of CD80 and CD86: a molecular basis for the cell-extrinsic function of CTLA-4. *Science* **332**, 600-603, doi:10.1126/science.1202947 (2011).

70 Schneider, H., Valk, E., Leung, R. & Rudd, C. E. CTLA-4 activation of phosphatidylinositol 3-kinase (PI 3-K) and protein kinase B (PKB/AKT) sustains T-cell anergy without cell death. *PLoS One* **3**, e3842, doi:10.1371/journal.pone.0003842 (2008).

71 Hu, H., Rudd, C. E. & Schneider, H. Src kinases Fyn and Lck facilitate the accumulation of phosphorylated CTLA-4 and its association with PI-3 kinase in intracellular compartments of T-cells. *Biochem Biophys Res Commun* **288**, 573-578, doi:10.1006/bbrc.2001.5814 (2001).

72 Berg, M. & Zavazava, N. Regulation of CD28 expression on CD8+ T cells by CTLA-4. *J Leukoc Biol* **83**, 853-863 (2008).

73 Walker, L. S. & Sansom, D. M. Confusing signals: recent progress in CTLA-4 biology. *Trends Immunol* **36**, 63-70, doi:10.1016/j.it.2014.12.001 (2015).

74 Iqbal, J., Weisenburger, D. D., Greiner, T. C., Vose, J. M., McKeithan, T., Kucuk, C., Geng, H., Deffenbacher, K., Smith, L., Dybkaer, K., Nakamura, S., Seto, M., Delabie, J., Berger, F., Loong, F., Au, W. Y., Ko, Y. H., Sng, I., Armitage, J. O. & Chan, W. C. Molecular signatures to improve diagnosis in peripheral T-cell lymphoma and prognostication in angioimmunoblastic T-cell lymphoma. *Blood* **115**, 1026-1036 (2010).

75 de Leval, L., Rickman, D. S., Thielen, C., Reynies, A., Huang, Y. L., Delsol, G., Lamant, L., Leroy, K., Briere, J., Molina, T., Berger, F., Gisselbrecht, C., Xerri, L. & Gaulard, P. The gene expression profile of nodal peripheral T-cell lymphoma demonstrates a molecular link between angioimmunoblastic T-cell lymphoma (AITL) and follicular helper T (TFH) cells. *Blood* **109**, 4952-4963 (2007).

76 Crotty, S. Follicular helper CD4 T cells (TFH). *Annu Rev Immunol* **29**, 621-663, doi:10.1146/annurev-immunol-031210-101400 (2011).

77 Johnston, R. J., Poholek, A. C., DiToro, D., Yusuf, I., Eto, D., Barnett, B., Dent, A. L., Craft, J. & Crotty, S. Bcl6 and Blimp-1 are reciprocal and antagonistic regulators of T follicular helper cell differentiation. *Science* **325**, 1006-1010, doi:10.1126/science.1175870 (2009).

78 Nurieva, R. I., Chung, Y., Martinez, G. J., Yang, X. O., Tanaka, S., Matskevitch, T. D., Wang, Y. H. & Dong, C. Bcl6 mediates the development of T follicular helper cells. *Science* **325**, 1001-1005, doi:10.1126/science.1176676 (2009).

79 Yu, D., Rao, S., Tsai, L. M., Lee, S. K., He, Y., Sutcliffe, E. L., Srivastava, M., Linterman, M., Zheng, L., Simpson, N., Ellyard, J. I., Parish, I. A., Ma, C. S., Li, Q. J., Parish, C. R., Mackay, C. R. & Vinuesa, C. G. The transcriptional repressor Bcl-6 directs T follicular helper cell lineage commitment. *Immunity* **31**, 457-468, doi:10.1016/j.immuni.2009.07.002 (2009).

80 Gong, D. & Malek, T. R. Cytokine-dependent Blimp-1 expression in activated T cells inhibits IL-2 production. *J Immunol* **178**, 242-252 (2007).

81 Martins, G. A., Cimmino, L., Shapiro-Shelef, M., Szabolcs, M., Herron, A., Magnusdottir, E. & Calame, K. Transcriptional repressor Blimp-1 regulates T cell homeostasis and function. *Nat Immunol* **7**, 457-465, doi:10.1038/ni1320 (2006).

82 Suto, A., Kashiwakuma, D., Kagami, S., Hirose, K., Watanabe, N., Yokote, K., Saito, Y., Nakayama, T., Grusby, M. J., Iwamoto, I. & Nakajima, H. Development and characterization of IL-21-producing CD4+ T cells. *J Exp Med* **205**, 1369-1379, doi:10.1084/jem.20072057 (2008).

83 Nurieva, R. I., Chung, Y., Hwang, D., Yang, X. O., Kang, H. S., Ma, L., Wang, Y. H., Watowich, S. S., Jetten, A. M., Tian, Q. & Dong, C. Generation of T follicular helper cells is mediated by interleukin-21 but independent of T helper 1, 2, or 17 cell lineages. *Immunity* **29**, 138-149, doi:10.1016/j.immuni.2008.05.009 (2008).

84 Eto, D., Lao, C., DiToro, D., Barnett, B., Escobar, T. C., Kageyama, R., Yusuf, I. & Crotty, S. IL-21 and IL-6 are critical for different aspects of B cell immunity and redundantly induce optimal follicular helper CD4 T cell (Tfh) differentiation. *PLoS One* **6**, e17739, doi:10.1371/journal.pone.0017739 (2011).

85 Allman, D., Jain, A., Dent, A., Maile, R. R., Selvaggi, T., Kehry, M. R. & Staudt, L. M. BCL-6 expression during B-cell activation. *Blood* **87**, 5257-5268 (1996).

86 Hirata, Y., Ogasawara, N., Sasaki, M., Mizushima, T., Shimura, T., Mizoshita, T., Mori, Y., Kubota, E., Wada, T., Tanida, S., Kataoka, H., Kamiya, T., Higashiyama, S. & Joh, T. BCL6 degradation caused by the interaction with the C-terminus of pro-HB-EGF induces cyclin D2 expression in gastric cancers. *Br J Cancer* **100**, 1320-1329, doi:10.1038/sj.bjc.6605010 (2009).

87 Ivanova, E. A. & Orekhov, A. N. T Helper Lymphocyte Subsets and Plasticity in Autoimmunity and Cancer: An Overview. *Biomed Res Int* **2015**, 327470, doi:10.1155/2015/327470 (2015).

88 Ma, C. S., Suryani, S., Avery, D. T., Chan, A., Nanan, R., Santner-Nanan, B., Deenick, E. K. & Tangye, S. G. Early commitment of naive human CD4(+) T cells to the T follicular helper (T(FH)) cell lineage is induced by IL-12. *Immunol Cell Biol* **87**, 590-600, doi:10.1038/icb.2009.64 (2009).

89 Yusuf, I., Kageyama, R., Monticelli, L., Johnston, R. J., Ditoro, D., Hansen, K., Barnett, B. & Crotty, S. Germinal center T follicular helper cell IL-4 production is dependent on signaling lymphocytic activation molecule receptor (CD150). *J Immunol* **185**, 190-202, doi:10.4049/jimmunol.0903505 (2010).

90 Hardtke, S., Ohl, L. & Forster, R. Balanced expression of CXCR5 and CCR7 on follicular T helper cells determines their transient positioning to lymph node follicles and is essential for efficient B-cell help. *Blood* **106**, 1924-1931, doi:10.1182/blood-2004-11-4494 (2005).

91 Haynes, N. M., Allen, C. D., Lesley, R., Ansel, K. M., Killeen, N. & Cyster, J. G. Role of CXCR5 and CCR7 in follicular Th cell positioning and appearance of a programmed cell death gene-1high germinal center-associated subpopulation. *J Immunol* **179**, 5099-5108 (2007).

92 Choi, Y. S., Kageyama, R., Eto, D., Escobar, T. C., Johnston, R. J., Monticelli, L., Lao, C. & Crotty, S. ICOS receptor instructs T follicular helper cell versus effector cell differentiation via induction of the transcriptional repressor Bcl6. *Immunity* **34**, 932-946, doi:10.1016/j.immuni.2011.03.023 (2011).

93 Celli, S., Lemaitre, F. & Bousso, P. Real-time manipulation of T cell-dendritic cell interactions in vivo reveals the importance of prolonged contacts for CD4+ T cell activation. *Immunity* **27**, 625-634, doi:10.1016/j.immuni.2007.08.018 (2007).

94 Fazilleau, N., McHeyzer-Williams, L. J., Rosen, H. & McHeyzer-Williams, M. G. The function of follicular helper T cells is regulated by the strength of T cell antigen receptor binding. *Nat Immunol* **10**, 375-384, doi:10.1038/ni.1704 (2009).

95 Ferguson, S. E., Han, S., Kelsoe, G. & Thompson, C. B. CD28 is required for germinal center formation. *J Immunol* **156**, 4576-4581 (1996).

96 Shahinian, A., Pfeffer, K., Lee, K. P., Kundig, T. M., Kishihara, K., Wakeham, A., Kawai, K., Ohashi, P. S., Thompson, C. B. & Mak, T. W. Differential T cell costimulatory requirements in CD28-deficient mice. *Science* **261**, 609-612 (1993).

97 Flynn, S., Toellner, K. M., Raykundalia, C., Goodall, M. & Lane, P. CD4 T cell cytokine differentiation: the B cell activation molecule, OX40 ligand, instructs CD4 T cells to express interleukin 4 and upregulates expression of the chemokine receptor, Blr-1. *J Exp Med* **188**, 297-304 (1998).

98 Akiba, H., Takeda, K., Kojima, Y., Usui, Y., Harada, N., Yamazaki, T., Ma, J., Tezuka, K., Yagita, H. & Okumura, K. The role of ICOS in the CXCR5+ follicular B helper T cell maintenance in vivo. *J Immunol* **175**, 2340-2348 (2005).

99 Kopf, M., Ruedl, C., Schmitz, N., Gallimore, A., Lefrang, K., Ecabert, B., Odermatt, B. & Bachmann, M. F. OX40-deficient mice are defective in Th cell proliferation but are competent in generating B cell and CTL Responses after virus infection. *Immunity* **11**, 699-708 (1999).

100 Glasmacher, E., Hoefig, K. P., Vogel, K. U., Rath, N., Du, L., Wolf, C., Kremmer, E., Wang, X. & Heissmeyer, V. Roquin binds inducible costimulator mRNA and effectors of mRNA decay to induce microRNA-independent post-transcriptional repression. *Nat Immunol* **11**, 725-733, doi:10.1038/ni.1902 (2010).

101 Vinuesa, C. G., Cook, M. C., Angelucci, C., Athanasopoulos, V., Rui, L., Hill, K. M., Yu, D., Domaschenz, H., Whittle, B., Lambe, T., Roberts, I. S., Copley, R. R., Bell, J. I., Cornall, R. J. & Goodnow, C. C. A RING-type ubiquitin ligase family member required to repress follicular helper T cells and autoimmunity. *Nature* **435**, 452-458, doi:10.1038/nature03555 (2005).

102 Vogel, K. U., Edelmann, S. L., Jeltsch, K. M., Bertossi, A., Heger, K., Heinz, G. A., Zoller, J., Warth, S. C., Hoefig, K. P., Lohs, C., Neff, F., Kremmer, E., Schick, J., Repsilber, D., Geerlof, A., Blum, H., Wurst, W., Heikenwalder, M., Schmidt-Supprian, M. & Heissmeyer, V. Roquin paralogs 1 and 2 redundantly repress the Icos and Ox40 costimulator mRNAs and control follicular helper T cell differentiation. *Immunity* **38**, 655-668, doi:10.1016/j.immuni.2012.12.004 (2013).

103 Good-Jacobson, K. L., Szumilas, C. G., Chen, L., Sharpe, A. H., Tomayko, M. M. & Shlomchik, M. J. PD-1 regulates germinal center B cell survival and the formation and affinity of long-lived plasma cells. *Nat Immunol* **11**, 535-542, doi:10.1038/ni.1877 (2010).

104 Kashiwakuma, D., Suto, A., Hiramatsu, Y., Ikeda, K., Takatori, H., Suzuki, K., Kagami, S., Hirose, K., Watanabe, N., Iwamoto, I. & Nakajima, H. B and T lymphocyte attenuator suppresses IL-21 production from follicular Th cells and subsequent humoral immune responses. *J Immunol* **185**, 2730-2736, doi:10.4049/jimmunol.0903839 (2010).

105 Cai, G. & Freeman, G. J. The CD160, BTLA, LIGHT/HVEM pathway: a bidirectional switch regulating T-cell activation. *Immunol Rev* **229**, 244-258, doi:10.1111/j.1600-065X.2009.00783.x (2009).

106 Iqbal, J., Wright, G., Wang, C., Rosenwald, A., Gascoyne, R. D., Weisenburger, D. D., Greiner, T. C., Smith, L., Guo, S., Wilcox, R. A., Teh, B. T., Lim, S. T., Tan, S. Y., Rimsza, L. M., Jaffe, E. S., Campo, E., Martinez, A., Delabie, J., Braziel, R. M., Cook, J. R. *et al.* Gene expression signatures delineate biological and prognostic subgroups in peripheral T-cell lymphoma. *Blood* **123**, 2915-2923 (2014).

107 Glimcher, L. H. & Murphy, K. M. Lineage commitment in the immune system: the T helper lymphocyte grows up. *Genes Dev* **14**, 1693-1711 (2000).

108 Zhu, J., Yamane, H. & Paul, W. E. Differentiation of effector CD4 T cell populations (*). *Annu Rev Immunol* **28**, 445-489, doi:10.1146/annurev-immunol-030409-101212 (2010).

109 Leavy, O. T cells: The TFH-like transition of TH1 cells. *Nat Rev Immunol* **12**, 74, doi:10.1038/nri3161 (2012).

110 Nakayamada, S., Kanno, Y., Takahashi, H., Jankovic, D., Lu, K. T., Johnson, T. A., Sun, H. W., Vahedi, G., Hakim, O., Handon, R., Schwartzberg, P. L., Hager, G. L. & O'Shea, J. J. Early Th1 cell differentiation is marked by a Tfh cell-like transition. *Immunity* **35**, 919-931, doi:10.1016/j.immuni.2011.11.012 (2011).

111 Bruneau, J., Canioni, D., Renand, A., Marafioti, T., Paterson, J. C., Martin-Garcia, N., Gaulard, P., Delfau, M. H., Hermine, O., Macintyre, E., Brousse, N. & Asnafi, V. Regulatory T-cell depletion in angioimmunoblastic T-cell lymphoma. *Am J Pathol* **177**, 570-574, doi:10.2353/ajpath.2010.100150 (2010).

112 Bonzheim, I., Geissinger, E., Tinguely, M., Roth, S., Grieb, T., Reimer, P., Wilhelm, M., Rosenwald, A., Muller-Hermelink, H. K. & Rudiger, T. Evaluation of FoxP3 expression in peripheral T-cell lymphoma. *Am J Clin Pathol* **130**, 613-619, doi:10.1309/L65GWEQ803PP6VX1 (2008).

113 Williams, C., Ponten, F., Moberg, C., Soderkvist, P., Uhlen, M., Ponten, J., Sitbon, G. & Lundeberg, J. A high frequency of sequence alterations is due to formalin fixation of archival specimens. *Am J Pathol* **155**, 1467-1471, doi:10.1016/S0002-9440(10)65461-2 (1999).

114 Yost, S. E., Smith, E. N., Schwab, R. B., Bao, L., Jung, H., Wang, X., Voest, E., Pierce, J. P., Messer, K., Parker, B. A., Harismendy, O. & Frazer, K. A. Identification of high-confidence somatic mutations in whole genome sequence of formalin-fixed breast cancer specimens. *Nucleic Acids Res* **40**, e107, doi:10.1093/nar/gks299 (2012).

115 Mardis, E. R. A decade's perspective on DNA sequencing technology. *Nature* **470**, 198-203, doi:10.1038/nature09796 (2011).

116 Sanger, F., Nicklen, S. & Coulson, A. R. DNA sequencing with chain-terminating inhibitors. *Proc Natl Acad Sci U S A* **74**, 5463-5467 (1977).

117 Ozsolak, F. & Milos, P. M. RNA sequencing: advances, challenges and opportunities. *Nat Rev Genet* **12**, 87-98, doi:10.1038/nrg2934 (2011).

118 Illumina, I. *Specifications Sheet: HiSeq X 10*, <http://www.illumina.com/content/dam/illumina-marketing/documents/products/datasheets/datasheet-hiseq-x-ten.pdf> (2015).

119 Choi, M., Scholl, U. I., Ji, W., Liu, T., Tikhonova, I. R., Zumbo, P., Nayir, A., Bakkaloglu, A., Ozen, S., Sanjad, S., Nelson-Williams, C., Farhi, A., Mane, S. & Lifton, R. P. Genetic diagnosis by whole exome capture and massively parallel DNA sequencing. *Proc Natl Acad Sci U S A* **106**, 19096-19101, doi:10.1073/pnas.0910672106 (2009).

120 Illumina, I. *NextSeq Series Amplicon Sequencing Solution*, <http://www.illumina.com/content/dam/illumina-marketing/documents/products/datasheets/datasheet_truseq_custom_amplicon.pdf> (2016).

121 Hodges, E., Xuan, Z., Balija, V., Kramer, M., Molla, M. N., Smith, S. W., Middle, C. M., Rodesch, M. J., Albert, T. J., Hannon, G. J. & McCombie, W. R. Genome-wide in situ exon capture for selective resequencing. *Nat Genet* **39**, 1522-1527, doi:10.1038/ng.2007.42 (2007).

122 Rohr, J., Guo, S., Huo, J., Bouska, A., Lachel, C., Li, Y., Simone, P. D., Zhang, W., Gong, Q., Wang, C., Cannon, A., Heavican, T., Mottok, A., Hung, S., Rosenwald, A., Gascoyne, R., Fu, K., Greiner, T. C., Weisenburger, D. D., Vose, J. M. *et al.* Recurrent activating mutations of CD28 in peripheral T-cell lymphomas. *Leukemia*, doi:10.1038/leu.2015.357 (2015).

123 Wang, C., McKeithan, T. W., Gong, Q., Zhang, W., Bouska, A., Rosenwald, A., Gascoyne, R. D., Wu, X., Wang, J., Muhammad, Z., Jiang, B., Rohr, J., Cannon, A., Steidl, C., Fu, K., Li, Y., Hung, S., Weisenburger, D. D., Greiner, T. C., Smith, L. *et al.* IDH2R172 mutations define a unique subgroup of patients with angioimmunoblastic T-cell lymphoma. *Blood* **126**, 1741-1752, doi:10.1182/blood-2015-05-644591 (2015).

124 Bouska, A., McKeithan, T. W., Deffenbacher, K. E., Lachel, C., Wright, G. W., Iqbal, J., Smith, L. M., Zhang, W., Kucuk, C., Rinaldi, A., Bertoni, F., Fitzgibbon, J., Fu, K., Weisenburger, D. D., Greiner, T. C., Dave, B. J., Gascoyne, R. D., Rosenwald, A., Ott, G., Campo, E. *et al.* Genome-wide copy-number analyses reveal genomic abnormalities involved in transformation of follicular lymphoma. *Blood* **123**, 1681-1690, doi:10.1182/blood-2013-05-500595 (2014).

125 Palomero, T., Couronne, L., Khiabanian, H., Kim, M. Y., Ambesi-Impiombato, A., Perez-Garcia, A., Carpenter, Z., Abate, F., Allegretta, M., Haydu, J. E., Jiang, X., Lossos, I. S., Nicolas, C., Balbin, M., Bastard, C., Bhagat, G., Piris, M. A., Campo, E., Bernard, O. A., Rabadan, R. *et al.* Recurrent mutations in epigenetic regulators, RHOA and FYN kinase in peripheral T cell lymphomas. *Nat Genet* **46**, 166-170 (2014).

126 Quivoron, C., Couronne, L., Della Valle, V., Lopez, C. K., Plo, I., Wagner-Ballon, O., Do Cruzeiro, M., Delhommeau, F., Arnulf, B., Stern, M. H., Godley, L., Opolon, P., Tilly, H., Solary, E., Duffourd, Y., Dessen, P., Merle-Beral, H., Nguyen-Khac, F., Fontenay, M., Vainchenker, W. *et al.* TET2 inactivation results in pleiotropic hematopoietic abnormalities in mouse and is a recurrent event during human lymphomagenesis. *Cancer Cell* **20**, 25-38 (2011).

127 Sakata-Yanagimoto, M., Enami, T., Yoshida, K., Shiraishi, Y., Ishii, R., Miyake, Y., Muto, H., Tsuyama, N., Sato-Otsubo, A., Okuno, Y., Sakata, S., Kamada, Y., Nakamoto-Matsubara, R., Tran, N. B., Izutsu, K., Sato, Y., Ohta, Y., Furuta, J., Shimizu, S., Komeno, T. *et al.* Somatic RHOA mutation in angioimmunoblastic T cell lymphoma. *Nat Genet* **46**, 171-175 (2014).

128 Yoo, H. Y., Sung, M. K., Lee, S. H., Kim, S., Lee, H., Park, S., Kim, S. C., Lee, B., Rho, K., Lee, J. E., Cho, K. H., Kim, W., Ju, H., Kim, J., Kim, S. J., Kim, W. S., Lee, S. & Ko, Y. H. A recurrent inactivating mutation in RHOA GTPase in angioimmunoblastic T cell lymphoma. *Nat Genet* **46**, 371-375 (2014).

129 Couronne, L., Bastard, C. & Bernard, O. A. TET2 and DNMT3A mutations in human T-cell lymphoma. *N Engl J Med* **366**, 95-96, doi:10.1056/NEJMc1111708 (2012).
130 Moran-Crusio, K., Reavie, L., Shih, A., Abdel-Wahab, O., Ndiaye-Lobry, D., Lobry, C., Figueroa, M. E., Vasanthakumar, A., Patel, J., Zhao, X., Perna, F., Pandey, S., Madzo, J., Song, C., Dai, Q., He, C., Ibrahim, S., Beran, M., Zavadil, J., Nimer, S. D. *et al.* Tet2 loss leads to increased hematopoietic stem cell self-renewal and myeloid transformation. *Cancer Cell* **20**, 11-24, doi:10.1016/j.ccr.2011.06.001 (2011).
131 Yu, L. & Qi, S. Ten-Eleven Translocation-2 gene mutations: A potential new molecular marker in malignant gliomas (Review). *Oncol Lett* **3**, 7-10, doi:10.3892/ol.2011.447 (2012).
132 Mardis, E. R., Ding, L., Dooling, D. J., Larson, D. E., McLellan, M. D., Chen, K., Koboldt, D. C., Fulton, R. S., Delehaunty, K. D., McGrath, S. D., Fulton, L. A., Locke, D. P., Magrini, V. J., Abbott, R. M., Vickery, T. L., Reed, J. S., Robinson, J. S., Wylie, T., Smith, S. M., Carmichael, L. *et al.* Recurring mutations found by sequencing an acute myeloid leukemia genome. *N Engl J Med* **361**, 1058-1066, doi:10.1056/NEJMoa0903840 (2009).
133 Abdel-Wahab, O., Mullally, A., Hedvat, C., Garcia-Manero, G., Patel, J., Wadleigh, M., Malinge, S., Yao, J., Kilpivaara, O., Bhat, R., Huberman, K., Thomas, S., Dolgalev, I., Heguy, A., Paietta, E., Le Beau, M. M., Beran, M., Tallman, M. S., Ebert, B. L., Kantarjian, H. M. *et al.* Genetic characterization of TET1, TET2, and TET3 alterations in myeloid malignancies. *Blood* **114**, 144-147, doi:10.1182/blood-2009-03-210039 (2009).
134 McKerrell, T., Park, N., Moreno, T., Grove, C. S., Ponstingl, H., Stephens, J., Understanding Society Scientific, G., Crawley, C., Craig, J., Scott, M. A., Hodkinson, C., Baxter, J., Rad, R., Forsyth, D. R., Quail, M. A., Zeggini, E., Ouwehand, W., Varela, I. & Vassiliou, G. S. Leukemia-associated somatic mutations drive distinct patterns of age-related clonal hemopoiesis. *Cell Rep* **10**, 1239-1245, doi:10.1016/j.celrep.2015.02.005 (2015).
135 Xie, M., Lu, C., Wang, J., McLellan, M. D., Johnson, K. J., Wendl, M. C., McMichael, J. F., Schmidt, H. K., Yellapantula, V., Miller, C. A., Ozenberger, B. A., Welch, J. S., Link, D. C., Walter, M. J., Mardis, E. R., Dipersio, J. F., Chen, F., Wilson, R. K., Ley, T. J. & Ding, L. Age-related mutations associated with clonal hematopoietic expansion and malignancies. *Nat Med* **20**, 1472-1478, doi:10.1038/nm.3733 (2014).
136 Odejide, O., Weigert, O., Lane, A. A., Toscano, D., Lunning, M. A., Kopp, N., Kim, S., van Bodegom, D., Bolla, S., Schatz, J. H., Teruya-Feldstein, J., Hochberg, E., Louissaint, A., Dorfman, D., Stevenson, K., Rodig, S. J., Piccaluga, P. P., Jacobsen, E., Pileri, S. A., Harris, N. L. *et al.* A targeted mutational landscape of angioimmunoblastic T-cell lymphoma. *Blood* **123**, 1293-1296 (2014).
137 Li, K. K., Luo, L. F., Shen, Y., Xu, J., Chen, Z. & Chen, S. J. DNA methyltransferases in hematologic malignancies. *Semin Hematol* **50**, 48-60, doi:10.1053/j.seminhematol.2013.01.005 (2013).
138 Cairns, R. A., Iqbal, J., Lemonnier, F., Kucuk, C., de Leval, L., Jais, J. P., Parrens, M., Martin, A., Xerri, L., Brousset, P., Chan, L. C., Chan, W. C., Gaulard, P. & Mak, T. W. IDH2 mutations are frequent in angioimmunoblastic T-cell lymphoma. *Blood* **119**, 1901-1903 (2012).
139 Xu, W., Yang, H., Liu, Y., Yang, Y., Wang, P., Kim, S. H., Ito, S., Yang, C., Wang, P., Xiao, M. T., Liu, L. X., Jiang, W. Q., Liu, J., Zhang, J. Y., Wang, B.,

Frye, S., Zhang, Y., Xu, Y. H., Lei, Q. Y., Guan, K. L. *et al.* Oncometabolite 2-hydroxyglutarate is a competitive inhibitor of alpha-ketoglutarate-dependent dioxygenases. *Cancer Cell* **19**, 17-30, doi:10.1016/j.ccr.2010.12.014 (2011).

140 Chowdhury, R., Yeoh, K. K., Tian, Y. M., Hillringhaus, L., Bagg, E. A., Rose, N. R., Leung, I. K., Li, X. S., Woon, E. C., Yang, M., McDonough, M. A., King, O. N., Clifton, I. J., Klose, R. J., Claridge, T. D., Ratcliffe, P. J., Schofield, C. J. & Kawamura, A. The oncometabolite 2-hydroxyglutarate inhibits histone lysine demethylases. *EMBO Rep* **12**, 463-469, doi:10.1038/embor.2011.43 (2011).

141 Yan, H., Parsons, D. W., Jin, G., McLendon, R., Rasheed, B. A., Yuan, W., Kos, I., Batinic-Haberle, I., Jones, S., Riggins, G. J., Friedman, H., Friedman, A., Reardon, D., Herndon, J., Kinzler, K. W., Velculescu, V. E., Vogelstein, B. & Bigner, D. D. IDH1 and IDH2 mutations in gliomas. *N Engl J Med* **360**, 765-773, doi:10.1056/NEJMoa0808710 (2009).

142 Lee, S. H., Kim, J. S., Kim, J., Kim, S. J., Kim, W. S., Lee, S., Ko, Y. H. & Yoo, H. Y. A highly recurrent novel missense mutation in CD28 among angioimmunoblastic T-cell lymphoma patients. *Haematologica* **100**, e505-507, doi:10.3324/haematol.2015.133074 (2015).

143 Pechloff, K., Holch, J., Ferch, U., Schweneker, M., Brunner, K., Kremer, M., Sparwasser, T., Quintanilla-Martinez, L., Zimber-Strobl, U., Streubel, B., Gewies, A., Peschel, C. & Ruland, J. The fusion kinase ITK-SYK mimics a T cell receptor signal and drives oncogenesis in conditional mouse models of peripheral T cell lymphoma. *J Exp Med* **207**, 1031-1044, doi:10.1084/jem.20092042 (2010).

144 Piccaluga, P. P., Rossi, M., Agostinelli, C., Ricci, F., Gazzola, A., Righi, S., Fuligni, F., Laginestra, M. A., Mancini, M., Sapienza, M. R., De Renzo, A., Tazzari, P. L., Gibellini, D., Went, P., Alviano, F., Zinzani, P. L., Bagnara, G. P., Inghirami, G., Tripodo, C. & Pileri, S. A. Platelet-derived growth factor alpha mediates the proliferation of peripheral T-cell lymphoma cells via an autocrine regulatory pathway. *Leukemia* **28**, 1687-1697, doi:10.1038/leu.2014.50 (2014).

145 Manso, R., Rodriguez-Pinilla, S. M., Gonzalez-Rincon, J., Gomez, S., Monsalvo, S., Llamas, P., Rojo, F., Perez-Callejo, D., Cereceda, L., Limeres, M. A., Maeso, C., Ferrando, L., Perez-Seoane, C., Rodriguez, G., Arrinda, J. M., Garcia-Bragado, F., Franco, R., Rodriguez-Peralto, J. L., Gonzalez-Carrero, J., Martin-Davila, F. *et al.* Recurrent presence of the PLCG1 S345F mutation in nodal peripheral T-cell lymphomas. *Haematologica* **100**, e25-27, doi:10.3324/haematol.2014.113696 (2015).

146 Vaque, J. P., Gomez-Lopez, G., Monsalvez, V., Varela, I., Martinez, N., Perez, C., Dominguez, O., Grana, O., Rodriguez-Peralto, J. L., Rodriguez-Pinilla, S. M., Gonzalez-Vela, C., Rubio-Camarillo, M., Martin-Sanchez, E., Pisano, D. G., Papadavid, E., Papadaki, T., Requena, L., Garcia-Marco, J. A., Mendez, M., Provencio, M. *et al.* PLCG1 mutations in cutaneous T-cell lymphomas. *Blood* **123**, 2034-2043, doi:10.1182/blood-2013-05-504308 (2014).

147 Trapnell, C., Pachter, L. & Salzberg, S. L. TopHat: discovering splice junctions with RNA-Seq. *Bioinformatics* **25**, 1105-1111 (2009).

148 Trapnell, C., Williams, B. A., Pertea, G., Mortazavi, A., Kwan, G., van Baren, M. J., Salzberg, S. L., Wold, B. J. & Pachter, L. Transcript assembly and quantification by RNA-Seq reveals unannotated transcripts and isoform switching during cell differentiation. *Nat Biotechnol* **28**, 511-515 (2010).

149 Kim, D. & Salzberg, S. L. TopHat-Fusion: an algorithm for discovery of novel fusion transcripts. *Genome Biol* **12**, R72 (2011).

150 Langmead, B., Trapnell, C., Pop, M. & Salzberg, S. L. Ultrafast and memory-efficient alignment of short DNA sequences to the human genome. *Genome Biol* **10**, R25 (2009).
151 Yost, S. E., Alakus, H., Matsui, H., Schwab, R. B., Jepsen, K., Frazer, K. A. & Harismendy, O. Mutascope: sensitive detection of somatic mutations from deep amplicon sequencing. *Bioinformatics* **29**, 1908-1909 (2013).
152 Koboldt, D. C., Zhang, Q., Larson, D. E., Shen, D., McLellan, M. D., Lin, L., Miller, C. A., Mardis, E. R., Ding, L. & Wilson, R. K. VarScan 2: somatic mutation and copy number alteration discovery in cancer by exome sequencing. *Genome Res* **22**, 568-576 (2012).
153 Therneau, T. M. *A Package for Survival Analysis in S*, <http://CRAN.R-project.org/package=survival> (2015).
154 Evans, E. J., Castro, M. A., O'Brien, R., Kearney, A., Walsh, H., Sparks, L. M., Tucknott, M. G., Davies, E. A., Carmo, A. M., van der Merwe, P. A., Stuart, D. I., Jones, E. Y., Ladbury, J. E., Ikemizu, S. & Davis, S. J. Crystal structure and binding properties of the CD2 and CD244 (2B4)-binding protein, CD48. *J Biol Chem* **281**, 29309-29320 (2006).
155 Evans, E. J., Esnouf, R. M., Manso-Sancho, R., Gilbert, R. J., James, J. R., Yu, C., Fennelly, J. A., Vowles, C., Hanke, T., Walse, B., Hunig, T., Sorensen, P., Stuart, D. I. & Davis, S. J. Crystal structure of a soluble CD28-Fab complex. *Nat Immunol* **6**, 271-279 (2005).
156 Schwartz, J. C., Zhang, X., Fedorov, A. A., Nathenson, S. G. & Almo, S. C. Structural basis for co-stimulation by the human CTLA-4/B7-2 complex. *Nature* **410**, 604-608 (2001).
157 Stamper, C. C., Zhang, Y., Tobin, J. F., Erbe, D. V., Ikemizu, S., Davis, S. J., Stahl, M. L., Seehra, J., Somers, W. S. & Mosyak, L. Crystal structure of the B7-1/CTLA-4 complex that inhibits human immune responses. *Nature* **410**, 608-611 (2001).
158 Emsley, P., Lohkamp, B., Scott, W. G. & Cowtan, K. Features and development of Coot. *Acta Crystallogr D Biol Crystallogr* **66**, 486-501 (2010).
159 Chen, V. B., Arendall, W. B., 3rd, Headd, J. J., Keedy, D. A., Immormino, R. M., Kapral, G. J., Murray, L. W., Richardson, J. S. & Richardson, D. C. MolProbity: all-atom structure validation for macromolecular crystallography. *Acta Crystallogr D Biol Crystallogr* **66**, 12-21 (2010).
160 Kabsch, W. A solution for the best rotation to relate two sets of vectors. *Acta Crystallogr. A Found. Crystallogr.* **32**, 922-923 (1976).
161 Winn, M. D., Ballard, C. C., Cowtan, K. D., Dodson, E. J., Emsley, P., Evans, P. R., Keegan, R. M., Krissinel, E. B., Leslie, A. G., McCoy, A., McNicholas, S. J., Murshudov, G. N., Pannu, N. S., Potterton, E. A., Powell, H. R., Read, R. J., Vagin, A. & Wilson, K. S. Overview of the CCP4 suite and current developments. *Acta Crystallogr D Biol Crystallogr* **67**, 235-242 (2011).
162 Adams, P. D., Afonine, P. V., Bunkoczi, G., Chen, V. B., Davis, I. W., Echols, N., Headd, J. J., Hung, L. W., Kapral, G. J., Grosse-Kunstleve, R. W., McCoy, A. J., Moriarty, N. W., Oeffner, R., Read, R. J., Richardson, D. C., Richardson, J. S., Terwilliger, T. C. & Zwart, P. H. PHENIX: a comprehensive Python-based system for macromolecular structure solution. *Acta Crystallogr D Biol Crystallogr* **66**, 213-221 (2010).
163 Laskowski, R. A. & Swindells, M. B. LigPlot+: multiple ligand-protein interaction diagrams for drug discovery. *J Chem Inf Model* **51**, 2778-2786 (2011).

164 Dominguez, C., Boelens, R. & Bonvin, A. M. HADDOCK: a protein-protein docking approach based on biochemical or biophysical information. *J Am Chem Soc* **125**, 1731-1737 (2003).

165 Baker, N. A., Sept, D., Joseph, S., Holst, M. J. & McCammon, J. A. Electrostatics of nanosystems: application to microtubules and the ribosome. *Proc Natl Acad Sci U S A* **98**, 10037-10041, doi:10.1073/pnas.181342398 (2001).

166 Dolinsky, T. J., Nielsen, J. E., McCammon, J. A. & Baker, N. A. PDB2PQR: an automated pipeline for the setup of Poisson-Boltzmann electrostatics calculations. *Nucleic Acids Res* **32**, W665-667 (2004).

167 Lerner, M. G. & Carlson, H. A. APBS Tools 2.1 plugin for PyMOL. University of Michigan, Ann Arbor (2009).

168 Schrödinger, L. The PyMOL Molecular Graphics System. **Version 1.6.9** (2013).

169 Higo, K., Ikura, T., Oda, M., Morii, H., Takahashi, J., Abe, R. & Ito, N. High resolution crystal structure of the Grb2 SH2 domain with a phosphopeptide derived from CD28. *PLoS One* **8**, e74482 (2013).

170 Kucuk, C., Iqbal, J., Hu, X., Gaulard, P., De Leval, L., Srivastava, G., Au, W. Y., McKeithan, T. W. & Chan, W. C. PRDM1 is a tumor suppressor gene in natural killer cell malignancies. *Proc Natl Acad Sci U S A* **108**, 20119-20124 (2011).

171 Morgenstern, J. P. & Land, H. Advanced mammalian gene transfer: high titre retroviral vectors with multiple drug selection markers and a complementary helper-free packaging cell line. *Nucleic Acids Res* **18**, 3587-3596 (1990).

172 Mitchell, T. C., Hildeman, D., Kedl, R. M., Teague, T. K., Schaefer, B. C., White, J., Zhu, Y., Kappler, J. & Marrack, P. Immunological adjuvants promote activated T cell survival via induction of Bcl-3. *Nat Immunol* **2**, 397-402, doi:10.1038/87692 (2001).

173 Cao, Y., Janssen, E. M., Duncan, A. W., Altman, A., Billadeau, D. D. & Abraham, R. T. Pleiotropic defects in TCR signaling in a Vav-1-null Jurkat T-cell line. *EMBO J* **21**, 4809-4819 (2002).

174 Geiss, G. K., Bumgarner, R. E., Birditt, B., Dahl, T., Dowidar, N., Dunaway, D. L., Fell, H. P., Ferree, S., George, R. D., Grogan, T., James, J. J., Maysuria, M., Mitton, J. D., Oliveri, P., Osborn, J. L., Peng, T., Ratcliffe, A. L., Webster, P. J., Davidson, E. H., Hood, L. *et al.* Direct multiplexed measurement of gene expression with color-coded probe pairs. *Nat Biotechnol* **26**, 317-325 (2008).

175 Weinstein, J. S., Lezon-Geyda, K., Maksimova, Y., Craft, S., Zhang, Y., Su, M., Schulz, V. P., Craft, J. & Gallagher, P. G. Global transcriptome analysis and enhancer landscape of human primary T follicular helper and T effector lymphocytes. *Blood* **124**, 3719-3729, doi:10.1182/blood-2014-06-582700 (2014).

176 Ren, J., Wen, L., Gao, X., Jin, C., Xue, Y. & Yao, X. DOG 1.0: illustrator of protein domain structures. *Cell Res* **19**, 271-273 (2009).

177 Hindson, B. J., Ness, K. D., Masquelier, D. A., Belgrader, P., Heredia, N. J., Makarewicz, A. J., Bright, I. J., Lucero, M. Y., Hiddessen, A. L., Legler, T. C., Kitano, T. K., Hodel, M. R., Petersen, J. F., Wyatt, P. W., Steenblock, E. R., Shah, P. H., Bousse, L. J., Troup, C. B., Mellen, J. C., Wittmann, D. K. *et al.* High-throughput droplet digital PCR system for absolute quantitation of DNA copy number. *Anal Chem* **83**, 8604-8610, doi:10.1021/ac202028g (2011).

178 Ungewickell, A., Bhaduri, A., Rios, E., Reuter, J., Lee, C. S., Mah, A., Zehnder, A., Ohgami, R., Kulkarni, S., Armstrong, R., Weng, W. K., Gratzinger, D., Tavallaee, M., Rook, A., Snyder, M., Kim, Y. & Khavari, P. A. Genomic analysis of mycosis fungoides and Sezary syndrome identifies recurrent alterations in TNFR2. *Nat Genet* **47**, 1056-1060, doi:10.1038/ng.3370 (2015).

179 Choi, J., Goh, G., Walradt, T., Hong, B. S., Bunick, C. G., Chen, K., Bjornson, R. D., Maman, Y., Wang, T., Tordoff, J., Carlson, K., Overton, J. D., Liu, K. J., Lewis, J. M., Devine, L., Barbarotta, L., Foss, F. M., Subtil, A., Vonderheid, E. C., Edelson, R. L. *et al.* Genomic landscape of cutaneous T cell lymphoma. *Nat Genet* **47**, 1011-1019, doi:10.1038/ng.3356 (2015).

180 Kataoka, K., Nagata, Y., Kitanaka, A., Shiraishi, Y., Shimamura, T., Yasunaga, J., Totoki, Y., Chiba, K., Sato-Otsubo, A., Nagae, G., Ishii, R., Muto, S., Kotani, S., Watatani, Y., Takeda, J., Sanada, M., Tanaka, H., Suzuki, H., Sato, Y., Shiozawa, Y. *et al.* Integrated molecular analysis of adult T cell leukemia/lymphoma. *Nat Genet* **47**, 1304-1315, doi:10.1038/ng.3415 (2015).

181 Kucuk, C., Jiang, B., Hu, X., Zhang, W., Chan, J. K., Xiao, W., Lack, N., Alkan, C., Williams, J. C., Avery, K. N., Kavak, P., Scuto, A., Sen, E., Gaulard, P., Staudt, L., Iqbal, J., Zhang, W., Cornish, A., Gong, Q., Yang, Q. *et al.* Activating mutations of STAT5B and STAT3 in lymphomas derived from gammadelta-T or NK cells. *Nat Commun* **6**, 6025, doi:10.1038/ncomms7025 (2015).

182 Watanabe, R., Harada, Y., Takeda, K., Takahashi, J., Ohnuki, K., Ogawa, S., Ohgai, D., Kaibara, N., Koiwai, O., Tanabe, K., Toma, H., Sugamura, K. & Abe, R. Grb2 and Gads exhibit different interactions with CD28 and play distinct roles in CD28-mediated costimulation. *J Immunol* **177**, 1085-1091 (2006).

183 Obenauer, J. C., Cantley, L. C. & Yaffe, M. B. Scansite 2.0: Proteome-wide prediction of cell signaling interactions using short sequence motifs. *Nucleic Acids Res* **31**, 3635-3641 (2003).

184 Riley, J. L., Mao, M., Kobayashi, S., Biery, M., Burchard, J., Cavet, G., Gregson, B. P., June, C. H. & Linsley, P. S. Modulation of TCR-induced transcriptional profiles by ligation of CD28, ICOS, and CTLA-4 receptors. *Proc Natl Acad Sci U S A* **99**, 11790-11795 (2002).

185 Bahlis, N. J., King, A. M., Kolonias, D., Carlson, L. M., Liu, H. Y., Hussein, M. A., Terebelo, H. R., Byrne, G. E., Jr., Levine, B. L., Boise, L. H. & Lee, K. P. CD28-mediated regulation of multiple myeloma cell proliferation and survival. *Blood* **109**, 5002-5010 (2007).

186 Pope, B., Brown, R. D., Gibson, J., Yuen, E. & Joshua, D. B7-2-positive myeloma: incidence, clinical characteristics, prognostic significance, and implications for tumor immunotherapy. *Blood* **96**, 1274-1279 (2000).

187 Robillard, N., Jego, G., Pellat-Deceunynck, C., Pineau, D., Puthier, D., Mellerin, M. P., Barille, S., Rapp, M. J., Harousseau, J. L., Amiot, M. & Bataille, R. CD28, a marker associated with tumoral expansion in multiple myeloma. *Clin Cancer Res* **4**, 1521-1526 (1998).

188 Johnston, R. J., Comps-Agrar, L., Hackney, J., Yu, X., Huseni, M., Yang, Y., Park, S., Javinal, V., Chiu, H., Irving, B., Eaton, D. L. & Grogan, J. L. The immunoreceptor TIGIT regulates antitumor and antiviral CD8(+) T cell effector function. *Cancer Cell* **26**, 923-937 (2014).

189 Sakurai, H., Suzuki, S., Kawasaki, N., Nakano, H., Okazaki, T., Chino, A., Doi, T. & Saiki, I. Tumor necrosis factor-alpha-induced IKK phosphorylation of NF-kappaB p65 on serine 536 is mediated through the TRAF2, TRAF5, and TAK1 signaling pathway. *J Biol Chem* **278**, 36916-36923 (2003).

190 Dunleavy, K. & Wilson, W. H. Appropriate management of molecular subtypes of diffuse large B-cell lymphoma. *Oncology (Williston Park)* **28**, 326-334 (2014).

191 Yoo, H. Y., Kim, P., Kim, W. S., Lee, S. H., Kim, S., Kang, S. Y., Jang, H. Y., Lee, J. E., Kim, J., Kim, S. J., Ko, Y. H. & Lee, S. Frequent CTLA4-CD28 gene fusion in diverse types of T cell lymphoma. *Haematologica*, doi:10.3324/haematol.2015.139253 (2016).

192 Gong, Q., Wang, C., Rohr, J., Feldman, A., Chan, W. & McKeithan, T. Comment on Yoo et al.: Frequent CTLA4-CD28 gene fusion in diverse types of T cell lymphoma. *Haematologica* **Submitted**.

193 Houlard, M., Arudchandran, R., Regnier-Ricard, F., Germani, A., Gisselbrecht, S., Blank, U., Rivera, J. & Varin-Blank, N. Vav1 is a component of transcriptionally active complexes. *J Exp Med* **195**, 1115-1127 (2002).

194 McClary, K. B. & Grainger, D. W. RhoA-induced changes in fibroblasts cultured on organic monolayers. *Biomaterials* **20**, 2435-2446 (1999).

195 Bellizzi, A., Mangia, A., Chiriatti, A., Petroni, S., Quaranta, M., Schittulli, F., Malfettone, A., Cardone, R. A., Paradiso, A. & Reshkin, S. J. RhoA protein expression in primary breast cancers and matched lymphocytes is associated with progression of the disease. *Int J Mol Med* **22**, 25-31 (2008).

196 Schmidt, L. J., Duncan, K., Yadav, N., Regan, K. M., Verone, A. R., Lohse, C. M., Pop, E. A., Attwood, K., Wilding, G., Mohler, J. L., Sebo, T. J., Tindall, D. J. & Heemers, H. V. RhoA as a mediator of clinically relevant androgen action in prostate cancer cells. *Mol Endocrinol* **26**, 716-735, doi:10.1210/me.2011-1130 (2012).

197 Rohde, M., Richter, J., Schlesner, M., Betts, M. J., Claviez, A., Bonn, B. R., Zimmermann, M., Damm-Welk, C., Russell, R. B., Borkhardt, A., Eils, R., Hoell, J. I., Szczepanowski, M., Oschlies, I., Klapper, W., Burkhardt, B., Siebert, R., German, I. M.-S.-P. & Group, N.-B. S. Recurrent RHOA mutations in pediatric Burkitt lymphoma treated according to the NHL-BFM protocols. *Genes Chromosomes Cancer* **53**, 911-916, doi:10.1002/gcc.22202 (2014).

198 Liu, L., Schwartz, B. R., Lin, N., Winn, R. K. & Harlan, J. M. Requirement for RhoA kinase activation in leukocyte de-adhesion. *J Immunol* **169**, 2330-2336 (2002).

199 Cleverley, S. C., Costello, P. S., Henning, S. W. & Cantrell, D. A. Loss of Rho function in the thymus is accompanied by the development of thymic lymphoma. *Oncogene* **19**, 13-20 (2000).

200 Manser, E. J. The GTPase cycle. How dominant inhibitory mutants block the biological functions of small GTPases. *Methods Mol Biol* **189**, 3-11, doi:10.1385/1-59259-281-3:003 (2002).

201 Vunjak-Novakovic, G., Lui, K. O., Tandon, N. & Chien, K. R. Bioengineering heart muscle: a paradigm for regenerative medicine. *Annu Rev Biomed Eng* **13**, 245-267, doi:10.1146/annurev-bioeng-071910-124701 (2011).

202 Tilles, A. W., Berthiaume, F., Yarmush, M. L., Tompkins, R. G. & Toner, M. Bioengineering of liver assist devices. *J Hepatobiliary Pancreat Surg* **9**, 686-696, doi:10.1007/s005340200095 (2002).

203 Berman, D. M., Molano, R. D., Fotino, C., Ulissi, U., Gimeno, J., Mendez, A. J., Kenyon, N. M., Kenyon, N. S., Andrews, D. M., Ricordi, C. & Pileggi, A. Bioengineering the endocrine pancreas: intraomental islet transplantation within a biologic resorbable scaffold. *Diabetes*, doi:10.2337/db15-1525 (2016).

204 Sato, F., Ishida, T., Ito, A., Mori, F., Masaki, A., Takino, H., Narita, T., Ri, M., Kusumoto, S., Suzuki, S., Komatsu, H., Niimi, A., Ueda, R., Inagaki, H. & Iida, S. Angioimmunoblastic T-cell lymphoma mice model. *Leuk Res* **37**, 21-27, doi:10.1016/j.leukres.2012.09.009 (2013).

205 Suntharalingam, G., Perry, M. R., Ward, S., Brett, S. J., Castello-Cortes, A., Brunner, M. D. & Panoskaltsis, N. Cytokine storm in a phase 1 trial of the anti-CD28 monoclonal antibody TGN1412. *N Engl J Med* **355**, 1018-1028, doi:10.1056/NEJMoa063842 (2006).

206 Ossevoort, M. A., Ringers, J., Kuhn, E. M., Boon, L., Lorre, K., van den Hout, Y., Bruijn, J. A., de Boer, M., Jonker, M. & de Waele, P. Prevention of renal allograft rejection in primates by blocking the B7/CD28 pathway. *Transplantation* **68**, 1010-1018 (1999).

207 Haspot, F., Seveno, C., Dugast, A. S., Coulon, F., Renaudin, K., Usal, C., Hill, M., Anegon, I., Heslan, M., Josien, R., Brouard, S., Soulillou, J. P. & Vanhove, B. Anti-CD28 antibody-induced kidney allograft tolerance related to tryptophan degradation and TCR class II B7 regulatory cells. *Am J Transplant* **5**, 2339-2348, doi:10.1111/j.1600-6143.2005.01018.x (2005).

208 Das, S., Ariizumi, K. & Cruz, P. D., Jr. T-cell inhibitors: a bench-to-bedside review. *Dermatitis* **23**, 195-202, doi:10.1097/DER.0b013e31826e43ed (2012).